Non-axisymmetric magnetic flux transport in the Sun

Dissertation
zur Erlangung des mathematisch-naturwissenschaftlichen Doktorgrades

“Doctor rerum naturalium”

der Georg-August-Universität Göttingen

im Promotionsprogramm PROPHYS
der Georg-August University School of Science (GAUSS)

vorgelegt von

David Martín Belda

aus Salamanca, Spanien

Göttingen, 2017

Betreuungsausschuss

Dr. Robert H. Cameron
Max-Planck-Institut für Sonnensystemforschung, Göttingen, Germany

Prof. Dr. Manfred Schüssler
Max-Planck-Institut für Sonnensystemforschung, Göttingen, Germany

Prof. Dr. Laurent Gizon
Institut für Astrophysik, Georg-August Universität Göttingen, Göttingen, Germany und
Max-Planck-Institut für Sonnensystemforschung, Göttingen, Germany

Mitglieder der Prüfungskommision

Referent: Prof. Dr. Manfred Schüssler
Max-Planck-Institut für Sonnensystemforschung, Göttingen, Germany

Korreferent: Prof. Dr. Laurent Gizon
Institut für Astrophysik, Georg-August Universität Göttingen, Göttingen, Germany und
Max-Planck-Institut für Sonnensystemforschung, Göttingen, Germany

Weitere Mitglieder der Prüfungskommission:

Prof. Dr. Ansgar Reiners
Institut für Astrophysik, Georg-August Universität Göttingen, Göttingen, Germany

Prof. Dr. Andreas Tilgner
Institut für Geophysik, Georg-August Universität Göttingen, Göttingen, Germany

Prof. Dr. Wolfgang Glatzel
Institut für Astrophysik, Georg-August Universität Göttingen, Göttingen, Germany

Dr. Michael Wilczek
Max-Planck-Institut für Dynamik und Selbstorganisation, Göttingen

Tag der mündlichen Prüfung: 19.04.2017

Contents

Summary

The magnetic field of the Sun is maintained by a hydromagnetic dynamo. In recent years, observational evidence in support of the dynamo being of the Babcock-Leighton type has accumulated. In this kind of dynamo models, the regeneration of the large scale dipole field occurs through the decay of active regions on the solar surface. Hence, surface fields play a central role on the global dynamo, as opposed to being a mere by-product of a turbulent dynamo operating below the surface.

Most kinematic models of the solar cycle are formulated in terms of azimuthal averages. The critical role of the non-axisymmetric flows on the evolution of the magnetic field is incorporated through the mean field coefficients. In particular, the effect of the non-axisymmetric convective flows on the generation of magnetic field is parametrized through a linear relationship between the mean poloidal field and the mean toroidal field (the mean field α effect). On the intermediate scales, an example of non-axisymmetric flows are the near-surface, converging flows towards active regions that have been detected by helioseismology. These flows can provide a non-linear saturation mechanism for the global dynamo and contribute to the modulation of the cycle strength.

The first study presented in this thesis is concerned with the effect of the inflows on the evolution of a single bipolar magnetic region (BMR) and its contribution to the global dipole field. The latter depends on the flux contents of the active region and its tilt with respect to the East-West direction. We build a simple surface flux transport model in which small magnetic flux concentrations are passively advected by the differential rotation, random convective flows and the inflows. We find that flux cancellation leads to a quick decrease in the strength of the inflows, which allows for the flux inside the active region to disperse rather than clumping. The contribution of a BMR to the global dipole decreases by a $\sim$ 30% compared to a no-inflows scenario, with little dependence on the BMR's tilt and the latitude of emergence in most cases. When the initial tilt of the BMR is very close to zero, we find that the interplay between the inflows, the differential rotation and the convective flows leads to an increase in the BMR's tilt angle and its contribution to the global dipole field.

In our second study, we investigate the global effect of the inflows on the scale of a solar cycle. By using global surface flux transport simulations, we determine that the strength and extension of the inflows have a large impact on the build-up of the global dipole. Stronger (weaker) inflows lead to a weaker (stronger) axial dipole moment at the end of the cycle. We also find that the reduction in the dipole moment at the end of the cycle caused by the inflows is $\sim$ 9% stronger in stronger activity cycles. This is a non-linear effect which may provide a means to saturating the global dynamo.

In the third study, we formulate a non-axisymmetric version of the Babcock-Leighton dynamo. We then employ this model to infer observation-based latitude-longitude maps of the sub-surface azimuthal flux. We obtain that the non-axisymmetric structure of the sub-surface azimuthal flux system is very weak (about 3% on average). By comparing the inferred maps with the properties of the sunspot groups observed during cycle 23, we find that the probability of emergence, per unit time and surface area, is a function of the ratio between the amount of emerged flux and the amount of flux underlying the emergence site.

1 Introduction

The Sun is a magnetically active star, i.e., it shows a magnetic field that varies with time. One conspicuous manifestation of the solar magnetism is the occurrence of sunspots. These are dark spots that appear on the surface of the Sun as a consecuence of the emergence of strong magnetic fields from beneath the surface. The phenomenon of sunspots is cyclic, with a period of approximately eleven years. At the beginning of each cycle, sunspots appear at a latitude of $\sim 30^\circ$ on both hemispheres. Throughout the cycle, the mean emergence latitude drifts towards the equator, and the rate of appearance of sunspots increases, peaks and declines. The last stages of a magnetic activity cycle normally overlap with the first sunspots of the new cycle.

The Sun's large scale magnetic field is thought to be maintained against Ohmic dissipation by a hydromagnetic dynamo. Since the global field is largely axisymmetric, quantitative models of the solar cycle are traditionally based on azimuthal averages of the magnetic field and the plasma flows. The aim of this thesis is to study the implications of relaxing the axial symmetry assumption for modeling the Sun's global dynamo. The first part of the thesis is dedicated to study the impact of the near-surface, converging flows towards active regions (Gizon et al. 2001) on the large scale solar magnetic field. These flows affect the surface transport of magnetic flux substantially, and may provide a mechanism for limiting the amplitude of the magnetic field generated by the global dynamo (Cameron and Schüssler 2012). In the second part of the thesis, a method for inferring the non-axisymmetric structure and evolution of the sub-surface magnetic flux from observations is provided. The relationship between the so inferred subsurface azimuthal flux and the observed sunspots is then studied.

1.1 Historical overview

The appearance of sunspots on the solar disk was already known to ancient civilizations, well before the telescopic era (e.g. Clark and Stephenson 1978, Wittmann and Xu 1988). By contrast, the magnetic nature of the solar activity was only discovered one century ago. In this section, we present an overview of the key findings that led to the development of hydromagnetic dynamo models of the solar cycle.

1.1.1 The discovery of the sunspot cycle

The periodicity of the sunspot phenomenon was discovered by Schwabe (1844). Aiming to detect the transit of a hypothetical planet inside the orbit of Mercury, he registered daily observations of sunspots over 18 years (1826-1843), which led him to propose the existence of a sunspot cycle having a period of about 10 years. Wolf (1861) compiled past data from multiple observers, which allowed him to reconstruct the sunspot counts back to the middle of the 18th century. To make the comparison of data sets recorded by different observers easier, he introduced the relative sunspot number r, defined as

$$r = k(10g + n), \tag{1.1}$$

where g and n are, respectively, the number of sunspot groups and individual sunspots, and the calibration constant k is specific to each observer (for Wolf, $k = 1$). This definition is still in use today, although r has been renamed to International Sunspot Number.

By the mid-1800s, observers became concerned with the latitudes at which sunspots appeared. Carrington (1858) noticed a sudden jump on the average sunspot latitude immediately after the activity minimum of 1856, from very low latitudes to two distinct belts between 20 and 40° in both hemispheres, with some indication of an equatorward drift of the active zones:

> [T]hroughout the two years preceding the minimum ... the spots were confined to an equatoreal belt ... [but] shortly after that epoch, ... two new belts of disturbance abruptly commenced, the limits of which in both hemispheres may be roughly set at between 20° and 40° ... The tendency at the present time appears to be to contraction of the parallels.

Further observations (Carrington 1863, Spörer 1887) made the discovery of the latitudinal drift of the activity belts unambiguous, and the phenomenon became known as “Spörer’s Law of Zones". The rate of sunspot occurrence and the latitudinal drift of the activity belts can be easily visualized in a butterfly diagram (Fig. 1.1).

1.1.2 The magnetic nature of solar activity

The early observational knowledge on the solar magnetic field can be credited to George Ellery Hale and his team at Mount Wilson Observatory. The first breakthrough came in 1908. Hale (1908b) had observed a helical motion of the gas around sunspots, which led him to postulate the existence of a sunspot magnetic field induced by the circulation of electrically charged particles in the solar atmosphere.[1] By measuring the Zeeman splitting of magnetically sensitive lines in the spectrum of sunspots, he was able to estimate an average sunspot magnetic field of 2600 to 2900 G (Hale 1908a).

Continued observations of sunspot magnetic fields led Hale et al. (1919) to propose the existence of cycle-related laws governing the polarity of the spots (Fig. 1.2):

> The present investigation should ultimately lead to the formulation of a definite law of sun-spot polarities ... We already know that the preceding and following spots of binary groups, with few exceptions, are of opposite polarity, and that the corresponding spots of such groups in the Northern and Southern hemispheres are also opposite in sign. Furthermore, the spots of the present cycle are opposite in polarity to those of the last cycle.

---

[1] Hale’s explanation of the origin of the sunspot magnetic field required a charge separation that is not present in the solar plasma. Additionally, the cyclonic motion observed by Hale is not a common feature of sunspots. It was Biermann (1941) who first proposed that the strong magnetic field suppressed the convective heat transport, resulting in a temperature deficit that made the spots darker than their surroundings.

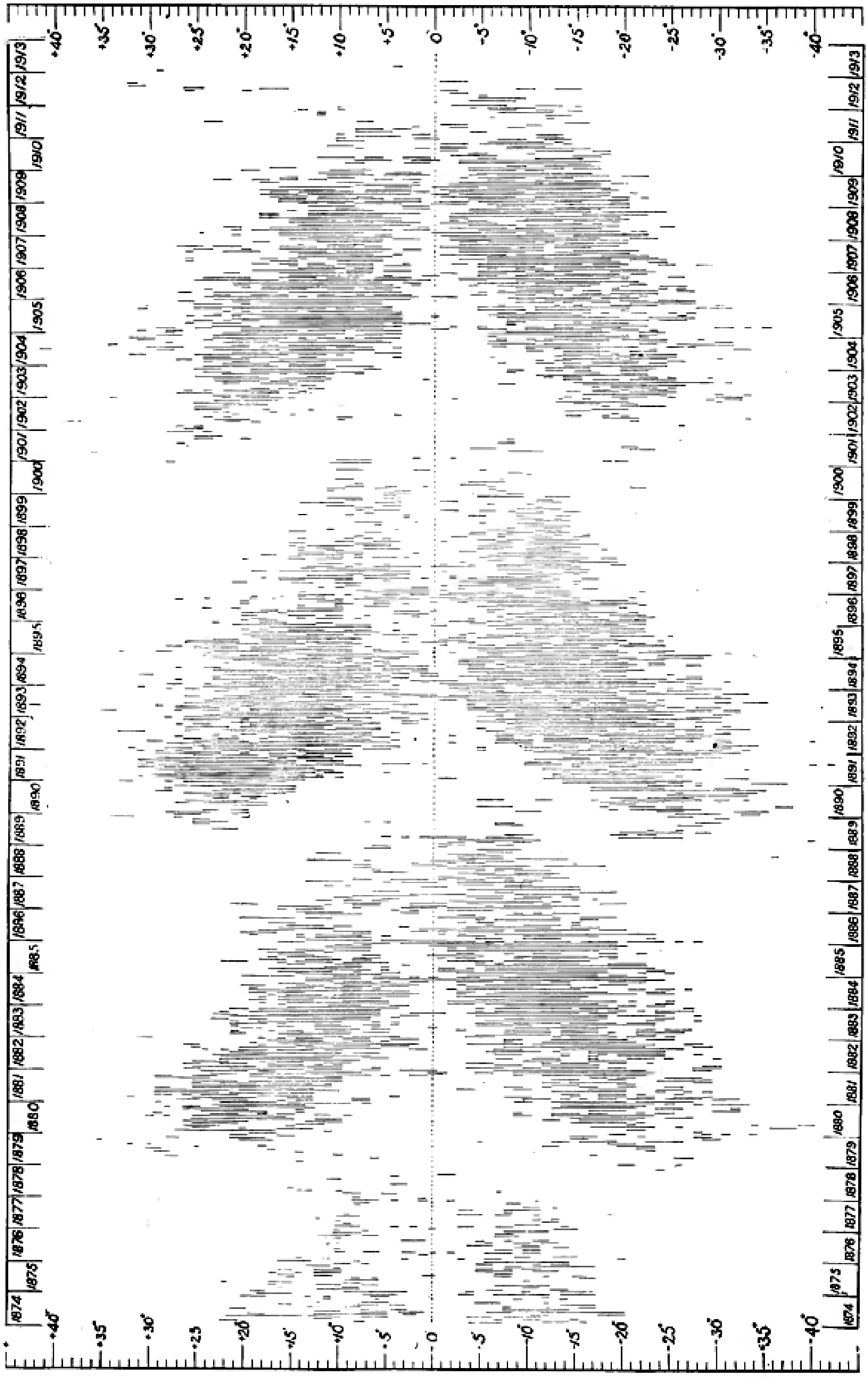

Figure 1.1: Latitude of sunspot emergences versus time for the period 1874–1913. Figure 4 of Maunder (1922).

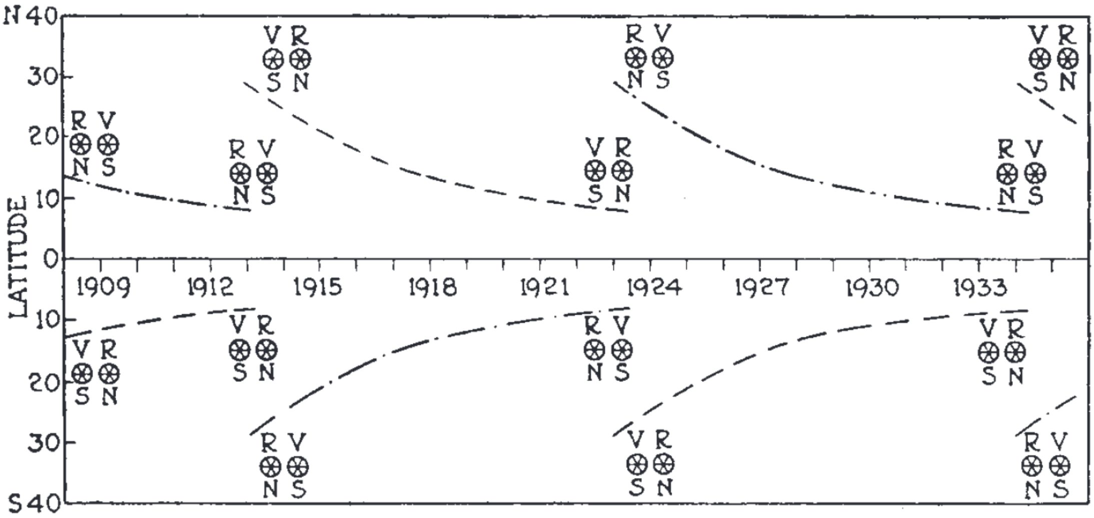

Figure 1.2: Sketch by Hale (1935) illustrating his polarity laws. The curves represent the evolution of the mean emergence latitude over several cycles. The pairs of symbols represent the following (left) and leading (right) polarities of the sunspot groups. Reprinted by permission from Macmillan Publishers Ltd: Nature 136, 703–705, copyright 1935.

In the same work, these authors also reported a systematic tilt of the axis of the bipolar sunspot groups with respect to the East-West direction, now known as Joy's law:

> The following spot of the pair tends to appear farther from the equator than the preceding spot, and the higher the latitude, the greater is the inclination of the axis to the equator.

The observation of a sunspot polarity reversal at the beginning of cycle 16 validated Hale's polarity laws, and established that the complete magnetic cycle had a period of ~ 22 years (Hale and Nicholson 1925)

> Thus, while the $11\frac{1}{2}$-year interval correctly represents the periodic variation in the number or total area of sun-spots, the full sun-spot period, corresponding to the interval between the successive appearances in high latitudes of spots of the same magnetic polarity, is twice as long.

1.1.3 The Sun's global magnetic field

In parallel with their research on the magnetism of sunspots, Hale's team also directed efforts towards detecting the much weaker global dipole field of the Sun. The existence of such a field had been postulated on the basis of the resemblance of the coronal streamers to the force lines of a magnetized sphere (Bigelow 1889). Schuster (1892) had put forward that every large rotating body has a magnetic field. Aiming to test this hypothesis, Hale (1913) confirmed the presence of a general solar magnetic field:

> [I]t is probable that [the measured displacements of spectral lines] represent the Zeeman effect due to the sun's general magnetic field ... [T]he magnetic poles of the sun lie at or near the poles of rotation ... [and] the

> polarity of the sun corresponds with that of the earth ... A first approximate value for the vertical intensity of the sun's general field at the poles is 50 gausses.

The next key clue to understanding the nature of the solar global magnetic field was gathered by Harold D. Babcock and Horace W. Babcock when, in the context of their program of systematic observations of the solar magnetic field, these authors reported, for the first time, a reversal of the global dipole (Babcock and Babcock 1952, 1955, Babcock and Livingston 1958, Babcock 1959):

> The polarity of the high-latitude dipolar magnetic field of the sun was opposite to that of the earth's field from 1953 to 1957. About the middle of 1957, the polarity of the magnetic field near the south heliographic pole was reversed; reversal of the field near the north pole was not observed until November, 1958. At present, the sun's polar field is parallel to that of the earth.

1.1.4 Early models of the solar cycle

The discovery of the Sun's global field prompted the appearance of a number of theories that tried to explain its origin. The earliest ideas suggested that the difference in mobilities of ions and electrons could give rise to some electric charge separation which, owing to the Sun's rotation, would induce a magnetic field. This mechanism was shown to be largely insufficient to explain the observed field (Brunt 1913). Other possibilities invoked self-induced toroidal electric currents, arising from convective motions (Elsasser 1939) or from a circulation of the solar material in meridional planes (Larmor 1919, 1934). These and other hypotheses were considered and proved wrong by Cowling (1933, 1945). One important result of his work, known as Cowling's anti-dynamo theorem, is that a dynamo cannot sustain an axisymmetric magnetic field (Cowling 1933). Cowling's theorem imposes a strong constraint on astrophysical dynamo models, since the observed magnetic fields are often almost axisymmetric on the larger scales.

The development of magnetohydrodynamics was crucial to advancing the understanding of astrophysical dynamos. Alfvén (1942) showed that magnetic field lines are effectively frozen into a perfectly conducting material. Based on this idea, Cowling (1946) proposed that the field of sunspots most likely originated from a pre-existing subsurface toroidal structure:

> We are therefore led to the view that the field is not generated in situ, but that it exists before the spot comes into being ... [One] possibility is that a field exists below the surface, lines of force running as "girdles" round the Sun's axis, and a pair of spots arises when part of this field is convected to the surface.

It was soon realized that such a toroidal field could be generated from the global poloidal field in the presence of non-uniform rotation (Elsasser 1950, Bullard and Gellman 1954, Parker 1955). The main difficulty was then to produce a reversed global dipole

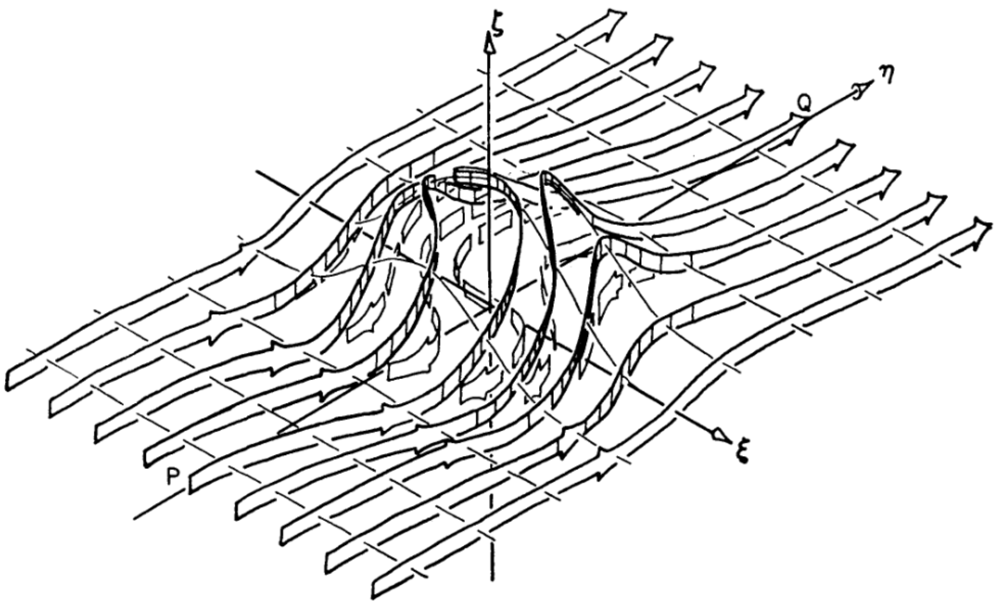

Figure 1.3: Illustration of the generation of a poloidal component from a toroidal magnetic field by a cyclonic motion (α-effect). The thick arrows represent the magnetic field. The greek letters ξ, η, and ζ denote, respectively, the meridional, azimuthal and vertical directions. Figure from Parker (1955), courtesy of E. Parker. ©AAS. Reproduced with permission.

from the subsurface toroidal field, bypassing the limitations imposed by Cowling's theorem. Two different mechanisms were proposed to solve this problem, each of which gave rise to a whole family of models.

The first mechanism was proposed by Parker (1955) (Fig. 1.3). He postulated that cyclonic motions, arising from the effect of the Coriolis force on convective flows, can twist the toroidal field and produce small scale poloidal loops, which then coalesce into a large scale poloidal field:

> [O]ne result of the interaction of cyclonic fluid motions with the toroidal field is to generate loops of flux in meridional planes. In the limit as the number of cyclones becomes large, this produces no fields other than these meridional loops ... [whose] gross result ... is a dipole field ... [which] completes the problem of the generation of poloidal field from toroidal field.

This mechanism for the regeneration of the poloidal field (known as the "α-effect") was later incorporated into the formalism of mean field electrodynamics (Braginskii 1964, Steenbeck et al. 1966, Steenbeck and Krause 1969), giving rise to the turbulent dynamo paradigm.

The second mechanism was proposed by Babcock and Babcock (1955), and integrated in a phenomenological model of the solar cycle in Babcock (1961) (Fig. 1.4). In Babcock's model, the toroidal field is amplified by the Sun's differential rotation until it becomes magnetically buoyant and rises, piercing through the surface and originating

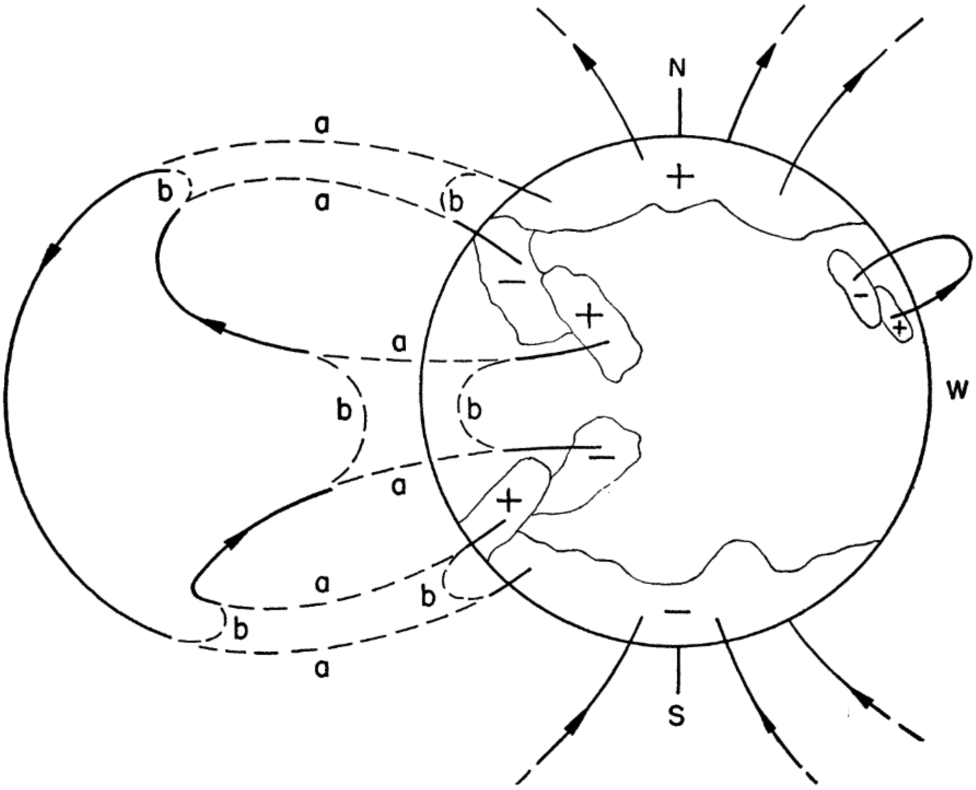

Figure 1.4: Illustration of Babcock's mechanism for the regeneration of the Sun's global poloidal field. Figure from Babcock (1961). ©AAS. Reproduced with permission.

tilted bipolar magnetic regions (BMRs). The surface decay of the BMRs causes the cancellation and reversal of the global poloidal field of the Sun, providing the seed for the amplification of the next cycle's reversed toroidal field:

> We could speculate at this stage that the polar magnetic field is the result of a poleward migration of the *f* portions of disintegrating BMR's in the first few years of each sunspot cycle. If this were true, the main poloidal field should reverse its polarity every $11\frac{1}{2}$ years, but out of phase with the frequency-curve for sunspots. On this theory the residual *p* portions of BMR's should either be neutralized by merging of low-latitude fields of the northern and southern hemispheres, or there should be evidences of a general quadrupolar field.

The apparent migration of the polarities of the BMRs was later explained by Leighton (1964) as result of the random motions caused by the surface convective flows, which he parametrized as a diffusion process. Later, Leighton (1969) put forward a quantitative version of Babcock's model. These three papers provide the basis for the Babcock-Leighton dynamo framework.

1.2 Elements of dynamo theory

1.2.1 The dynamo problem

The evolution of the magnetic field **B** in a conducting fluid is given by the magnetohydrodynamical (MHD) induction equation,

$$\frac{\partial \mathbf{B}}{\partial t} = \nabla \times (\mathbf{u} \times \mathbf{B}) - \nabla \times (\eta \nabla \times \mathbf{B}), \tag{1.2}$$

where **u** is the velocity of the fluid and η is the magnetic diffusivity, defined as

$$\eta = \frac{1}{\mu_0 \sigma} \quad [\mathrm{cm}^2 \mathrm{s}^{-1}]. \tag{1.3}$$

In the above expression, σ is the electrical conductivity of the fluid and μ_0 is the vacuum magnetic permeability.

The first term on the right hand side of Eq. (1.2) describes the induction of magnetic field by the plasma flows, while the second one represents the decay of the magnetic field by means of the ohmic dissipation of the electric currents that support it. The relative importance of the two terms is measured by the magnetic Reynolds number:

$$R_m = \frac{ul}{\eta}, \tag{1.4}$$

where u is a typical value for the flow velocity, and l is a characteristic spatial scale.

The induction term of Eq. (1.2) can act to amplify the magnetic field and oppose its resistive decay. A hydromagnetic dynamo is defined as a set of flows **u** capable of maintaining a magnetic field against resistive decay through inductive action.

The full set of MHD equations is extremely difficult to solve in its most general form. One common simplification of the dynamo problem consists in prescribing the flow field **u**, rather than computing it self-consistently from the MHD equations. The so-called kinematic approximation is justified when the magnetic energy is much smaller than the kinetic energy of the plasma flows. In this regime, Eq. (1.2) becomes linear in **B**.

To examine the temporal behaviour of the solutions of Eq. (1.2) in the kinematic regime, we consider the evolution of the eigenvectors of the linear operator acting on **B** on the right hand side of the equation. Let $\mathbf{B}_\lambda$ be an eigenvector of the operator, and let λ be the corresponding eigenvalue. From Eq. (1.2) we obtain:

$$\frac{\partial \mathbf{B}_\lambda}{\partial t} = \lambda \mathbf{B}_\lambda. \tag{1.5}$$

We allow the eigenvalues to be complex numbers, $\lambda = \lambda_\mathrm{r} + \mathrm{i}\lambda_\mathrm{i}$. Integrating Eq. (1.5) yields

$$\mathbf{B}_\lambda = \mathbf{B}_0 \exp[(\lambda_\mathrm{r} + \mathrm{i}\lambda_\mathrm{i})t]. \tag{1.6}$$

Here, $\mathbf{B}_0$ is an integration constant which can be set by specifying initial conditions. The imaginary part of the eigenvalue is the frequency of the possible oscillatory solutions, while its real part is the growth rate of the magnetic field. Solutions for which $\lambda_\mathrm{r} \geq 0$ correspond to dynamo action. By contrast, solutions with $\lambda_\mathrm{r} < 0$ describe decaying magnetic fields.

1.2.2 Mean field electrodynamics

The development of mean field electrodynamics established a dynamo framework in which turbulent flows play a central role. The main assumption is that the magnetic and velocity fields can be decomposed into a mean part and a fluctuating part:

$$\begin{aligned}\mathbf{B} &= \langle\mathbf{B}\rangle + \mathbf{B}', \\ \mathbf{u} &= \langle\mathbf{u}\rangle + \mathbf{u}'.\end{aligned} \tag{1.7}$$

The averaging operation can be in space, time or over an ensemble, as long as it satisfies the Reynolds rules:

$$\begin{aligned}\langle f+g\rangle &= \langle f\rangle + \langle g\rangle, \\ \langle f\langle g\rangle\rangle &= \langle f\rangle\langle g\rangle, \\ \langle c\rangle &= c,\end{aligned} \tag{1.8}$$

where f and g are functions of position and time and c is a constant. Solar dynamo models mostly consider azimuthal averages.

By substituting Eqs. (1.7) in Eq. (1.2) and averaging we obtain an evolution equation for the mean field:

$$\frac{\partial\langle\mathbf{B}\rangle}{\partial t} = \nabla\times\left(\langle\mathbf{u}\rangle\times\langle\mathbf{B}\rangle + \boldsymbol{\varepsilon} - \eta\nabla\times\langle\mathbf{B}\rangle\right), \tag{1.9}$$

where

$$\boldsymbol{\varepsilon} = \langle\mathbf{u}'\times\mathbf{B}'\rangle \tag{1.10}$$

is the mean electromotive force (emf). Subtracting Eq. (1.9) from Eq. (1.2) yields an evolution equation for the fluctuating part:

$$\frac{\partial\mathbf{B}'}{\partial t} = \nabla\times(\langle\mathbf{u}\rangle\times\mathbf{B}' + \mathbf{u}'\times\langle\mathbf{B}\rangle + \mathbf{G} - \eta\nabla\times\mathbf{B}'), \tag{1.11}$$

where

$$\mathbf{G} = \mathbf{u}'\times\mathbf{B}' + \langle\mathbf{u}'\times\mathbf{B}'\rangle. \tag{1.12}$$

Equation (1.11) establishes a linear relationship between $\langle\mathbf{B}\rangle$ and $\mathbf{B}'$, which implies a linear relationship between $\langle\mathbf{B}\rangle$ and $\boldsymbol{\varepsilon}$. We can therefore expand

$$\varepsilon_i = \alpha_{ij}\langle B\rangle_j + \beta_{ijk}\partial_k\langle B\rangle_j + \cdots \tag{1.13}$$

where summation over repeated indices is implied. The coefficients in Eq. (1.13) will depend on the mean velocity field $\langle\mathbf{u}\rangle$, the statistical properties of the fluctuating velocities $\mathbf{u}'$, and the diffusivity η.

To gain insight on the effect that fluctuating, turbulent motions can have on the mean magnetic field $\langle\mathbf{B}\rangle$ we consider the case of homogeneous, stationary, isotropic turbulence. In that case, the emf can be written as (e.g., Charbonneau 2013)

$$\boldsymbol{\varepsilon} = \alpha\langle\mathbf{B}\rangle + \beta\nabla\times\langle\mathbf{B}\rangle, \tag{1.14}$$

where α and β are scalars. Equation (1.9) then becomes

$$\frac{\partial\langle\mathbf{B}\rangle}{\partial t} = \nabla\times\left(\langle\mathbf{u}\rangle\times\langle\mathbf{B}\rangle + \alpha\langle\mathbf{B}\rangle - \eta_t\nabla\times\langle\mathbf{B}\rangle\right), \tag{1.15}$$

where $\eta_t = \eta + \beta$ is a turbulent diffusivity. In the convection zone of the Sun, $\beta \gg \eta$, which means that turbulence greatly enhances the diffusion rate of the mean field.

The term $\alpha\langle\mathbf{B}\rangle$ acts as a source term for the mean field, and is responsible for the generation of poloidal field out of toroidal field in turbulent dynamo models (the turbulent α-effect). Since this source term describes the effect on the mean field of a fundamentally non-axisymmetric process (the coupling between the magnetic field and turbulent convection in a rotating system) it allows to circumvent the constraint imposed by Cowling's theorem, thus making dynamo action possible.

Parker (1955) showed that an $\alpha\Omega$ dynamo (in which the toroidal field is generated by differential rotation and the poloidal field is generated by the α-effect) supports propagating solutions (dynamo waves). The direction of propagation of such dynamo waves is given by the Parker-Yoshimura rule (Yoshimura 1975):

$$\mathbf{s} = \alpha \nabla\Omega \times \hat{\mathbf{e}}_\phi \tag{1.16}$$

where Ω denotes angular velocity and $\mathbf{e}_\phi$ is a unit vector pointing in the azimuthal direction. In turbulent solar dynamo models, this dynamo waves explain the latitudinal propagation of the latitude of emergence of sunspots over the cycle.

In more general cases, the α_{ij} tensor may also provide an effective velocity term for the mean field. By separating the symmetric and antisymmetric components of the tensor, the emf can be written as

$$\varepsilon_i = \alpha_{ij}^{\text{sym.}} B_j + (\boldsymbol{\gamma} \times \langle\mathbf{B}\rangle)_i + \cdots \tag{1.17}$$

The effective mean-field velocity $\boldsymbol{\gamma}$ arising from the antisymmetric part of the α_{ij} tensor is called turbulent pumping.

1.2.3 Babcock-Leighton dynamos

The distinctive feature of Babcock-Leighton (BL) models is that the generation of poloidal field from toroidal field is achieved through the decay of BMRs on the solar surface (Babcock 1961, Leighton 1964, 1969). At the beginning of an activity cycle, the surface field is strongly dipolar, and is mostly concentrated at the polar caps. This surface configuration reflects the global dipole field, which is the main source of the internal toroidal field generated by the differential rotation (Cameron and Schüssler 2015). Bipolar magnetic regions, which originate from the toroidal field, show a systematic tilt with respect to the East-West direction, the leading polarity (in the direction of rotation) being, on average, closer to the equator than the following polarity (Joy's law). Additionally, the sign of the following polarity is opposite to the polar field at the beginning of the cycle. The surface flows redistribute the magnetic flux of BMRs, which, owing to Joy's and Hale's laws, results in a preferential transport of leading polarity flux across the equator. This leads to a gradual cancellation of the global axial dipole and the build-up of a new, reversed global dipole. After reaching a new activity minimum the process repeats itself, but all the polarities are now reversed with respect to the previous activity cycle. The full magnetic cycle spans approximately 22 years.

In recent years, observational evidence has accumulated in favor of the solar dynamo being of the BL type. Surface flux transport (SFT) models describe the evolution of the surface magnetic flux as a passive transport by the observed surface flows (Leighton 1964, DeVore et al. 1984, Wang et al. 1989b). In particular, SFT models can reproduce the strength of the polar fields at cycle minimum, which is the main source of net toroidal flux in each hemisphere (Cameron and Schüssler 2015). The polar fields are also a good precursor of the strength of the next activity cycle (e.g. Schrijver and Liu 2008, Wang et al. 2009, Cameron et al. 2010, Upton and Hathaway 2014). Dasi-Espuig et al. (2010) found a strong correlation between the cycle-averaged tilt angles observed during cycles 15 through 21 and the strength of the next cycle. Kitchatinov and Olemskoy (2011) found that the aggregate contribution of active regions to the strength of the axial dipole correlates with the strength of the global dipole field at cycle minimum, as inferred by the A-index (Makarov and Tlatov 2000).

The BL mechanism can be incorporated in the mean-field formalism via an α-like term concentrated near the solar surface. Since the mathematical structure of the equations is the same as in the case of the turbulent α-effect, latitudinally-propagating dynamo solutions are in principle allowed. Joy's law determines a positive (negative) α term in the northern (southern) hemisphere. Equatorward propagation of dynamo waves then requires, by Eq. (1.16), that the angular velocity of the plasma increases with depth. Assuming such a negative radial shear, Leighton (1969) obtained equatorward-propagating solutions[2]. However, the shear in the convection zone is manly latitudinal (Christensen-Dalsgaard and Schou 1988). Additionally, a surface poleward meridional flow, not present in Leighton's original model, was detected (Howard 1979). These discoveries led to the introduction of an alternative mechanism to explain the equatorward propagation of activity, namely a subsurface return meridional flow that could advect the toroidal field towards the equator (Wang et al. 1991). Soon, more sophisticated 2D models, solving the axisymmetric dynamo equations in a meridional plane, appeared (Durney 1995, Choudhuri et al. 1995). Dynamo models in which the meridional circulation is important are called flux transport dynamo (FTD) models.

One important parameter in FTD models is the turbulent diffusivity in the convection zone. In low-diffusivity ($\sim 1\,\mathrm{km^2s^{-1}}$), advection dominated models (e.g. Choudhuri et al. 1995, Durney 1995, Dikpati and Charbonneau 1999, Bonanno et al. 2002) the meridional flow transports the poloidal field from the surface to the interior, where it is amplified by the differential rotation. In high-diffusivity ($\sim 100\,\mathrm{km^2s^{-1}}$) models (Jiang et al. 2007, Yeates et al. 2008), the downward transport of poloidal flux is dominated by turbulent diffusion. In both types of model the cycle period is set by the strength of the return flow. However, high-diffusivity models reproduce better some observed features of the solar cycle, such as its dipolar parity (Chatterjee et al. 2004, Hotta and Yokoyama 2010), the symmetry between the two hemispheres (Chatterjee and Choudhuri 2006, Goel and Choudhuri 2009, Norton et al. 2014), and the strength of past cycles (Karak 2010).

The most recent update of the Leighton's 1969 model has been proposed by Cameron and Schüssler (2017). In this work, the authors consider the toroidal flux per unit colatitude as the variable representing the toroidal field in the convection zone. The updated model includes the effect of several important recent results:

---

[2] Leighton (1969) also obtained equatorward-propagating solutions in a model without radial shear. However, this was due to an error in his formulation, leading to unphysical solutions that violated $\nabla \cdot \mathbf{B} = 0$ (Cameron and Schüssler 2017).

- Cameron and Schüssler (2016) inferred an effective diffusivity of the toroidal field in the range 150-450 $\mathrm{km^2 s^{-1}}$ from the properties of the declining phase of the activity cycles.

- The differential rotation in the convection zone is mainly latitudinal and maintains the profile measured at the surface. There is a layer of negative radial shear near the surface (the near-surface shear layer, NSSL, Thompson et al. 1996, Barekat et al. 2014).

- Near-surface downwards turbulent pumping removes the horizontal components of the magnetic field from the NSSL. Additionally, it suppresses the diffusion of the magnetic field through the solar surface. Downwards turbulent pumping has been shown to be required to make FTD models compatible with the evolution of the surface fields (Cameron et al. 2012). It also contributes to obtaining solutions with a periodicity of $\sim$ 11 years in high-diffusivity FTD models, which otherwise yield substantially shorter cycles (Karak and Cameron 2016).

1.2.4 Nonlinear saturation of the dynamo

Dynamo solutions of the induction equation in the kinematic approximation grow exponentially with time. Therefore, at least one nonlinear feedback mechanism is needed to stop the exponential growth when the field becomes sufficiently strong. In the solar dynamo, the magnetic field could in principle backreact on the differential rotation or on the mechanism of regeneration of the poloidal field. The only observed dependence of the rotation rate on the magnetic activity is the torsional oscillations (Howard and Labonte 1980, Zhao and Kosovichev 2004, Gizon 2004). However, these are too weak (a few m/s) to have a significant impact on the generation of toroidal field. Possible nonlinear feedback mechanisms that affect the generation of poloidal field are:

Alpha quenching. In the context of turbulent dynamos, once the energy of the toroidal field becomes comparable to the kinetic energy of the turbulent motions (equipartition) the Lorentz force can suppress the helical turbulent motions that give rise to the α-effect, thus quenching the regeneration of the poloidal field.

Backreaction of the magnetic field on the tilt of rising flux tubes. In the BL framework, a cyclic variation of Joy's law can provide a nonlinear saturation mechanism. Such a cyclic dependence of the tilt angle of active regions has been reported by Dasi-Espuig et al. (2010). In BL models, it is often considered that the toroidal field is stored in a stable overshoot layer below the convection zone in the form of flux tubes. A flux tube can become buoyantly unstable and rise through the convection zone. During its rise the Coriolis force twists the toroidal structure, which emerges with a tilt with respect to the E-W direction. The strength of the toroidal field affects the efficiency of the Coriolis force, thus making the tilt angle dependent on the field strength (e.g. D'Silva and Choudhuri 1993, Fan et al. 1994, Caligari et al. 1995, 1998). A possible way the strength of the flux tubes could depend on the strength of the cycle is through thermal effects in the convection zone. The stratification of the convection zone may be more stable in strong cycles, resulting in flux tubes becoming unstable at higher field strengths (Işık 2015).

Inflows towards active regions. Large-scale, near-surface converging flows around active regions were first reported by Gizon et al. (2001), and have been systematically observed since then (Zhao and Kosovichev 2004, Gizon 2004, Gizon and Rempel 2008, Švanda et al. 2008, González Hernández et al. 2010).

The inflows are possibly due to enhanced radiative surface cooling, caused by bright magnetic elements in active regions (Spruit 2003). Pressure balance leads to a reduced opacity inside the magnetic elements, which enhances radiative heat loss near the surface (Spruit 1977). The colder gas is transported downwards by the convective downflows at the intergranular lanes, leading to a temperature decrease beneath the active region. This causes the pressure deficit in active regions that drives the converging flows.

The inflows were proposed as a possible nonlinear saturation mechanism for a Babcock-Leighton dynamo by Cameron and Schüssler (2012). The converging flows limit the latitudinal separation of the following and leading polarities of emerged BMRs (Jiang et al. 2010). In strong cycles, the collective action of the inflows towards the activity belts causes a greater reduction in the latitudinal separation of the polarities of individual BMRs, which leads to a weaker global dipole at the end of the cycle. A second effect is the enhancement of the cross-equatorial transport of preceding polarity flux by inflows driven by low-latitude BMRs, which leads to a stronger global dipole at the end of the cycle. This effect is more pronounced in weak cycles, where the emergence rate peaks at lower latitudes than in strong cycles (Waldmeier effect). In strong cycles, the activity peaks further away from the equator, and the first effect dominates.

1.3 Motivation and thesis outline

Ideally, the solar dynamo problem should be tackled through 3D, convective MHD simulations. Considerable effort has been and continues to be made in this direction (e.g. Ghizaru et al. 2010, Käpylä et al. 2012, Nelson et al. 2013, 2014, Augustson et al. 2015, Duarte et al. 2016, Hotta et al. 2016, Käpylä et al. 2016). However, the parameter regime accesible by today's computational capabilities is still very far from resolving the huge range of spatial and temporal scales involved in the problem. For this reason, highly parametrized models of the solar dynamo, such as the kinematic mean field models discussed in the above sections, remain useful to describe the evolution of the large scale magnetic field and make contact with observations. These models are commonly based on longitudinal averages of the magnetic field, and consider purely axisymmetric flows. The main aim of the present thesis is to consider the effects of the departures from the axial symmetry assumption on modeling the evolution of the global solar magnetic field.

This thesis is composed of three papers. In the first two papers we study the way inflows towards active regions affect the surface transport of magnetic flux, and their possible impact on the generation of global poloidal field. In **Paper I** (Ch. 2) we consider the evolution of a single, isolated active region. An unsolved problem is how active regions decay in the presence of strong converging flows (De Rosa and Schrijver 2006). We show that the dispersal of surface flux due to random convective motions is enough to explain the decay of a BMR. Next, we carry out a parameter study to ascertain the way inflows impact the contribution of an isolated BMR, emerging at different latitudes and with different tilt angles, to the global dipole field. We also include a discussion on the validity of the diffusion approximation to describe the surface decay of active regions. In **Paper II** (Ch. 3) we include the inflows in global surface flux transport simulations spanning several cycles. By means of a parameter study, we evaluate the way inflows with different strengths and extensions influence the build-up of the global dipole. Finally, we show that the inflows enhance the efficiency of the BL mechanism in weak cycles. This result further supports the inflows as a non-linear feedback mechanism capable of saturating the global solar dynamo.

In **Paper III** (Ch. 4) we study the non-axisymmetric structure of the toroidal field that may arise from the (non-axisymmetric) emergence process. We extend the updated Leighton model of Cameron and Schüssler (2017) to the non-axisymmetric case. We then use synoptic magnetograms to build the poloidal source term. This allows us to produce observation-based maps of the sub-surface toroidal flux system. We find that the structure of the toroidal flux is largely axisymmetric. The maps of toroidal flux are then compared to the observed properties of active regions, as given by the USAF/NOAA sunspot record. Our main finding is that the probability of sunspot emergence is a function of the ratio between the flux contents of the active region and the amount of toroidal flux lying directly beneath the emergence site.

In Ch. 5 we provide a brief discussion and an outlook on the future work.

2 Paper I. Surface Flux Transport Simulations: Effect of Inflows Toward Active Regions and Random Velocities on the Sun's Large Scale Magnetic Field

Abstract

Aims We aim to determine the effect of converging flows on the evolution of a bipolar magnetic region (BMR), and to investigate the role of these inflows in the generation of poloidal flux. We also discuss whether the flux dispersal due to turbulent flows can be described as a diffusion process.

Methods We developed a simple surface flux transport model based on point-like magnetic concentrations. We tracked the tilt angle, the magnetic flux and the axial dipole moment of a BMR in simulations with and without inflows and compared the results. To test the diffusion approximation, simulations of random walk dispersal of magnetic features were compared against the predictions of the diffusion treatment.

Results We confirm the validity of the diffusion approximation to describe flux dispersal on large scales. We find that the inflows enhance flux cancellation, but at the same time affect the latitudinal separation of the polarities of the bipolar region. In most cases the latitudinal separation is limited by the inflows, resulting in a reduction of the axial dipole moment of the BMR. However, when the initial tilt angle of the BMR is small, the inflows produce an increase in latitudinal separation that leads to an increase in the axial dipole moment in spite of the enhanced flux destruction. This can give rise to a tilt of the BMR even when the BMR was originally aligned parallel to the equator. [1]

---

[1] This chapter reproduces the article *Surface flux transport simulations: Effect of inflows toward active regions and random velocities on the evolution of the Sun's large-scale magnetic field* by D. Martin-Belda and R. H. Cameron, published in Astronomy & Astrophysics 586, A73 (2016), DOI 10.1051/0004-6361/201527213. Reproduced with permission of Astronomy & Astrophysics, © ESO. Contributions: D.M.B and R.C. designed the research. D.M.B carried out the research, analyzed the data and wrote the paper.

2.1 Introduction

Surface flux transport (SFT) simulations have been used with considerable success to describe the evolution of the large-scale photospheric magnetic field (see, e.g. DeVore et al. 1984, Wang et al. 1989a, Mackay et al. 2002b,a, Baumann et al. 2004). These models are based on the asumption that the field at the surface is nearly radial (Solanki 1993, Martínez Pillet et al. 1997), and thus its evolution can be described by the radial component of the MHD induction equation. The scalar quantity B_r is advected by the large-scale flows (differential rotation and meridional flow) and the variable patterns of convection. The latter have the effect of dispersing the magnetic field, and have commonly been modeled as a Fickian diffusion process (Leighton 1964), although some authors prefer a less parametrized treatment of the turbulent dispersal. In Schrijver (2001), an SFT model based on discrete flux concentrations is used to simulate the evolution of the surface field. Hathaway (2010) uses an observation-based, time-evolving spectrum of spherical harmonics to produce random patterns of turbulent flows that advect magnetic concentrations. This approach recovers some of the observed characteristics of the evolution of the photospheric field, such as the accumulation of flux in the network and the dispersal on multiple scales. One of the questions we want to address in this work is whether the effects of the turbulent dispersal on the large-scale, long-term evolution of the surface field are appropriately captured by the diffusion approximation.

A second question concerns the systematic tilt of emerged bipolar magnetic regions (BMRs), which plays a central role in the Babcock-Leighton dynamo mechanism. The leading polarity of a BMR tends to emerge at lower latitudes than the trailing polarity (Joy's law), and the latter is opposite to the polarity of the polar field at the preceding activity minimum (Hale's law). The tilt angle is thought to be caused by the action of the Coriolis force on rising flux ropes (see, e.g., Fan 2009), and provides a mechanism for generating poloidal field from toroidal field (Charbonneau 2010). The latitudinal separation of the polarity patches favors the cross-equatorial transport of leading polarity, which leads to the cancellation and eventual reversal of the polar fields. The nearly dipolar field at the end of an activity cycle represents the poloidal flux from which the toroidal flux of the next cycle is generated (Cameron and Schüssler 2015). Thus, a backreaction mechanism that affects the latitudinal separation of the polarities would limit the strength of the polar fields and explain the observed cycle variability. Cameron and Schüssler (2012) propose the converging flows toward active regions as a major candidate for this nonlinear cycle modulation. These near-surface, large-scale flows toward sunspot groups and active regions were first observed by Gizon et al. (2001). These flows have magnitudes of $\sim 50\,\mathrm{m/s}$ and can extend up to heliocentric angles of 30° around the active region center (see, e.g., Haber et al. 2002, Gizon and Rempel 2008, González Hernández et al. 2010, Gizon et al. 2010). De Rosa and Schrijver (2006) incorporated such inflows in their SFT model (see Schrijver 2001) to study their effect on the evolution of an active region. In their model they explicitly imposed a reduced diffusivity in regions of strong magnetic field in addition to the inflows. They found that, even for comparatively weak inflows, the inflows cause the magnetic concentrations to clump together and generate patterns that are inconsistent with observations. Jiang et al. (2010) included a magnetic-field-dependent, axisymmetric latitudinal perturbation of the meridional flow compatible with the inflows in SFT simulations and found that this reduced the latitudinal separation of the polari-

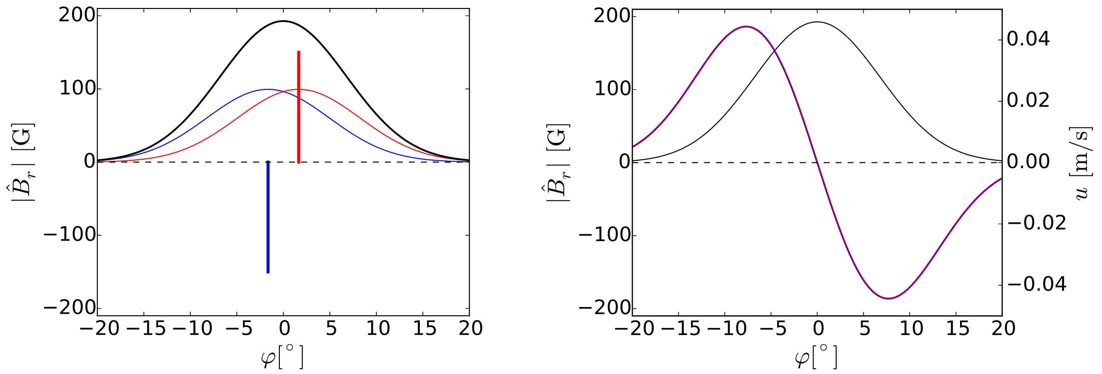

(a)

(b)

Figure 2.1: *Left:* Two concentrations of flux of different polarity (thick, vertical lines), smoothed absolute value of the magnetic field of the separate concentrations (red and blue Gaussian curves), and smoothed absolute value of the total magnetic field. *Right:* Smoothed absolute value of the total magnetic field (black line) and inflow velocity profile resulting from Equation (2.3) (purple line). We have assumed a flux of 4×10^{18} Mx for the single concentrations.

ties of the emerged BMRs, thus limiting the buildup of magnetic field at the polar caps. Cameron and Schüssler (2012) argue that this effect dominates in strong cycles, while in weak cycles the perturbation of the meridional flow enhances cross-equatorial flux transport and accelerates the reversal of the polar fields. The second question we investigate in this paper is the way inflows affect the evolution of a decaying BMR and their impact on the amount of poloidal flux generated.

2.2 Surface flux transport model

In our model, a magnetically active region is composed of a number N of point-like flux concentrations representing the radial photospheric magnetic field. We approximate the local solar surface as a plane domain centered at a latitude λ_0 and an arbitrary longitude that we take as 0. The flux concentrations are subject to advection by differential rotation and convective flows, the latter of which we model as a two-dimensional random walk. If two concentrations of opposite polarity approach each other within a distance of 1 Mm, the pair cancels and we remove them from the simulation. We assume the differential rotation profile determined by Snodgrass (1983):

$$\omega(\lambda) = 13.38 - 2.30 \sin^2 \lambda - 1.62 \sin^4 \lambda \ [^\circ/\text{day}]. \tag{2.1}$$

In this reference frame a solid body rotation translates into a uniform velocity field.

In one of the experiments described later, we include a meridional flow. The exact form of this flow is not critical, since we are performing a local study. We use the form from previous studies such as van Ballegooijen et al. (1998) or Baumann et al. (2004):

$$v_\lambda(\lambda) = v_m \sin(2.4\lambda), \tag{2.2}$$

where $v_m = 11\text{m/s}$.

De Rosa and Schrijver (2006) parametrize the inflows toward active regions in the following way:

$$\mathbf{u}_{\text{in}} = a\nabla|\hat{B}_r|^b, \tag{2.3}$$

where $|\hat{B}_r|$ is the absolute value of the magnetic flux density, smoothed with a Gaussian having a full width at half maximum of 15°. In Fig. 2.1 we sketch the inflow profile resulting from Equation (2.3) in the case of two close flux concentrations of opposite polarity placed at the same latitude. Figure 2.1a shows the smoothed absolute value of the magnetic fields of the two concentrations and the total smoothed unsigned magnetic field. Figure 2.1b shows the inflow velocity profile, proportional to the gradient of the smoothed absolute value of the magnetic field. In our simulations we use a FWHM of 15.5°, and set $b = 1$. In this case, we can equivalently calculate the inflow velocity field as the sum of the inflows driven by the single concentrations:

$$\mathbf{u}_{\text{in}}(\varphi, \lambda) = \sum_{i=1}^{N} \mathbf{u}_{\text{single}}(\varphi - \varphi_i, \lambda - \lambda_i), \tag{2.4}$$

where $\mathbf{u}_{\text{single}}(\varphi, \lambda)$ is the single-concentration inflow profile and (φ_i, λ_i) is the position of the $i-$th concentration. The parameter a is chosen such that the initial aggregate inflow velocity averaged over the 10% of the domain area with highest inflow velocities amounts to ~50m/s. We stress that we are not considering that the driving of such an extended inflow by a single concentration is a physical process that actually occurs on the Sun. Our aim is to reproduce a field of converging flows toward the BMR that is somewhat similar to what is observed.

2.3 Recovering the diffusion limit

2.3.1 Preliminary discussion

When describing the dispersive effect of convective flows on the magnetic concentrations as the Fickian diffusion of a continuous quantity (here the radial magnetic field), at least two assumptions are made. The first one is that each of the magnetic field concentrations performs an independent random walk, uncorrelated with the motion of all the other concentrations. The second one is that the random walk steps are small compared to the scale of interest. We now examine these assumptions.

We consider a specific pattern of convective cells (a *realization*): The magnetic field elements are advected toward the border of the cells, adopting a network-like arrangement. In a different realization, a given magnetic element travels a different distance, in a different direction, and takes a different time to reach the border of the cell. Repeating this experiment over a large number of realizations, the statistically expected distribution of magnetic elements at a certain time can be inferred. Similarly fragmentation and merging of flux concentrations strongly affect the correlations in particular realizations, but do not affect the averaged distribution. When the length of the random walk steps is small compared to the scale of interest, the evolution of the expectation value of the flux distribution is approximated well by the diffusion of a continuous flux density. In the following sections we employ our SFT model to investigate whether random steps of the size of the convective cells can be considered small enough to describe the dispersal of magnetic flux on intermediate and large scales as a diffusion process.

2.3.2 Methods

In the limit of small random walk steps, the evolution of the expectation value of the magnetic flux distribution can be described as the diffusion of a continuous quantity representing the radial field with a diffusion coefficient η given by

$$\eta = \frac{1}{4}\frac{(\Delta l)^2}{\Delta t} \tag{2.5}$$

(Leighton 1964). In what follows we consider the number density of concentrations. Solving the diffusion equation shows that an initial Gaussian density distribution $\rho(r, t_0)$ remains Gaussian at all times, and its standard deviation is given by

$$\sigma(t) = \sqrt{2\eta t + \sigma_0^2}, \tag{2.6}$$

where σ_0 is the standard deviation at $t = 0$.

In our experiment, we set up a patch of $N = 8000$ concentrations randomly placed about the center of the domain according to a Gaussian density distribution with an initial standard deviation of $\sigma_0 = 20\,\mathrm{Mm}$. The concentrations undergo random walks for 35 days. The experiment was carried out for two different random walk step sizes ($\Delta l = 500\,\mathrm{km}$ and $\Delta l = 20\,\mathrm{Mm}$), corresponding to small, short-lived granules and large, long-lived supergranules. To compare with the diffusion approximation, we consider random walks corresponding to a fixed diffusion coefficient of $\eta = 250\,\mathrm{km}^2/\mathrm{s}$. This value is similar to the $\sim 257\,\mathrm{km}^2/\mathrm{s}$ value reported by Jafarzadeh et al. (2014) from observations. It is also in the range of diffusivities found in radiative MHD simulations by Cameron et al. (2011), and compatible with the evolution of the large-scale fields (Cameron et al. 2010). The time interval between random walk steps is different for granules and supergranules and corresponds to different lifetimes. Equation 2.5 gives a lifetime of $\Delta t = 250\,\mathrm{s} \sim 4\,\mathrm{min}$ for the granule and $\Delta t = 4 \cdot 10^5\,\mathrm{s} \sim 4.5$ days for the supergranule.

We now consider an annulus centered on the origin of coordinates of the domain. The mean flux density $\bar{\rho}_a$ in the annulus is calculated as the number of concentrations enclosed within it divided by its surface area. If the annulus is sufficiently narrow, its mean density can be directly compared with the diffusion prediction $\rho(\bar{r}, t)$, where $\bar{r}$ is an arbitrary point within the annulus. If the random walk steps are short enough, the two quantities should be similar, provided that there are enough realizations or, equivalently, the number of random walkers is very large. To better approach this limit, we average over 1000 realizations of the experiment.

2.3.3 Results

Figure 2.2 shows the solution of the diffusion equation and the averaged number of flux concentrations per unit area at times $t = 0$, $t = 11.5$ days, and $t = 34.6$ days. The agreement is very good, and the point concentrations continue matching a Gaussian distribution

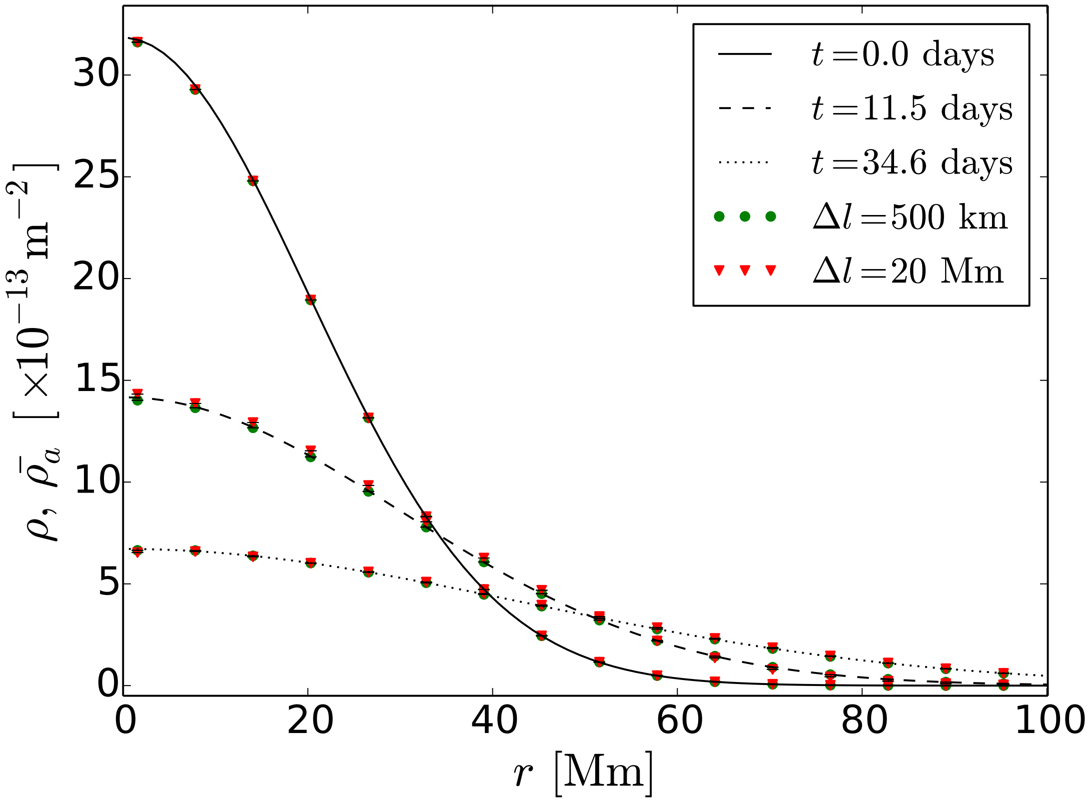

Figure 2.2: Comparison between the density distribution resulting from the diffusion equation (line plots) and the averaged number of concentrations per unit area in the simulations. The annuli used to count the concentrations are 2.5 Mm wide. Only one third of the points have been plotted for better visualization.

over time. Fitting the data points from the simulations to Gaussian curves, we can compare the spread of the distributions with the diffusion prediction (2.6). In Fig. 2.3 the standard deviation of the distributions is plotted as a function of time. We see that in the $\Delta l = 500\,\mathrm{km}$ case, the spread matches the diffusion approximation fairly well, whereas in the $\Delta l = 20\,\mathrm{Mm}$ case it is slightly lower than expected from a diffusion process. This is because at this scale the random walk step cannot be considered small with respect to the characteristic scale of the BMR. We also note that the larger discrepancy occurs over the first days of evolution (when the size of the patch is closer to the size of the random walk steps), while we normally are interested in substantially longer evolution times when using SFT models. Moreover, the random walk does not seem to diverge from the diffusion solution. Therefore, we conclude that the diffusion approximation can be safely used when studying the mid- and long-term evolution of magnetic field distributions on the length scales of a typical active region (tens of megameters) or larger, and it is the appropriate treatment when we are interested in, e.g., the evolution of the polar field.

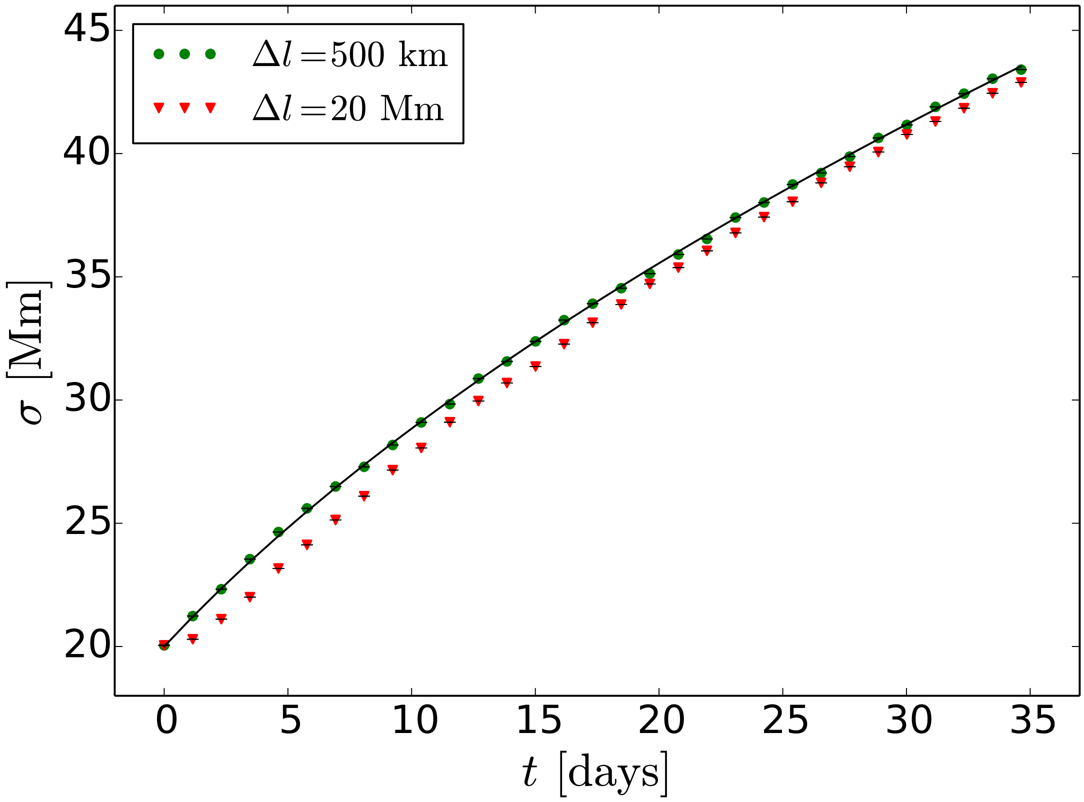

Figure 2.3: Full width at half maximum of the averaged distribution of concentrations as a function of time (symbols) compared to the spread of the equivalent diffusion process (continuous line).

2.4 Evolution of a bipolar magnetic region

2.4.1 Setup

We now consider the effects of the inflows on an isolated BMR. Figure 2.4 shows the initial configuration of our model of BMR for one of the experiments we carried out. The flux concentrations are evenly distributed in two circular regions of opposite polarities, each of which has a radius of 10 Mm and contains 1250 concentrations. The BMR is placed at latitude λ_0 with an initial tilt angle α_0. To study the evolution of the BMR, we track the changes of the longitudinal and latitudinal separations of the centers of gravity of the two polarity patches, as well as the tilt angle, the total unsigned flux, and the axial dipole moment. We ran 500 realizations of each experiment in order to reduce statistical noise. The tilt angle is calculated as the angle between the negative half of the φ-axis and the line connecting the two centers of gravity (the *dipole axis*); i.e.,

$$\alpha = \arctan\left(\frac{\bar{\lambda}^+ - \bar{\lambda}^-}{\bar{\varphi}^- - \bar{\varphi}^+}\right), \tag{2.7}$$

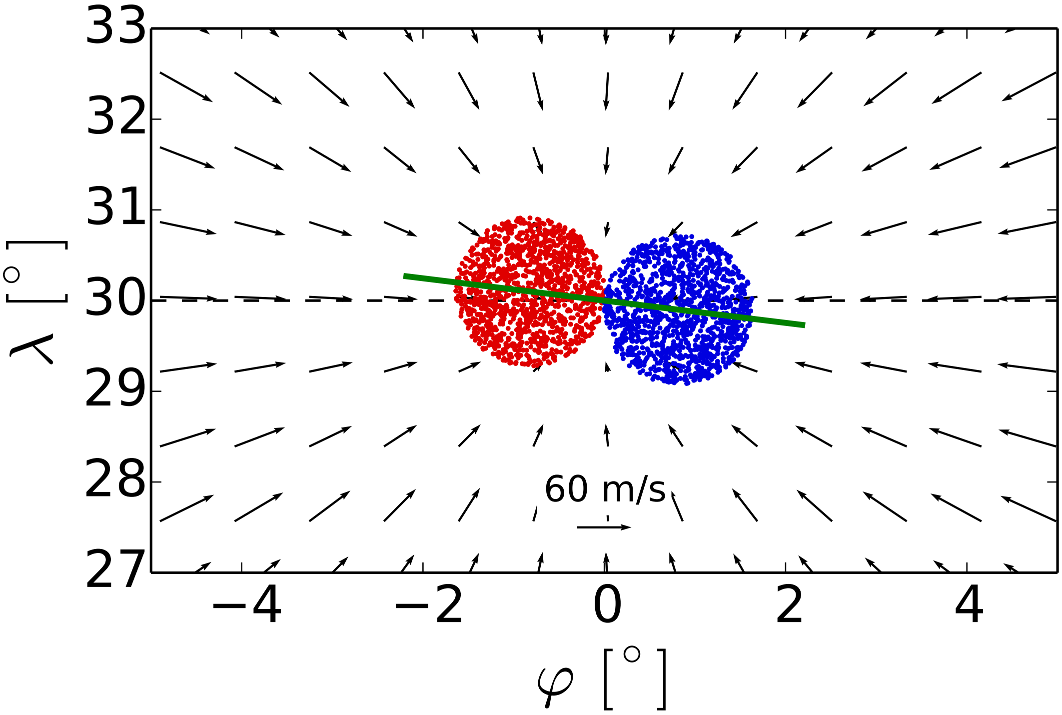

Figure 2.4: Initial distribution of magnetic flux concentrations in one of the realizations of the experiment with $\alpha_0 = 7°$ and $\lambda_0 = 30°$. The red and blue colors represent opposite polarities. The gray dashed line indicates the latitude of emergence. The solid green line indicates an angle of 7° with respect to the longitudinal direction and approximately bisects the BMR. The quiver plot represents the inflows.

where

$$\bar{\varphi}^{\pm} = \frac{1}{N^{\pm}} \sum_{i=1}^{N^{\pm}} \varphi_i^{\pm}; \quad \bar{\lambda}^{\pm} = \frac{1}{N^{\pm}} \sum_{i=1}^{N^{\pm}} \lambda_i^{\pm}. \tag{2.8}$$

Here, $\varphi_i^{\pm}$ and $\lambda_i^{\pm}$ are the coordinates of the i-th concentration of the polarity indicated by the superscript, and $N^{\pm}$ the total number of concentrations of each polarity.

The contribution of the bipolar region to the cancellation and build up of the polar fields depends on its total flux and the latitudinal separation of the polarity patches. To estimate this contribution we calculate the BMR's axial dipole moment, defined as

$$B_p = \int_0^{2\pi} \int_0^{\pi} B_r(\varphi, \theta) Y_1^0 \sin\theta \, \mathrm{d}\theta \mathrm{d}\varphi, \tag{2.9}$$

where θ is the colatitude, $\theta = \pi/2 - \lambda$. In our discrete representation and in terms of the latitude λ, the integral becomes

$$B_p = \frac{\phi_0}{R_\odot^2} \sqrt{\frac{3}{4\pi}} \sum_{i=1}^{N} p_i \sin(\lambda_i) \tag{2.10}$$

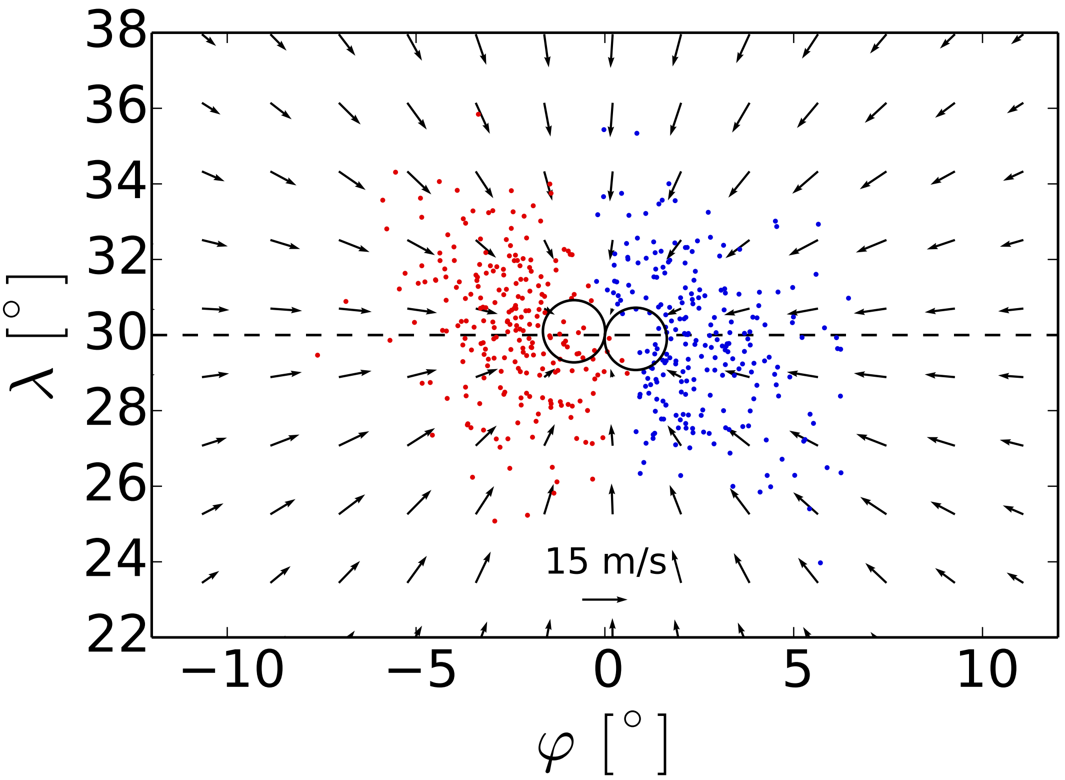

Figure 2.5: Positions and polarities of the magnetic flux concentrations shown in Fig. 2.4 after evolving for 17 days with inflows turned on. The two circles outline the initial configuration of the BMR as shown in Fig. 2.4. From the initial 2500 concentrations, only 480 remain.

where ϕ_0 is the flux of one concentration, and p_i the polarity (± 1) of the i−th concentration. Considering typical values for BMRs with moderate-to-strong magnetic fields, we assume a total unsigned flux of $\Phi_0 = 10^{22}$ Mx (see, e.g., Schrijver and Zwaan 2008), which gives a single concentration magnetic flux or $\phi_0 = 4 \cdot 10^{18}$ Mx. Under diffusion alone, the Sun's axial dipole moment would decay on a time scale $\tau_d = \frac{R_\odot^2}{\eta}$ (Leighton 1964). For a diffusion coefficient $\eta = 250\,\mathrm{km}^2/\mathrm{s}$, $\tau_d \sim 30$ years. In our plane domain approximation, the solar radius is infinite, so τ_d is infinite as well. Since Y_1^0 does not depend upon longitude, the axial dipole moment is expected to be conserved in the simulations where only differential rotation and random walks are included. In a more realistic spherical geometry, the axial dipole would decline on a time scale that is large compared to the length (35 days) of our simulations.

2.4.2 Results

Flux dispersal

The question we want to answer is how the inflows affect the dispersal of the magnetic field. In Fig. 2.5 we see the distribution of the magnetic concentrations starting from that shown in Fig. 2.4 after evolving for 17 days under the influence of differential rotation, random walk, and inflows. The BMR has been sheared by the differential rotation, while the random walk has dispersed the flux concentrations. At $t = 17$ days and in spite of the inflows, the BMR spans close to 10° in the longitudinal direction and around 8° in the latitudinal direction. The total flux decreases very rapidly owing to cancellation (see Fig. 2.7), especially in the first days, and the inflow velocity decays accordingly.

To compare the dispersive effect of the convective flows against the inflows, we begin by considering the two separately. At time t, a concentration undergoing a random walk alone is separated from its initial position by an average distance given by the diffusion length, $l_d(t) = 2\sqrt{\eta t}$. We define a mean expansion velocity $\bar{u}_d(t) = l_d(t)/t = 2\sqrt{\eta/t}$. The space- and time- averaged inflow velocity along such a path over a time t is given by

$$\bar{u}_{in}(t) = \frac{1}{t\,l_d(t)} \int_{l_0}^{l_0+l_d(t)} \int_0^t \mathbf{u}_{\mathrm{in}}[\varphi(l'), \lambda(l'), t'] \cdot \mathrm{d}\mathbf{l}'\mathrm{d}t', \tag{2.11}$$

where l' denotes the distance from the starting position l_0. To evaluate this integral, we take the inflow velocity $\mathbf{u}_{\mathrm{in}}[\varphi(l), \lambda(l), t]$ from one realization of the experiment. We choose the path l_d along the φ axis for simplicity and perform the calculation for $l_0 = 0$, 10 Mm, and 20 Mm from the origin. Both $\bar{u}_d(t)$ and $\bar{u}_{in}(t)$ are plotted in Fig. 2.6.

The mean expansion velocity decays as $t^{-1/2}$, but it remains higher than the mean inflow velocity at all times and for different values of l_0, most prominently during the first days. The differential rotation also contributes to the escape of magnetic flux. The shear flow velocity at $\lambda = 32\,°$ is ~14m/s, and it reaches ~30 m/s at $\lambda = 34°$. It is seen that the turbulent dispersal and the differential rotation dominate the (decaying) inflows. We therefore do not observe the clumping reported by De Rosa and Schrijver (2006). A possible cause for this discrepancy is the explicit additional damping of dispersal of large magnetic field concentrations that these authors include in their model (see Schrijver 2001) and we do not. This feature seeks to reproduce the reduced flux dispersal observed in areas of large magnetic field. (In Schrijver and Martin 1990, the authors report a flux dispersal characterized by a diffusion coefficient of ~250 km^2/s in areas surrounding the core of an active region, while within the core region the diffusion coefficient is ~110 km^2/s).

We point out here that the inflows alone will have the effect of reducing the apparent diffusivity in active regions. We can estimate this effect by considering the velocities involved. Assuming a random walk step of 15 Mm and a diffusion coefficient of 250 km^2/s, equation (2.5) gives a travel time of ~2.6 days. The concentrations travel with a velocity of ~67 m/s. A random walk with this travel time and characterized by a diffusion coefficient of 110 km^2/s has a step size of ~10 Mm and a travel velocity of ~44 m/s. The difference between travel velocities in the two cases is ~ 23 m/s, a value comparable with the averaged magnitude of the inflows.

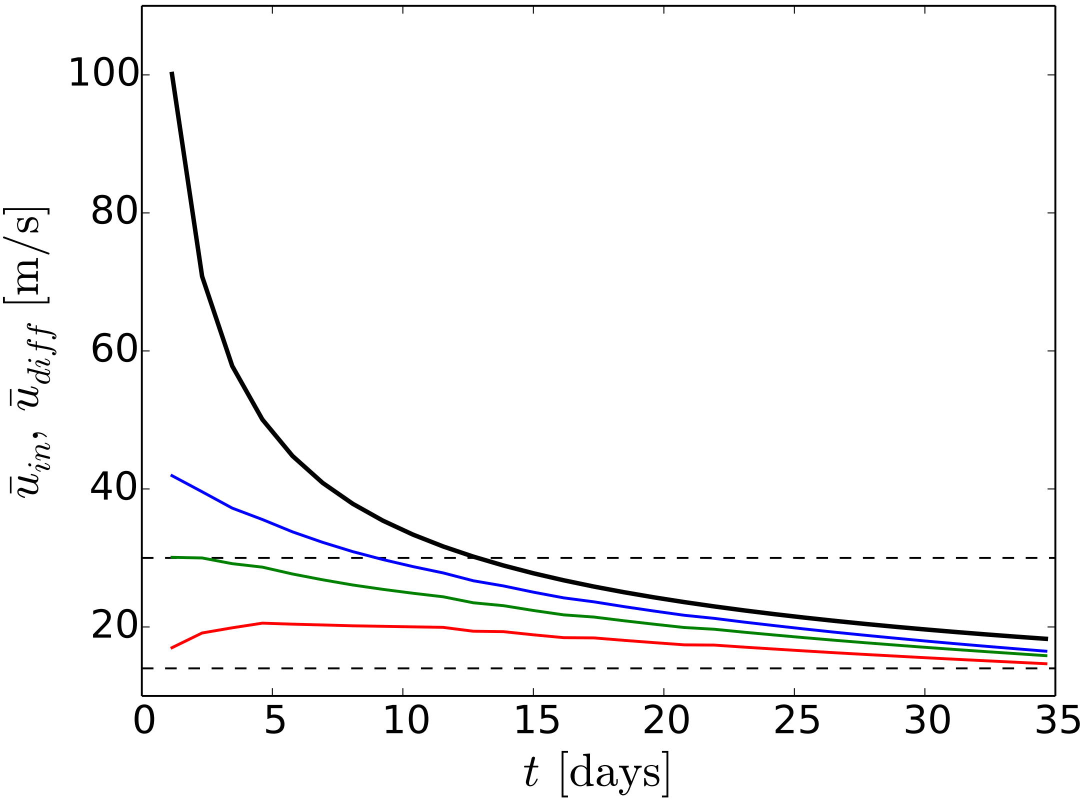

Figure 2.6: *Thick black line:* $\bar{u}_d(t)$ for the case under discussion ($\alpha_0 = 7°$, $\lambda_0 = 30°$). *Colored lines:* $\bar{u}_{in}(t)$ for 0 (red), 10 (green) and 20 Mm from the origin. *Dashed lines:* Shear flow velocities at ~ 12° (lower) and ~ 14° polewards from the central latitude.

Dependence upon initial tilt

Figure 2.8 shows the tilt angle of the BMR and the axial dipole moment as given by equation (2.10) for the case of a bipolar region placed at $\lambda_0 = 30°$ and initial tilt angles of $\alpha_0 = 0°$ (Fig. 2.8a), $\alpha_0 = 7°$ (Fig. 2.8b), and $\alpha_0 = -7°$ (Fig. 2.8c). We start by discussing the $\alpha_0 = 7°$ case. The longitudinal separation is initially greater than the separation in latitude, and the shear flow causes it to increase faster than the latter. This causes the dipole axis to rotate counter-clockwise, i.e., to decrease in tilt angle. When inflows are switched on, the growth of the longitudinal and latitudinal separations is restricted in such a way that the rotation of the dipole axis is slower, and flux cancellation is enhanced (see Fig. 2.7). The latter is expected since the converging flows tend to bring concentrations closer together, increasing the probability of pair cancellation.

As expected, the axial dipole moment remains constant when inflows are not present. When inflows are present B_p decays until reaching an approximately constant value after ~20-30 days, when the both the inflows-on and inflows-off plots essentially become parallel. At this point the inflows are so weak that the subsequent evolution of the BMR is dominated by the differential rotation and the random walk. It should be noted that inflows restrict the growth of the latitudinal separation of polarities over time rather than

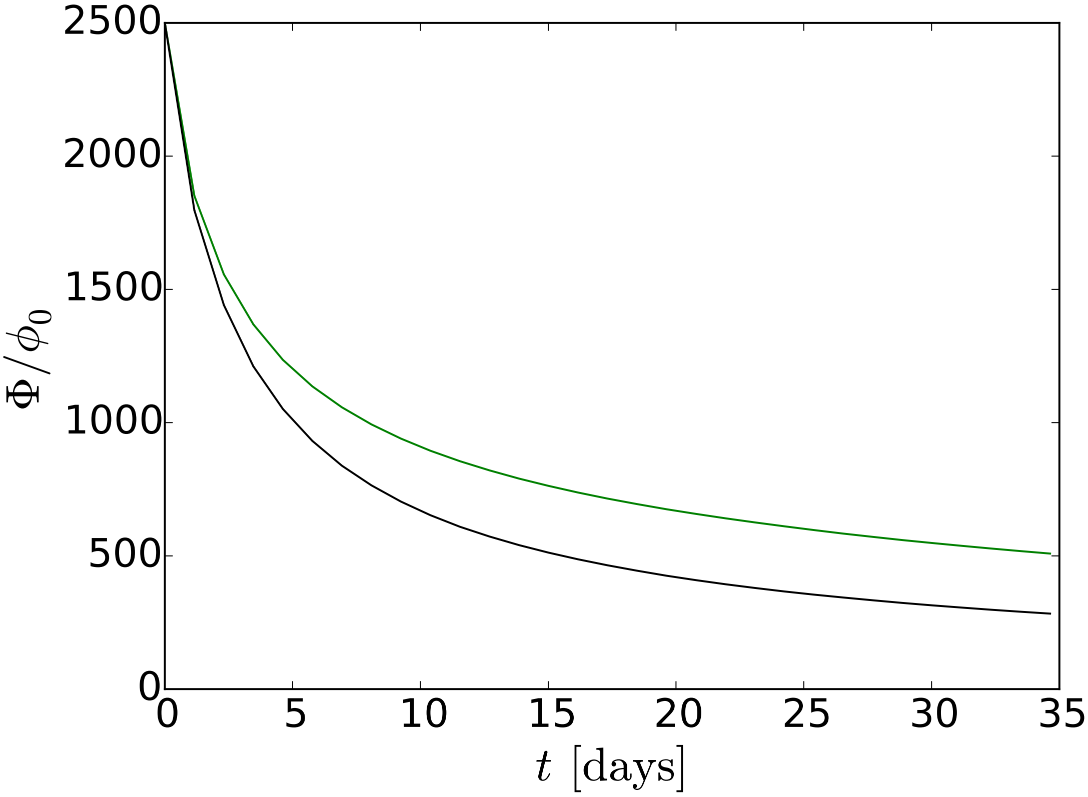

Figure 2.7: Total unsigned flux of a BMR placed at $\lambda_0 = 30°$ with an initial tilt of $\alpha_0 = 7°$. The black and green lines correspond to the simulations with and without inflows, respectively. The error bars indicating realization noise are too small to be visible. The enhanced flux destruction when inflows are present seen in the plot is very similar in all the cases studied.

reducing it (see Jiang et al. 2010). The decrease in B_p is a consequence of how the latitudinal separation and the enhanced flux destruction balance. In the case under discussion, the inflows cause a decrease in axial dipole moment.

The tilt angle and axial dipole moment for the case of an initial tilt angle of $-7°$ are presented in Fig. 2.8c. Now the trailing polarity is placed at a lower latitude than the preceding patch, so the shear flow tends to make the angle increase towards more negative values. When the inflows are included, the reduced latitudinal separation causes the tilt angle to be less negative than in the case without inflows, i.e., the dipole axis rotates more slowly. As before, flux destruction is enhanced by inflows, and the absolute value of the axial dipole moment is reduced.

Figure 2.8a shows the same magnitudes for the 0° initial tilt angle. The longitudinal separation is again restricted by the inflows, but the latitudinal separation increases with time, which produces a clockwise rotation of the dipole axis. This behavior departs from what could be expected from either diffusion, differential rotation or converging flows acting in isolation. In Fig. 2.9 we provide a schematic explanation of this effect. The differential rotation shears the BMR, and at the same time the inflows tend to bring the

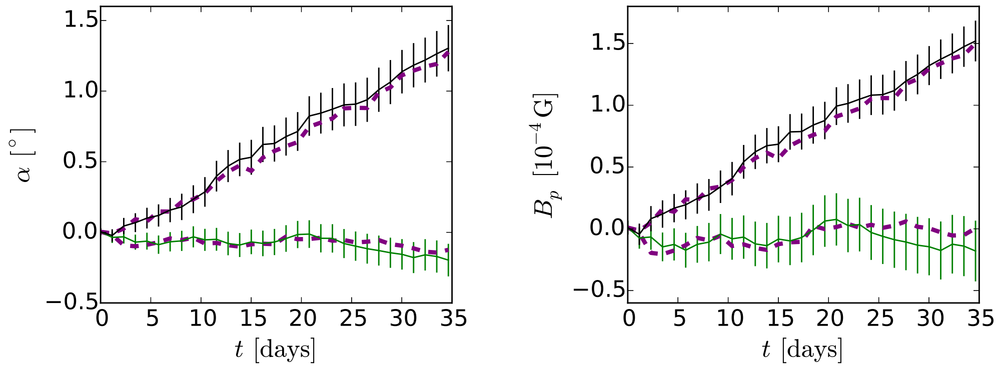

(a) $\alpha_0 = 0°$

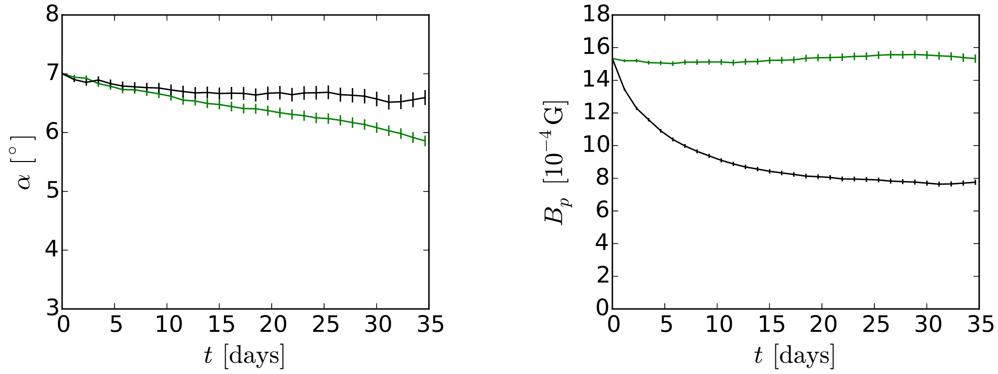

(b) $\alpha_0 = 7°$

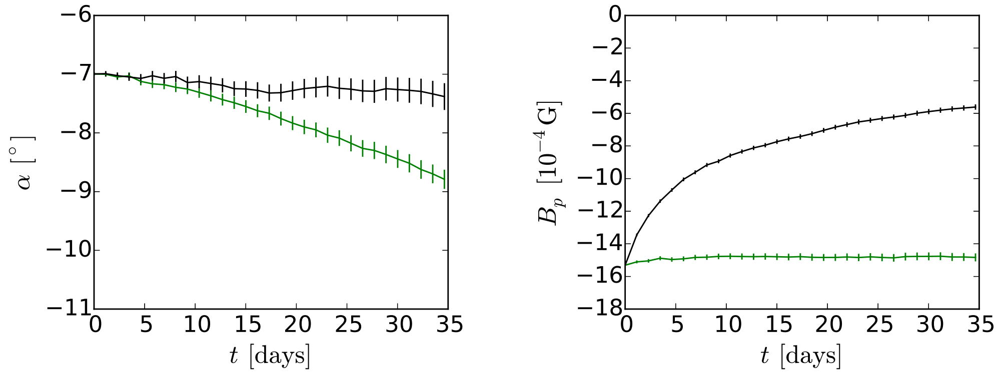

(c) $\alpha_0 = -7°$

Figure 2.8: Tilt angle and axial dipole moment of a BMR placed at $\lambda_0 = 30°$ with an initial tilt of $\alpha_0 = 0°$ (a), $\alpha_0 = 7°$ (b), $\alpha_0 = -7°$ (c). The black and green lines correspond to the simulations with and without inflows respectively. The purple dashed lines in (a) correspond to simulations where the meridional flow is included (error bars have not been plotted for clarity). The error bars represent the standard error of the mean values and indicate the realization noise. The errors for different times are correlated.

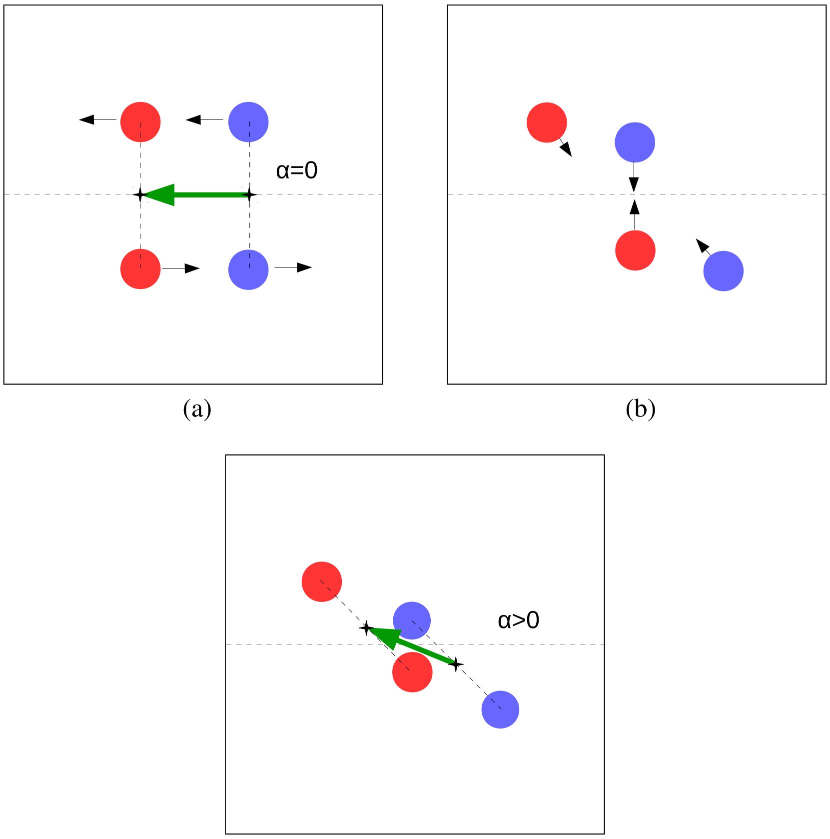

(a) (b) (c)

Figure 2.9: Schematic representation of the combined action of differential rotation and inflows leading to the latitudinal separation of the polarity patches giving rise to a non-zero axial dipole moment. The blue and red dots represent flux concentrations. The thin black arrows indicate plasma flows. The black plus signs indicate the location of the centers of gravity of each polarity. The thick green arrow outlines the dipole axis. (a). The flux concentrations of the BMR emerge at different latitudes. (b) Differential rotation shears the structure, and inflows tend to bring magnetic concentrations closer together. The effect of the inflows on the outermost concentrations is weaker. (c) This displaces the centroid of the polarity patches away from the central latitude, causing the dipole axis to rotate.

innermost concentrations closer to the central latitude, while the outermost concentrations are less affected. This displaces the centers of gravity of the polarity patches away from the central latitude: the trailing polarity is shifted poleward and the preceding polarity moves towards the equator. The rotation in the case considered here amounts to $\sim 1.3^\circ$ over 35 days. When inflows are off, the axial dipole moment remains close to zero, as expected from a BMR with no initial tilt. When inflows are present, however, there is an increase in latitudinal separation, and consequently B_p also increases.

Using observed positions and tilt angles of active regions as input to an SFT model, Cameron et al. (2010) were able to reproduce the main features of the open flux inferred from the *aa*-index of geomagnetic variations during solar cycles 15 to 21. However, the authors need to scale the tilt angles by a factor of 0.7 to reduce the amount of flux arriving at the poles and so match the observed amplitude of the open flux. The righthand column of Fig. 2.8 shows that the axial dipole moment of the BMR is indeed substantially decreased as a consequence of the inflows (except in the $\alpha_0 = 0$ case). The problem of how inflows affect the axial dipole moment of complex active regions and sunspot groups, rather than in an isolated BMR, has yet to be studied. Nevertheless, it is seen that the inflows can provide the physical mechanism needed to justify this scaling of the tilt angles.

Assuming the BMR emerges away from the equator, its contribution to the total axial dipole moment of the Sun is proportional to $\sin\theta$ and, under advection by the meridional flow alone, declines on a time scale $\tau_f = R_\odot/v_m \approx 2$ years (Wang and Sheeley 1991). This characteristic time becomes infinite in our plain domain approximation. As a result, the meridional flow does not have an appreciable effect on the axial dipole moment during the first month of evolution of the BMR, when inflows are non-negligible. This is shown in Fig. 2.8a, where the purple dashed lines represent the evolution of the corresponding quantities in simulations including meridional flow. These do not show any appreciable difference with the plots obtained in the simulations without meridional flow.

Dependence upon latitude of emergence

In Fig. 2.10 we present the same magnitudes as before for a BMR with an initial tilt angle of 7° placed at $\lambda_0 = 0$ (2.10a), $\lambda_0 = 15°$ (2.10b) and $\lambda_0 = 45°$ (2.10c). The case $\lambda_0 = 30°$ is presented in Fig. 2.8b. In all four cases, the inflows restrict the latitudinal and longitudinal separations of the centroids. This results in the tilt angle remaining roughly constant for the BMR at the equator, in the cases both with and without inflows. For the BMRs placed at higher latitudes, the tilt angle decreases over time; i.e., the dipole axis rotates counter-clockwise, and the rotation is slower when the inflows are on. As before, when inflows are switched on, the total unsigned flux decreases faster and the axial dipole moment decays over time. The stronger shearing at higher latitudes causes the inflows to decay faster, so the decrease in B_p is not as pronounced as at lower latitudes. Nevertheless, this decrease is very similar in all four cases, so the dependence of the effect of inflows upon the latitude of the BMR is not very strong.

2.5 Conclusion

In this study we used an SFT code to test the suitability of the diffusion treatment to describe the dispersal of magnetic flux by convective flows on the solar surface. The dispersal produced by the random walk is slightly lower than expected from a Fickian diffusion process when the step size is comparable to the typical size of an active region. However this discrepancy is not very important, even for lengths corresponding to the biggest and longest-lived supergranules. We therefore conclude that the diffusion treatment is appropriate for describing the flux dispersal due to supergranulation when the scales of interest resemble the size of a typical active region or higher.

We also investigated the role of the converging flows toward a BMR in its evolution and their impact on the axial dipolar field. We saw that the differential rotation and the

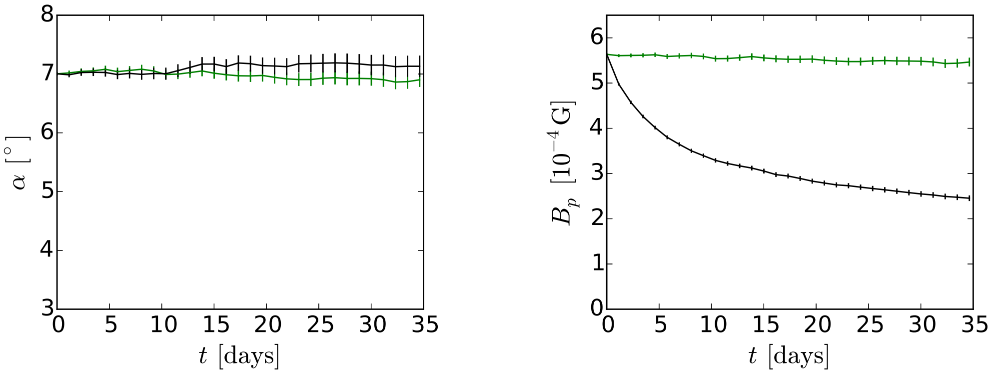

(a) λ_0 = 0°

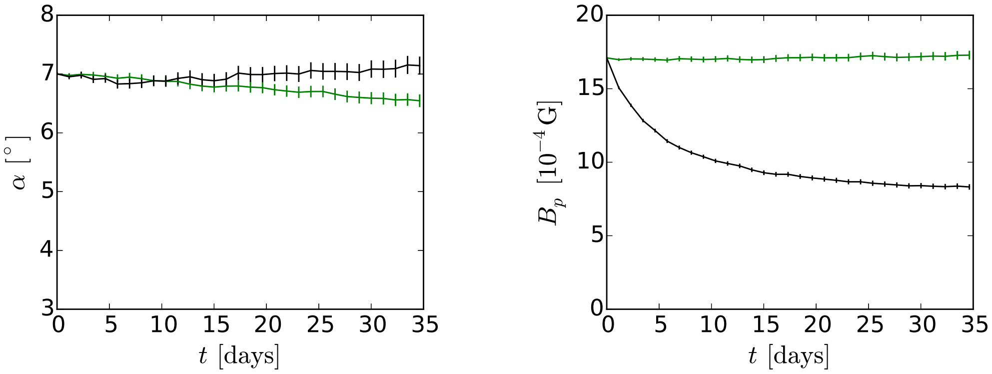

(b) λ_0 = 15°

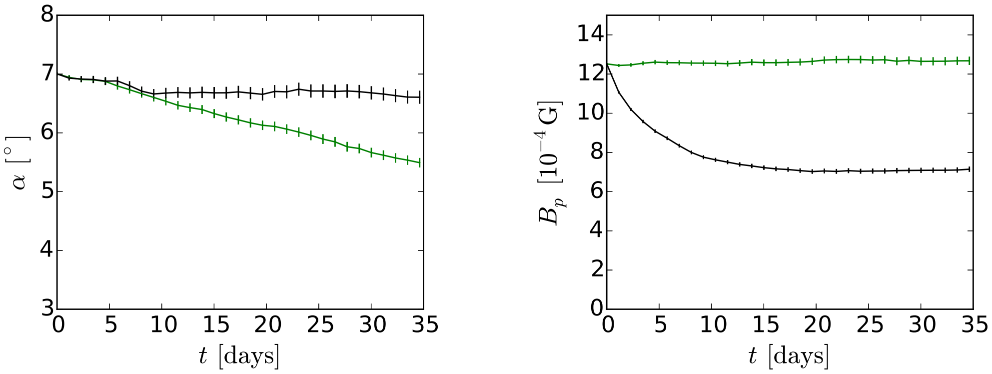

(c) λ_0 = 45°

Figure 2.10: Tilt angle, total unsigned flux, and poloidal flux for a BMR with an initial tilt angle of 7° placed at λ_0 = 0° (a), λ_0 = 15° (b), and λ_0 = 45° (c). The black and green lines correspond to the simulations with and without inflows, respectively. The error bars represent the standard error of the mean values and indicate the realization noise. The errors for different times are correlated.

dispersion by convective motions suffice to oppose the inflows, which decay very quickly owing to flux cancellation. We pointed out that the inflows may cause the apparent reduced rate at which strong magnetic fields appear to diffuse. We have also seen that, in most cases, the inflows limit the latitudinal separation of the polarities and enhance flux cancellation, which lowers the contribution of the emerged BMR to the axial dipole moment. This is an important effect for generating the polar fields. However, when the initial tilt angle is close to zero, the inflows increase the latitudinal separation of the polarities, which gives rise to a positive tilt angle and generates an axial dipole moment. Finally, it was shown that meridional flow does not have an appreciable influence on the early stages of the evolution of an emerged BMR, when the inflows are not negligible.

Aknowledgements

We want to thank Manfred Schüssler for his valuable suggestions and his thorough revisions of this manuscript. This work was carried out in the context of Deutsche Forschungsgemeinschaft SFB 963 “Astrophysical Flow Instabilities and Turbulence” (Project A16).

3 Paper II. Inflows Towards Active Regions and the Modulation of the Solar Cycle: a Parameter Study

Abstract

Aims We aim to investigate how converging flows towards active regions affect the surface transport of magnetic flux, as well as their impact on the generation of the Sun's poloidal field. The inflows constitute a potential non-linear mechanism for the saturation of the global dynamo and may contribute to the modulation of the solar cycle in the Babcock-Leighton framework.

Methods We build a surface flux transport code incorporating a parametrized model of the inflows and run simulations spanning several cycles. We carry out a parameter study to assess how the strength and extension of the inflows affect the build-up of the global dipole field. We also perform simulations with different levels of activity to investigate the potential role of the inflows in the saturation of the global dynamo.

Results We find that the interaction of neighbouring active regions can lead to the occasional formation of single-polarity magnetic flux clumps that are inconsistent with observations. We propose the darkening caused by pores in areas of high magnetic field strength as a possible mechanism preventing this flux-clumping. We find that inflows decrease the amplitude of the axial dipole moment by $\sim 30\,\%$, relative to a no-inflows scenario. Stronger (weaker) inflows lead to larger (smaller) reductions of the axial dipole moment. The relative amplitude of the generated axial dipole is about 9% larger after very weak cycles than after very strong cycles. This supports the idea that the inflows are a non-linear mechanism that is capable of saturating the global dynamo and contributing to the modulation of the solar cycle within the Babcock-Leighton framework. [1]

---

[1] This chapter reproduces the article *Inflows towards active regions and the modulation of the solar cycle: A parameter study* by D. Martin-Belda and R. H. Cameron, published in Astronomy & Astrophysics 597, A21 (2017), DOI 10.1051/0004-6361/201629061. Reproduced with permission of Astronomy & Astrophysics, © ESO. Contributions: D.M.B and R.C. designed the research. D.M.B carried out the research, analyzed the data and wrote the paper.

3.1 Introduction

The magnetic activity of the Sun follows an 11-year cycle. At the time of minimum activity, the surface magnetic field is concentrated at the polar caps and presents a strongly dipolar configuration. As the cycle progresses, new magnetic flux erupts in the form of bipolar magnetic regions (BMRs). The preceding polarity (relative to the Sun's sense of rotation) of the new BMRs tends to emerge closer to the equator (Joy's law), and is of the same sign as the polar field in the same hemisphere at the immediately previous activity minimum (Hale's law). The latitudinal separation of polarities favors the cross-equatorial transport of preceding polarity flux, which causes the gradual cancellation and eventual reversal of the polar fields. When the next activity minimum is reached, the global field is again nearly dipolar and reversed with respect to the previous activity minimum. The full magnetic cycle is therefore 22 years long. These activity cycles show pronounced variability, both cycle to cycle and on longer time scales (for a review of the solar cycle, see Hathaway 2015).

It has been shown that the strength of the polar fields at activity minima strongly correlates with the amplitude of the subsequent cycle (see, for example, Schatten et al. 1978, Choudhuri 2008, Wang and Sheeley 2009, Muñoz-Jaramillo et al. 2013). This is supportive of the Babcock-Leighton model of solar dynamo, in which the polar fields at activity minima represent the poloidal field threading the Sun, from which the toroidal field of the next cycle is generated, rather than being a secondary manifestation of a dynamo mechanism operating below the surface (Cameron and Schüssler 2015). It follows that, in this framework, an activity-related feedback mechanism affecting the surface transport of magnetic flux could provide a means for saturating the dynamo by limiting the build-up of the polar fields (and therefore the regeneration of the poloidal field) and possibly also contribute to the observed variability of the cycle amplitude. One candidate for such a mechanism are the near-surface, converging flows towards active regions (Cameron and Schüssler 2012). These flows, first reported by Gizon et al. (2001), have magnitudes of $\sim 50\,\mathrm{m\,s^{-1}}$ and can extend up to 30° away from the center of the active region. The inflows are possibly driven by the temperature gradient arising from the enhanced radiative loss in areas of strongly concentrated magnetic field (Spruit 2003, Gizon and Rempel 2008).

The question of how these inflows affect the surface transport of magnetic flux and the build-up of the polar fields has been addressed in a number of works. Their main effect is the limitation of the latitudinal separation of the polarities of BMRs, which causes a reduction of the global dipole with respect to a no-inflows scenario (Jiang et al. 2010). This effect dominates in strong cycles, while in weaker cycles the inflows driven by low-latitude BMRs mainly enhance the cross-equatorial transport of magnetic flux, resulting in stronger polar fields. The inclusion of the inflows in surface flux transport simulations improves the correlations of the amplitude of the global dipole with the inferred open heliospheric flux in cycles 13 to 21 (Cameron and Schüssler 2012), but produces a weaker match with the observed butterfly diagram and dipole reversal times in cycles 23 and 24 (Yeates 2014).

All the studies cited above modeled the inflows as an axisymmetric perturbation of the meridional flow converging toward the activity belts. De Rosa and Schrijver (2006) included a more realistic model of inflows in their surface flux transport model, but the converging flows severely affected the dispersal of magnetic flux in their simulations, leading to unrealistic clumping of magnetic flux despite the diffusion by supergranules. In a recent work (Martin-Belda and Cameron 2016), we studied the impact of the inflows in the evolution of an isolated BMR, and showed that turbulent diffusion and differential rotation are sufficiently strong to counteract the converging flows, which decline quickly owing to flux cancellation. A probable reason for the discrepancy with the aforementioned study is the additional damping of the turbulent diffusivity inside active regions, which these authors included to match observations. We argued that the inflows alone can cause this effect.

In this work we continue studying the effect of the inflows on the surface transport of magnetic flux. Our main question is the impact that realistic, non axisymmetric inflows may have on the generation of the large-scale poloidal field. As mentioned above, this could provide a non-linear saturation mechanism for the global dynamo and contribute to the solar cycle variability. A second problem concerns whether our previous result on the dispersal of flux against converging flows holds in global simulations. To address these questions, we incorporated two non-axisymmetric parametrizations of the inflows in a surface flux transport model. The paper is structured as follows: we first introduce our model (Sect. 3.2); then, we examine a case with inflows whose strength and extension are compatible with observations (Sect. 3.3); next, we carry out a parameter study to test how these two magnitudes, as well as the activity level, may affect the build-up of the global magnetic dipole at activity minima (Sect. 3.4); finally, the results are summarized and briefly discussed (Sect. 3.5).

3.2 Surface flux transport model

3.2.1 Surface flux transport equation

The evolution of the magnetic field on the solar surface is governed by the radial component of the induction equation (DeVore et al. 1984):

$$\begin{aligned}\frac{\partial B_r}{\partial t} = &-\frac{1}{R_\odot \sin\theta}\left[\frac{\partial(B_r u_\theta \sin\theta)}{\partial\theta} + \frac{\partial(B_r u_\phi)}{\partial\phi}\right]\\ &+\frac{\eta}{R_\odot^2}\left[\frac{1}{\sin\theta}\frac{\partial}{\partial\theta}\left(\sin\theta\frac{\partial B_r}{\partial\theta}\right) + \frac{1}{\sin^2\theta}\frac{\partial^2 B_r}{\partial\phi^2}\right]\\ &+S(\theta,\phi,t),\end{aligned} \tag{3.1}$$

where ϕ and θ denote solar longitude and colatitude, respectively. The first term on the right hand side represents the advection of magnetic flux by the surface flows, which include differential rotation, meridional flow, and inflows towards active regions:

$$u_\theta = v_m(\theta) + w_\theta(\theta,\phi) \tag{3.2}$$

$$u_\phi = R_\odot \sin\theta\,\Omega(\theta) + w_\phi(\theta,\phi). \tag{3.3}$$

Here, v_m is the velocity of the meridional flow, $\Omega(\theta)$ is the angular velocity of the differential rotation and w_ϕ and w_θ are the components in spherical coordinates of the inflows.

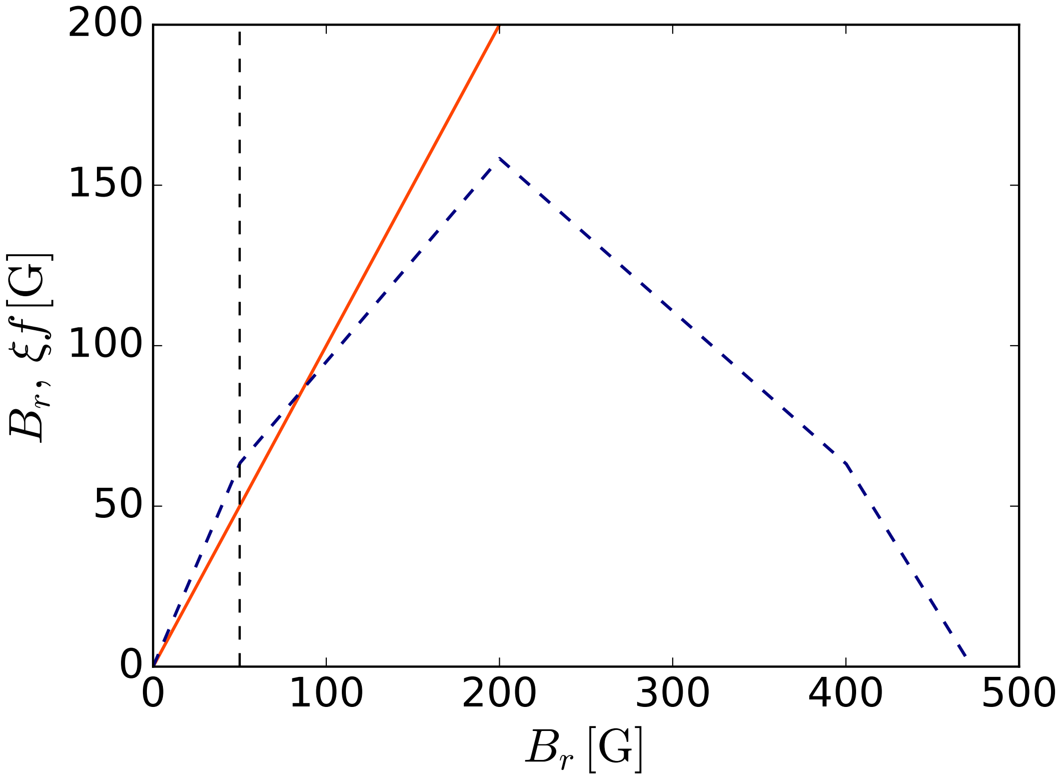

Figure 3.1: B_r (orange line) and ξf (dashed, blue line) as a function of B_r. The dashed vertical line indicates $B_r = 50\,\mathrm{G}$.

We adopt the differential rotation profile from Snodgrass (1983):

$$\Omega(\theta) = 13.38 - 2.30\cos^2\theta - 1.62\cos^4\theta\ [^\circ/\mathrm{day}]. \tag{3.4}$$

Following van Ballegooijen et al. (1998), we model the meridional flow as

$$v_m(\lambda) = \begin{cases} 11\sin(2.4\lambda)\ [\mathrm{m/s}] & \text{if } |\lambda| < \lambda_0; \\ 0 & \text{if } |\lambda| \geq \lambda_0, \end{cases} \tag{3.5}$$

where λ denotes solar latitude and $\lambda_0 = 75^\circ$.

The second term on the right hand side of Eq. (3.1) describes the flux dispersal by convective flows as a random walk/diffusion process (Leighton 1964). We choose $\eta = 250\,\mathrm{km}^2/\mathrm{s}$, a value in agreement with observations (Schrijver and Martin 1990, Jafarzadeh et al. 2014) and consistent with the evolution of the large scale fields (Cameron et al. 2010).

The term $S(\theta, \phi, t)$ describes the emergence of new active regions, and is described in detail in Baumann et al. (2004). The synthetic activity cycles in our simulations are 13 years long, with a two-year overlap between cycles, so the time distance between consecutive cycle minima is 11 years. The activity level (the number of new BMRs per day) is governed by a Gaussian function whose height peaks halfway into the the cycle. At the beginning of the cycle, the BMRs emerge at a mean latitude of 40° with a standard

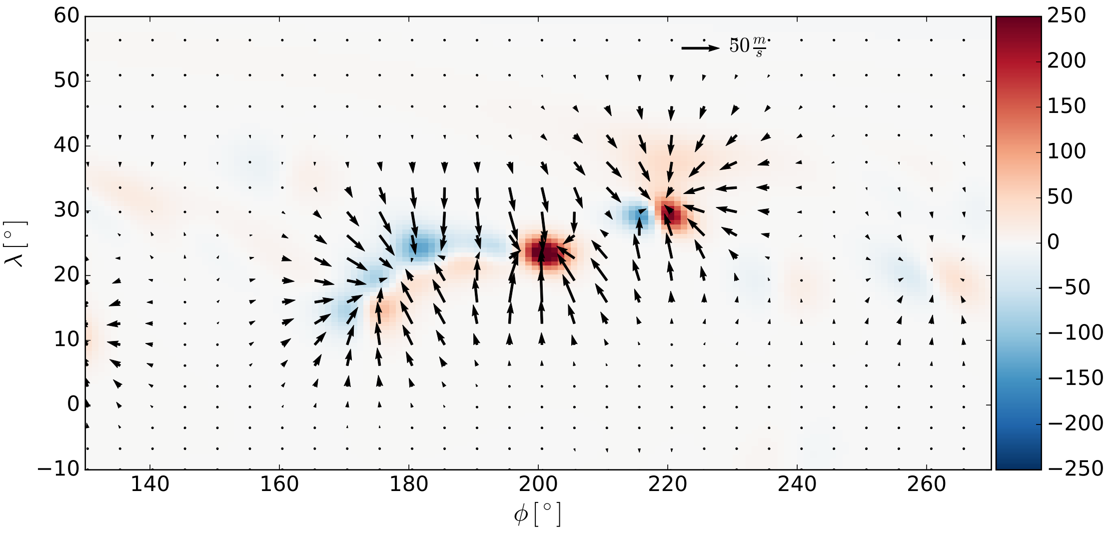

Figure 3.2: Model of inflows towards an activity complex formed by several emerged BMRs. The color scale encodes the strength of the magnetic field B_r in Gauss and saturates at 250 G. Red and blue indicate opposite polarities. The values of the parameters in Eq. (3.7) are $a = 1.8 \cdot 10^8\ \mathrm{m^2 G^{-1} s^{-1}}$ and FWHM = 15°.

deviation of 10°. These values decrease linearly and reach a mean latitude of 5° and a standard deviation of 5° at the end of the cycle. We do not consider active longitudes in this study, so the random distribution is uniform in ϕ. Following van Ballegooijen et al. (1998), we represent a BMR by two circular patches of opposite polarity. The magnetic field of each patch is given by:

$$B_r(\theta,\phi) = B_{max}\left(\frac{\delta}{\delta_0}\right)^2 \exp\left\{-\frac{2[1-\cos\beta_\pm(\theta,\phi)]}{\delta_0^2}\right\}, \tag{3.6}$$

where $\beta_\pm$ is the heliocentric angle between the center of the (±) polarity patch and the surface point (θ,ϕ); δ denotes the angular size of the *BMR* and $\delta_0 = 4^\circ$. The size of the BMRs follows a distribution $n(\delta) \propto \delta^4$. This distribution was derived by Schrijver and Harvey (1994) from observations for BMRs with sizes ranging from 3.5° to 10°. BMRs smaller than 3.5° cannot be well resolved in our simulations, so they are assumed to diffuse without interacting with the rest of the flux until they reach this size. The maximum field strength upon emergence, B_{max}, is adjusted so the total flux input per cycle is $\sim 8.9 \cdot 10^{24}$ Mx (Schrijver and Harvey 1994).

3.2.2 Parametrization of the inflows

We test two different models of inflows. The first one is based upon the parametrization of Cameron and Schüssler (2012),

$$\mathbf{w} = a\,\nabla\left(\frac{\cos\lambda}{\cos 30^\circ}|\hat{B}_r|\right), \tag{3.7}$$

where $|\hat{B}_r|$ is the absolute value of the magnetic field smoothed with a Gaussian. Adjusting the full width at half maximum (FWHM) of the Gaussian allows us to control the extension of the inflows. We note that the gradient of the smoothed magnetic field generally decreases with increasing width of the Gaussian. Hence, for a fixed value of a, wider inflows are weaker. The factor $\cos\lambda/\cos 30^\circ$ is introduced to quench unrealistically strong poleward flows arising from the gradient of the polar fields. Figure 3.2 shows the inflows around an activity complex for our reference values $a = 1.8 \cdot 10^8\,\mathrm{m^2/G\,s}$ and FWHM $= 15^\circ$. The value of a is chosen so that the peak inflow velocity around an isolated BMR of size 10° is $\sim 50\,\mathrm{m/s}$, in agreement with observations. Hereafter we refer to this parametrization as the $B-$parametrization.

The second parametrization of the inflows is motivated by the results of Vögler (2005). The author's radiative MHD simulations suggest that the relation between the average magnetic field in an active region and the integrated radiation flux is non-monotonic, peaking at about $\sim 200\,\mathrm{G}$. For stronger average fields, the formation of dark pores reduces the radiation output. This can effectively reduce the radiative cooling in active regions, and thus limit the strength of the inflows. We attempt to capture this effect by substituting B_r in Eq. (3.7) with the angle integrated radiation flux normalized to the quiet-sun value (which we denote by f), taken from the left panel of Fig. 2 in Vögler (2005),

$$\mathbf{w} = \xi a \nabla \left(\frac{\cos\lambda}{\cos 30^\circ} \hat{f} \right). \tag{3.8}$$

The prefactor $\xi = 6.3 \cdot 10^4$ was adjusted such that the peak inflow velocity around an isolated, $10^\circ-$sized BMR is $\sim 50\,\mathrm{m/s}$ for our reference values of a and the FWHM. This parametrization is referred to as $f-$ parametrization in the remainder of the paper. The $f-$ parametrization produces weaker inflow velocities in regions of strong magnetic field. However, since the slope of f is steeper than the slope of B between 0 and 50 G (see Fig. 3.1), the contribution to the inflows of areas with fields lower than 50 G value to the inflows will be stronger than in the $B-$ case.

One of the problems we address in this paper is the suppression of magnetic flux dispersal in the presence of inflows found by De Rosa and Schrijver (2006). These authors parametrize the inflows in the following way:

$$\mathbf{w} = a \nabla |B_r|^b \tag{3.9}$$

This parametrization (with $b = 1$) is the same as ours except for the geometric factor that is similar to the one introduced in Cameron and Schüssler (2012) to prevent strong inflows near the poles.

3.2.3 Numerical treatment

To integrate Eq. (3.1), we developed a surface flux transport code. The equation is expressed in terms of $x = \cos\theta$. We calculate the $x-$derivative in the advection term with a fourth-order centered finite differences scheme. The derivative in the ϕ direction is calculated in Fourier space. We use a fourth-order Runge-Kutta scheme to advance the advection terms in time. The diffusion term in the $x-$direction is treated with a Crank-Nicolson scheme. We treat the $\phi-$diffusion term by computing the exact solution of the diffusion equation for the Fourier components of B_r.

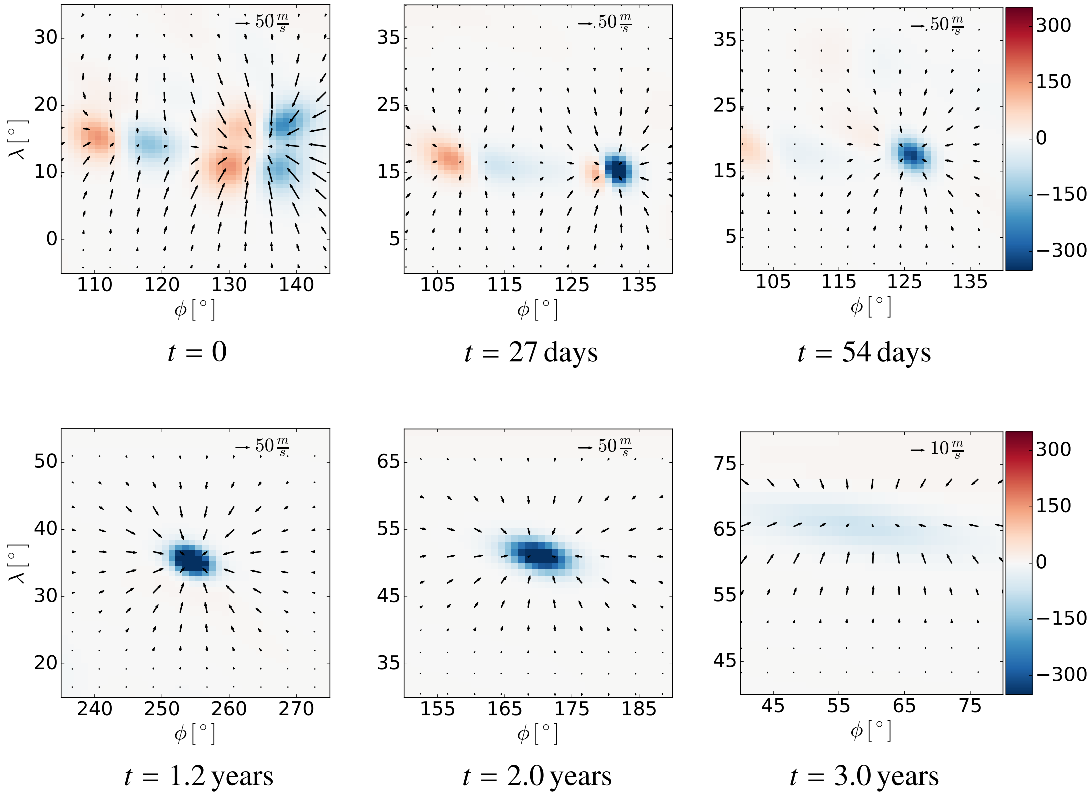

t = 0

t = 27 days

t = 54 days

t = 1.2 years

t = 2.0 years

t = 3.0 years

Figure 3.3: Time series showing the evolution of a long-standing, single-polarity magnetic flux clump. Time progresses from left to right and from top to bottom. The color scale indicates the magnetic field strength in Gauss and saturates at 350 G. The arrows represent the strength and direction of the inflows.

We validated the code by reproducing the results for the reference case of the study by Baumann et al. (2004).

Calculating the inflows requires smoothing the absolute value of the magnetic field (or the normalized radiation flux, in the $f-$ parametrization) with a Gaussian of given FWHM every time step. The result of this operation is identical to diffusing $|B_r|$ (or f) with a given diffusion coefficient η_s for a time interval $\Delta t'$, related to the FWHM of the smoothing Gaussian through

$$\mathrm{FWHM} = 4\sqrt{\Delta t'\,\eta_s\,\ln 2}. \tag{3.10}$$

We emphasize that the time t' in Eq. (3.10) is different to the simulation time t. The diffusion of $|B_r|$ or f is a mathematical resource that we employ to compute the inflows every time step, and is therefore unrelated to the diffusion term in Eq. (3.1), which describes the physical surface diffusion of B_r by the convective flows.

The numerical integration of the diffusion equation for $|B_r|$ or f is performed in a number n of time steps that must be large enough for the implicit scheme to produce a reasonably accurate solution and avoid Gibbs oscillations, which lead to instabilities in the simulation. The number n should also be as small as possible to minimize the computational cost. We tested two different approaches to matching this compromise.

The straightforward solution is to use time steps of equal size $\delta t' = \Delta t'/n$. By a process of trial and error, we find that $n = 50$ satisfies the required conditions. The second approach relies on the fact that the time steps need to be shorter when the gradient of the function to diffuse is steeper. Since the steepest gradients are reduced as the diffusion progresses, taking time steps of increasing size enables us to reduce n. If we allow every time step be longer than the preceding one by a factor γ, then

$$\delta t' = \frac{\Delta t'}{1 + \gamma + \gamma^2 + \ldots + \gamma^{n-1}} = \frac{1-\gamma}{1-\gamma^n}\Delta t', \tag{3.11}$$

where $\delta t'$ is now the size of the first step. We find that the combination $\gamma = 1.7$ and $n = 8$ satisfies the above requirements and leads to results that are consistent with the first approach.

Figure 3.2 shows an example of inflows towards an area of strong magnetic field.

3.3 Reference case

3.3.1 Setup

We first study the impact of the inflows on the amplitude of the polar fields for our reference values, $a = 1.8 \cdot 10^8\,\mathrm{m^2/G\,s}$ and FWHM $= 15°$. We ran three sets of simulations: without inflows, with inflows, and with an axisymmetric perturbation of the meridional flow calculated as the azimuthal average of the inflows. The latter is done for comparison with Cameron and Schüssler (2012). While our treatment is not equivalent to the one in the cited study, the calibration factors ensure that the axisymmetric inflows in both studies have similar strengths. To reduce the statistical noise arising from the random positioning of the sources, we ran 20 realizations for each set of parameters. Each realization spans 55 years.

The initial configuration of the magnetic field is chosen such that the rate of poleward flux transport by the meridional flow and the rate of equatorward transport by turbulent diffusion are approximately equal, $v_m B_r \approx (\eta/R_\odot)\partial B_r/\partial\theta$, which corresponds to a situation of activity minimum (see van Ballegooijen et al. 1998). Combining this with equation (3.5) yields

$$B_r(\lambda) = \begin{cases} \mathrm{sign}(\lambda) B_0 \exp[-a_0(\cos(\pi\lambda/\lambda_0) + 1)] & \text{if } |\lambda| < \lambda_0; \\ \mathrm{sign}(\lambda) B_0 & \text{if } |\lambda| \geq \lambda_0, \end{cases} \tag{3.12}$$

where $a_0 = v_m R_\odot \lambda_0/\theta\eta$. B_0 is chosen in each simulation by requiring that the strength of the polar fields at activity minima remains approximately constant from cycle to cycle.

3.3.2 Flux dispersal

Regarding the surface transport of magnetic flux, one of the main questions is how the magnetic flux contained in active regions that are surrounded by inflows spreads. De Rosa and Schrijver (2006) found that including the inflows in surface flux transport simulations led to a suppression of the flux dispersal by convective flows, resulting in the formation of magnetic flux clumps that are incompatible with observations. In Martin-Belda and Cameron (2016), we showed that, in the case of an isolated magnetic region, flux cancellation in the first days after emergence causes a decrease in the strength of the inflows, so that turbulent diffusion and the shearing caused by the differential rotation are sufficient to explain the flux dispersal. However, the interaction between neighbouring active regions can result in the formation of polarity-imbalanced magnetic patches. In such cases, flux cancellation no longer decreases the inflow strength. In our simulations, this leads to the occasional formation of highly concentrated, single-polarity flux clumps which can last for years. This is much longer than the typical decay time of active regions, which ranges from days to weeks (see, e.g., Schrijver and Zwaan 2008). By contrast, the flux clumping discussed in De Rosa and Schrijver (2006) possibly arises owing to the additional reduction of the diffusivity inside active regions that was included by these authors in their model. By reducing the diffusivity in active regions, these authors sought to account for the observed reduction of the flux dispersal in the core of active regions (Schrijver and Martin 1990). In Martin-Belda and Cameron (2016), we argued that the inflows alone would have a similar effect.

Figure 3.3 shows the formation and evolution of one such long-lasting polarity clump. The first panel shows an active region complex that consists of two large patches of magnetic flux, drawing strong inflows, and a BMR to the left of it. Some of the negative polarity of the BMR is attracted towards the active complex by the inflows, and cancels part of the complex's positive flux. The positive patch of the BMR, further away from the complex, is less affected and diffuses away rapidly. This causes a flux imbalance in the complex (we emphasize that magnetic flux is still conserved globally), leading to the formation of the single-polarity feature (top-middle). The persistent inflows further concentrate its flux, until an approximate equilibrium between diffusion and the inflows is reached. As the patch is advected towards higher latitudes, the shear that is caused by the differential rotation, the partial cancellation with the polar field, and the artificial decrease of the inflow strength that is caused by the prefactor $\cos\lambda/\cos 30^\circ$ of our parametrization lead to the dispersal of the single-polarity patch.

The formation and evolution of single-polarity features in simulations using the $f-$ parametrization is essentially parallel to the one described for the $B-$ parametrization, but the magnetic field is substantially less concentrated. This is demonstrated in Fig. 3.4, which represents the peak magnetic field of the single-polarity patch as a function of time in both parametrizations. An initial concentration of the magnetic field takes place in approximately the first two months of evolution. This is followed by a dip, possibly caused by the assimilation of positive polarity flux from a decaying BMR, much in the same way the single-polarity feature formed by mainly assimilating one of the polarities of a BMR. A plateau phase follows, in which the average magnetic field of the single-polarity feature, which we may estimate as $\sim B_{r,max}/2$, is $\sim 300\,\mathrm{G}$ in the $B-$ parametrization case and $\sim 150\,\mathrm{G}$ in the $f-$ parametrization (although a slightly increasing trend can be seen in the $B-$ parametrization case). This phase lasts slightly longer than a year, after which the feature begins to decay owing to the reasons stated above.

The lower concentration of magnetic flux in the long-standing clumps in the $f-$ parametrization suggests that a less idealized parametrization of this mechanism may solve the clumping problem completely.

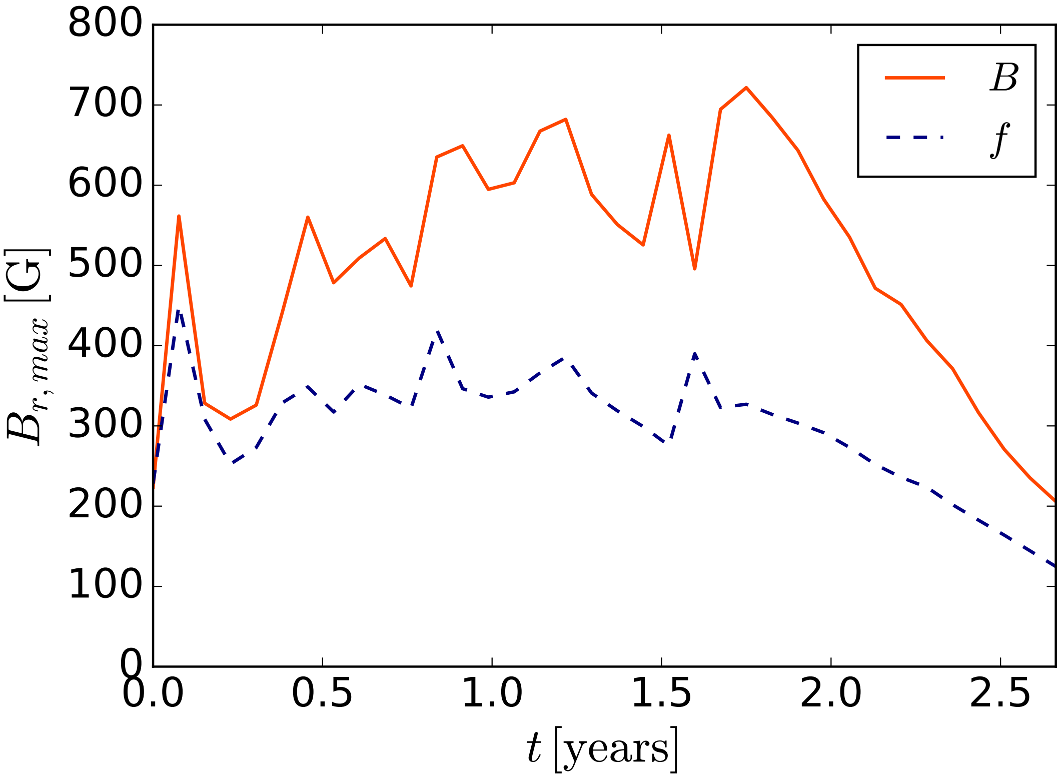

Figure 3.4: Maximum field strength of the single-polarity patch under discussion. The orange and dashed, blue lines correspond respectively to the $B-$ and the $f-$ parametrizations of the inflows.

3.3.3 Evolution of the axial dipole moment

To evaluate the impact of the inflows on the reversal and regeneration of the large-scale poloidal field we study the evolution of the axial dipole moment of the surface field, which is defined as:

$$D_M = \sqrt{\frac{3}{4\pi}} \int_0^{2\pi} \int_0^{\pi} B_r(\phi, \theta) \cos\theta \sin\theta \, \mathrm{d}\theta \mathrm{d}\phi. \tag{3.13}$$

Figure 3.5 shows the evolution of the axial dipole moment in three simulations (without inflows, with azimuthally averaged inflows and with full inflows) using the $B-$ parametrization of the inflows. The set of sources is identical in all three realizations. The dipole amplitude is larger in the run without inflows than in the runs with inflows and with azimuthally averaged inflows. In the case of non axisymmetric inflows, D_M is generally lower than in the case with averaged inflows, although values can occasionally be higher owing to statistical fluctuations. Averaging the peak values of the dipole moment over 20 realizations yields the following average axial dipole amplitudes:

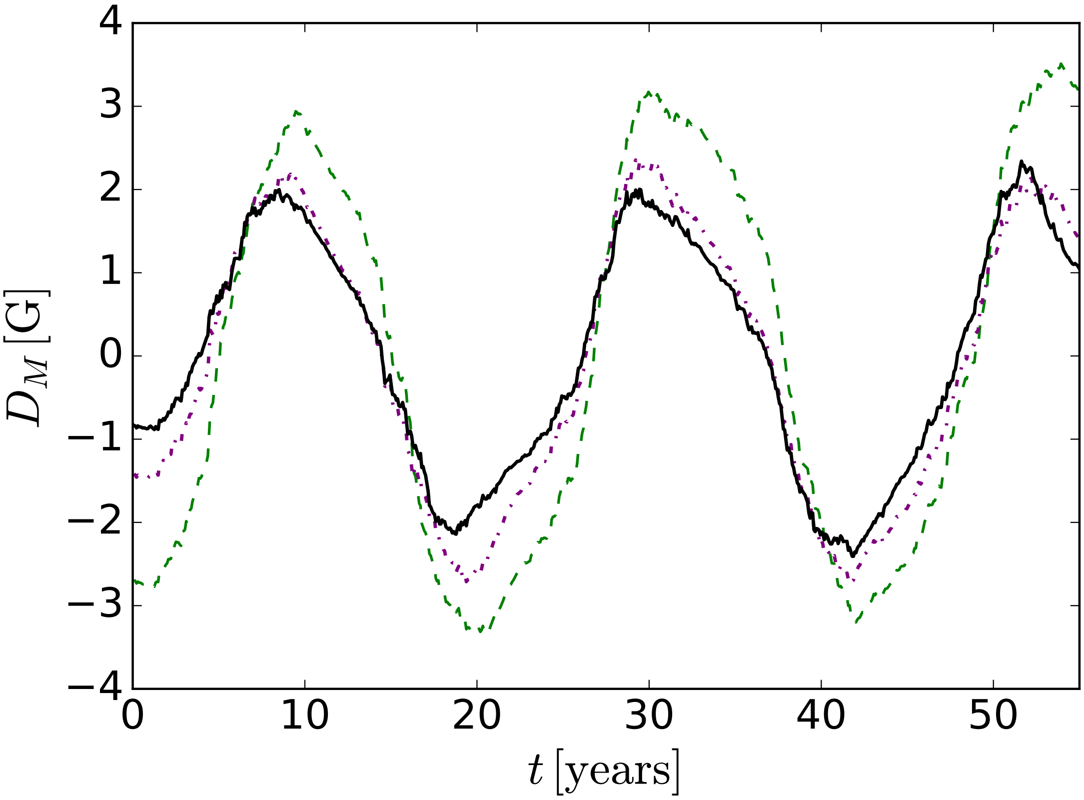

Figure 3.5: Evolution of the axial dipole moment in one realization with the $B-$ parametrization of the inflows. The (dashed) green, (dotted) purple and black lines correspond to simulations without inflows, with azimuthally averaged inflows and with non-axisymmetric inflows, respectively. Otherwise, the setup of all three simulations is identical.

$$
\begin{aligned}
\langle D_M \rangle &= 3.27 \pm 0.02\,\mathrm{G} \quad \text{(No inflows);}\\
\langle D_M \rangle &= 2.54 \pm 0.02\,\mathrm{G} \quad \text{(Averaged inflows);}\\
\langle D_M \rangle &= 2.27 \pm 0.02\,\mathrm{G} \quad \text{(Non-axisymmetric inflows).}
\end{aligned}
$$

The amplitude of the axial dipole moment in the case with azimuthally averaged inflows is, on average, $\sim$ 22% lower than in the case without inflows. In the case of non-axisymmetric inflows, the average amplitude is $\sim$ 30% lower.

The average dipole peak strength obtained from the simulations using the $f-$ parametrization is $\sim$ 3% lower than in the $B-$ case:

$$\langle D_M \rangle = 2.20 \pm 0.02\,\mathrm{G} \quad \text{(Non-axisymmetric, } f- \text{ parametrization).}$$

The slight difference is due to the stronger contribution of fields up to 50 G in this parametrization (see Sec. 3.2.2), which causes a greater restriction of the latitudinal separation of polarities than in the $B-$ case.

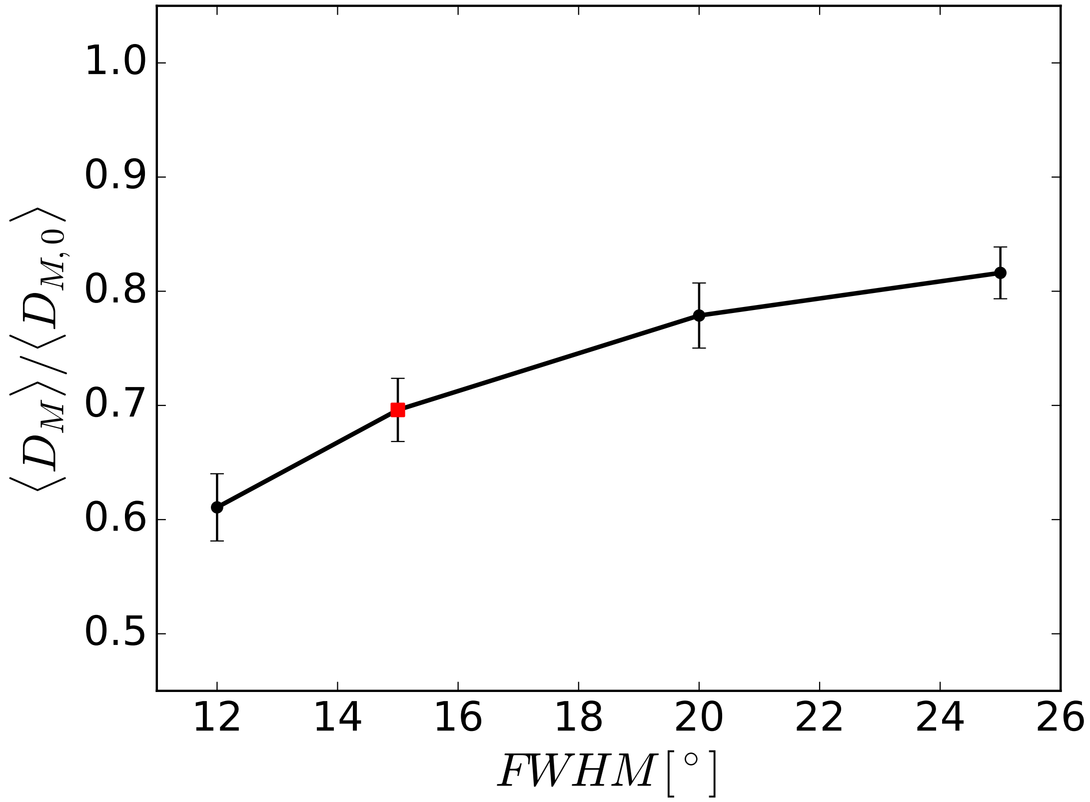

Figure 3.6: Average amplitude of the axial dipole moment ($\langle D_M \rangle$) relative to the no-inflows case ($\langle D_{M,0} \rangle$) as a function of the FWHM. The red square symbol indicates the reference case. The error bars indicate a deviation of 1σ from the mean.

The small difference between the average axial dipole moment in the $B-$ and $f-$ cases suggests that the occasional single-polarity clumps do not have a significant impact on the amplitude of the global dipole moment. This is because the single-polarity features occur only very occasionally, so the amount of flux that would have crossed the equator, had the feature been allowed to disperse, is much smaller than the total flux crossing the equator over the cycle. For this reason, we proceed by performing a parameter study of our inflow model using only the $B-$parametrization.

3.4 Parameter study

3.4.1 Inflow parameters

To understand the way the two parameters of our model influence the build-up of the axial dipole, we compared the strength of the dipole that results from simulations with and without inflows. The FWHM of the inflows was varied over the range $12\,^\circ$ to $25\,^\circ$, while keeping a to its reference value of $1.8 \cdot 10^8\,\mathrm{m^2G^{-1}s^{-1}}$. Similarly, a was varied from $2 \cdot 10^7$ to $3 \cdot 10^8\,\mathrm{m^2G^{-1}s^{-1}}$ with fixed FWHM $= 15\,^\circ$. We ran 20 realizations for each combination of parameters.

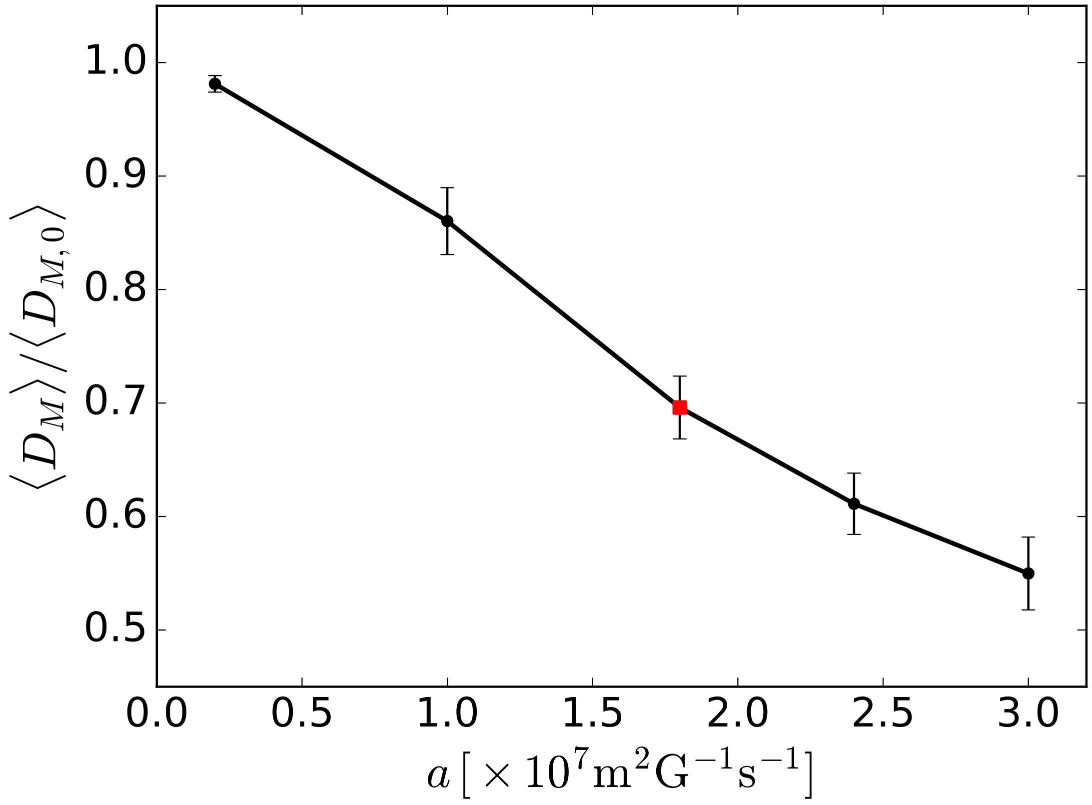

Figure 3.7: Average amplitude of the axial dipole moment ($\langle D_M \rangle$) relative to the no-inflows case ($\langle D_{M,0} \rangle$) as a function of the multiplicative parameter a in Eq. (3.7). The red square symbol indicates the reference case. The error bars indicate a deviation of 1σ from the mean.

Figure 3.6 shows the variation of the average dipole peak amplitude with the FWHM of the smoothing Gaussian. For all the values of the FWHM, the average amplitude of the axial dipole moment decreases relative to their no-inflows counterpart. This is due to the quenching of the contribution of the BMRs to the global dipole induced by the inflows, which is determined by the magnetic flux of the BMR and the latitudinal separation of the polarities (Martin-Belda and Cameron 2016). The inflows enhance the cancellation of opposite polarity flux and limit the latitudinal separation of the polarities, which results in a reduction of this contribution. With decreasing FWHM, the stronger and more localized inflows further enhance these effects, resulting in a larger reduction of the axial dipole moment. The axial dipole moment ratio varies from $\sim$ 60% to $\sim$ 80% in the range of FWHM under consideration.

Figure 3.7 shows the average peak amplitude of the axial dipole moment as a function of the multiplicative parameter a in Eqs. (3.7) and (3.8). For $a = 2 \cdot 10^7\ \mathrm{m}^2\mathrm{G}^{-1}\mathrm{s}^{-1}$, the average peak amplitude of the axial dipole is only slightly smaller than in the no-inflows case. Larger values of a render stronger inflows, and the amplitude of the dipole consequently decreases. For the strongest inflows that we considered ($a = 3 \cdot 10^8\ \mathrm{m}^2\mathrm{G}^{-1}\mathrm{s}^{-1}$), the amplitude of the axial dipole moment is $\sim$ 50% weaker than in the case without inflows.

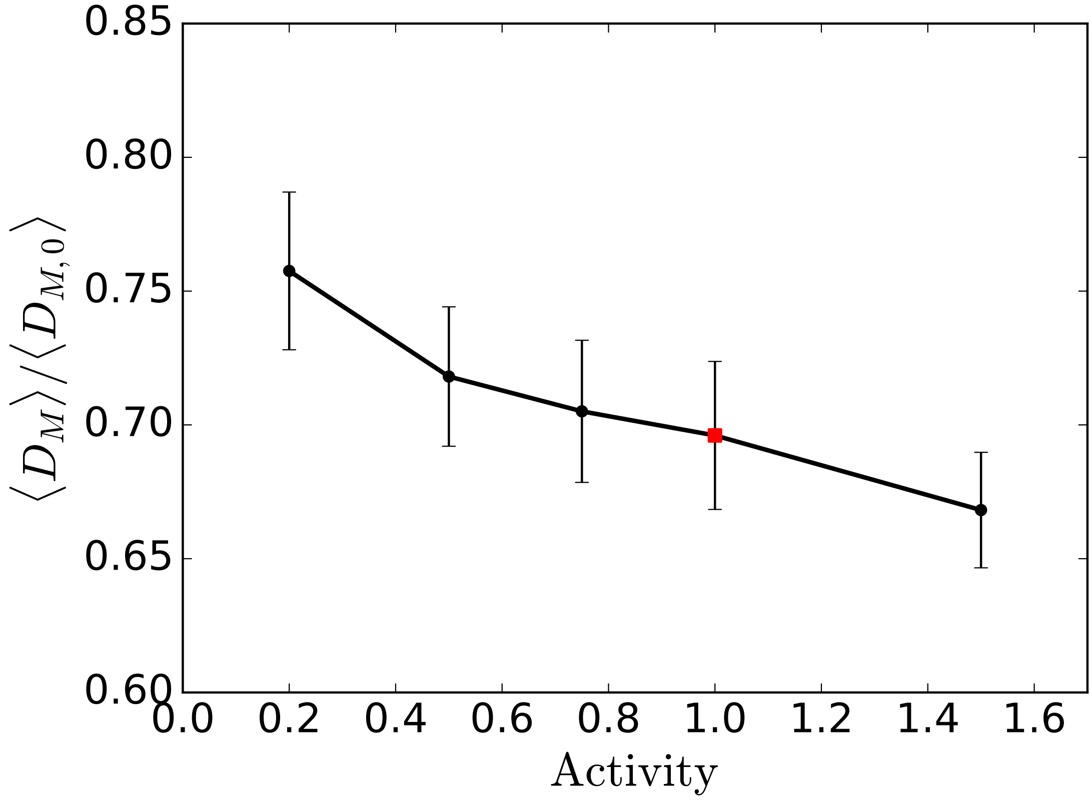

Figure 3.8: Average amplitude of the axial dipole moment ($\langle D_M \rangle$) relative to the corresponding no-inflows case ($\langle D_{M,0} \rangle$) as a function of the cycle strength. The symbols indicate the chosen values for the activity level, relative to the activity of the reference case (indicated with the red square symbol). The error bars indicate a deviation of 1σ from the mean.

3.4.2 Activity level

We ran simulations with an activity level, defined as the number of active regions per 11-year cycle, ranging from 0.2 to 1.5 times that of the reference case. The dependence of the average peak amplitude of the axial dipole moment (relative to the no-inflows scenario) with activity is shown in Fig. 3.8. The ratio of dipole moments decreases with the activity level by about a 9% over the whole activity range. This is because, in strong cycles, owing to the larger number of active regions, the collectively driven inflows have a stronger impact on the latitudinal separation of the polarities of individual BMRs. This decrease in the relative amplitude of the axial dipole moment with activity implies that, in the Babcock-Leighton framework, the generation of the poloidal field is more efficient in weak cycles than in strong ones. This constitutes a non-linearity, which may saturate the dynamo and possibly contribute to the modulation of the solar magnetic cycle.

There is a second way inflows can affect the build-up of the axial dipole, namely, enhanced cross-equatorial transport of flux owing to inflows driven by low-latitude active regions. This effect is less pronounced in strong cycles than in weak ones, since the former peak earlier than the latter (Waldmeier rule) and, as a consequence, the inflows during the maxima of strong cycles are further away from the equator. Since all our simulations peak halfway into the cycle, and thus do not include the Waldmeier effect, the influence of the activity level on the build-up of the axial dipole may be even more pronounced than found here.

3.5 Conclusion

We used a surface flux transport code to study the role of near-surface, converging flows towards active regions on the surface transport of magnetic flux and the build-up of an axial dipole at cycle minima. The inflows have been proposed as one possible non-linear mechanism behind the saturation of the global dynamo in the Babcock-Leighton framework (Cameron and Schüssler 2012). We stress that other mechanisms, such as alpha-quenching (Ruediger and Kichatinov 1993) or cycle-dependent thermal perturbations of the overshoot region affecting the stability of the flux tubes and, as a consequence, the tilt angle of the emerging flux tubes (Işık 2015), have also been proposed. Here we concentrate on the inflows, but we do not mean to suggest that in this paper we exclude other possibilities.

We first studied the evolution of the surface flux in a case with inflows that have strengths and extensions similar to those observed on the Sun. In Martin-Belda and Cameron (2016), we found that the strength of the inflows driven by an isolated BMR decays owing to the cancellation of opposite-polarity flux over approximately the first 30 days of evolution. Differential rotation and turbulent diffusion are strong enough to ensure the flux dispersal. However, as seen in Sect. 3.3.2, interaction between neighbouring active regions can occasionally give rise to large single-polarity concentrations. In these cases, a mechanism other than flux cancellation may be required to weaken the inflows and allow for the dispersal of the single-polarity clump. One possibility is that the darkening caused by the formation of pores in areas of strong magnetic field leads to a reduction in the cooling beneath the active region, rendering the inflows weaker. We explored this possibility in our simulations and saw that, although the clumping persists, the magnetic field of these features is substantially lower than in the simulations where the effect of pore-darkening is not considered. This result suggests that this mechanism may be operating in the Sun, although less idealized models of inflows may be necessary to fully account for the clumping problem. In any case, the occasional occurrence of single-polarity clumps in the simulations does not have a significant impact on the amplitude of the global dipole.

We also performed a parameter study in which we varied the strength and extension of the inflows and the activity of the cycles. In general, inflows decrease the axial dipole moment at the end of the cycle. This is due to the relative decrease in latitudinal separation of the polarities of BMRs caused by the inflows. Stronger (weaker) inflows lead to larger (smaller) reductions of the axial dipole moment.

Our main finding is that inflows with characteristics that are similar to those observed can reduce the axial dipole moment at the end of the cycle by $\sim 30\%$ with respect to the case without inflows in cycles of moderate activity. This ratio varies by $\sim 9\%$ from very weak cycles to very strong cycles, which supports the notion of inflows being a potential non-linear mechanism capable of limiting the field amplification in a Babcock-Leighton dynamo and contributing to the modulation of the solar cycle.

Aknowledgements

We want to thank Manfred Schüssler for his valuable suggestions and his thorough revision of this manuscript.

D.M.B. acknowledges postgraduate fellowship of the International Max Planck Research School on Physical Processes in the Solar System and Beyond.

This work was carried out in the context of Deutsche Forschungsgemeinschaft SFB 963 “Astrophysical Flow Instabilities and Turbulence” (Project A16).

4 Paper III. Evolution of the Sun’s Toroidal Field and the Flux Emergence Process

Abstract

Aims We aim to infer the sub-surface distribution of the Sun’s non-axisymmetric azimuthal magnetic flux from observable quantities, such as the surface magnetic field and the large scale plasma flows.

Methods We build a kinematic flux transport model of the solar dynamo based on the Babcock-Leighton framework. We construct the source term for the poloidal field using SOLIS magnetograms spanning three solar cycles. Based on this source we calculate the azimuthal flux below the surface. The flux transport model has two free parameters which we constrain using sunspot observations from cycle 22. We compare the model results with observations from cycle 23.

Results The structure of the azimuthal field is mainly axisymmetric. The departures from axisymmetry represent, on average, $\sim 3\%$ of the total azimuthal flux. Owing to its relative weakness, the non-axisymmetric structure of the azimuthal field does not have a significant impact on where the emergences appear or on the amount of flux contained in them. We find that the probability of emergence is a function of the ratio between the flux content of an active region and the underlying azimuthal flux. [1]

4.1 Introduction

The magnetic activity of the Sun and other stars is a manifestation of their internal magnetic field, which is thought to be sustained by a hydromagnetic dynamo. In the case of the Sun, it is generally thought that the differential rotation in the convection zone generates the toroidal magnetic field out of the poloidal field, but where exactly this field is

---

[1] This chapter reproduces the article *Evolution of the Sun’s non-axisymmetric toroidal field* by D. Martin-Belda and R. H. Cameron, published in Astronomy & Astrophysics 603, A53 (2017), DOI 10.1051/0004-6361/201730509. Reproduced with permission of Astronomy & Astrophysics, © ESO. Contributions: D.M.B and R.C. designed the research. D.M.B carried out the research, analyzed the data and wrote the paper.

amplified and stored is still an open question (see, e.g., Charbonneau 2010). The mechanism for the regeneration of the poloidal field from the azimuthal component is less agreed upon, with modeling approaches falling mainly into two categories: the turbulent dynamo models and the Babcock-Leighton models.

In Babcock-Leighton models (Babcock 1961, Leighton 1969), the poloidal field is regenerated by the surface transport of the magnetic flux of decaying active regions. Newly emerged bipolar magnetic regions (BMRs) show a systematic tilt with respect to the E-W direction, with the preceding polarity (in the Sun's sense of rotation) appearing closer to the equator than the trailing polarity (Joy's law). In addition, the preceding polarity of a BMR emerging in a given hemisphere tends to be of the same sign as the polar field in that hemisphere at the beginning of the ongoing activity cycle (Hale's law). This facilitates the cross-equatorial transport of preceding polarity flux, and leads to the cancellation of the polar fields and the build-up of a new, reversed axial dipole, which is the source of azimuthal field for the new activity cycle.

Babcock-Leighton models have gained substantial support in recent years. Dasi-Espuig et al. (2010) found a strong correlation between the strength of a Babcock-Leighton type source term in a given cycle, calculated from the observed tilt angle of active regions, and the strength of the next cycle. Kitchatinov and Olemskoy (2011) found that the aggregate contribution of active regions to the poloidal field during one cycle and the strength of the global dipole at the end of the same cycle (as inferred from the AA index) also correlate closely. Wang et al. (2009) showed that the build-up of the polar fields during cycles 20 through 23 is consistent with the passive transport of magnetic flux by the observed surface flows. On the theoretical side, Cameron and Schüssler (2015) showed that the main source of net azimuthal flux in each hemisphere is the winding up of poloidal flux that is connected to the polar fields at the surface.

One of the key features of dynamo models is the formulation of the poloidal source term as a function of the azimuthal field. One often considered possibility in Babcock-Leighton flux transport models is that magnetic flux tubes are stored in an overshoot region at the base of the convection zone. These develop a magnetic buoyancy instability and rise through the convection zone to emerge at the surface in the form of BMRs. For a review on this topic, see, e.g., Fan (2009).

Alternatively, 3D numerical calculations indicate that persistent, coherent azimuthal magnetic structures can arise in a turbulent convection zone, owing to turbulent intermittency (Brown et al. 2010, Nelson et al. 2013, 2014). Moreover, the transport of magnetic flux to the surface can be achieved by means of convective upflows, which might be at least as relevant as magnetic buoyancy.

In this work we consider the evolution of the radially integrated azimuthal flux density as a function of longitude and latitude. Our aim is to infer the distribution and evolution of the sub-surface azimuthal flux from observable quantities in order to gain insight on its relation with the observed properties of active regions. To do so, we construct a model of the magnetic flux transport in the Sun, based on the Babcock-Leighton framework. The poloidal field source term is determined by observational data (synoptic magnetograms). The paper is structured as follows: in Sec. 4.2 we introduce and calibrate our model; in Sec. 4.3 we present and discuss our results; and in Sec. 4.4 we briefly summarize our conclusions. In the appendices we derive the equation for the evolution of the azimuthal flux density and other supplementary quantities in our model.

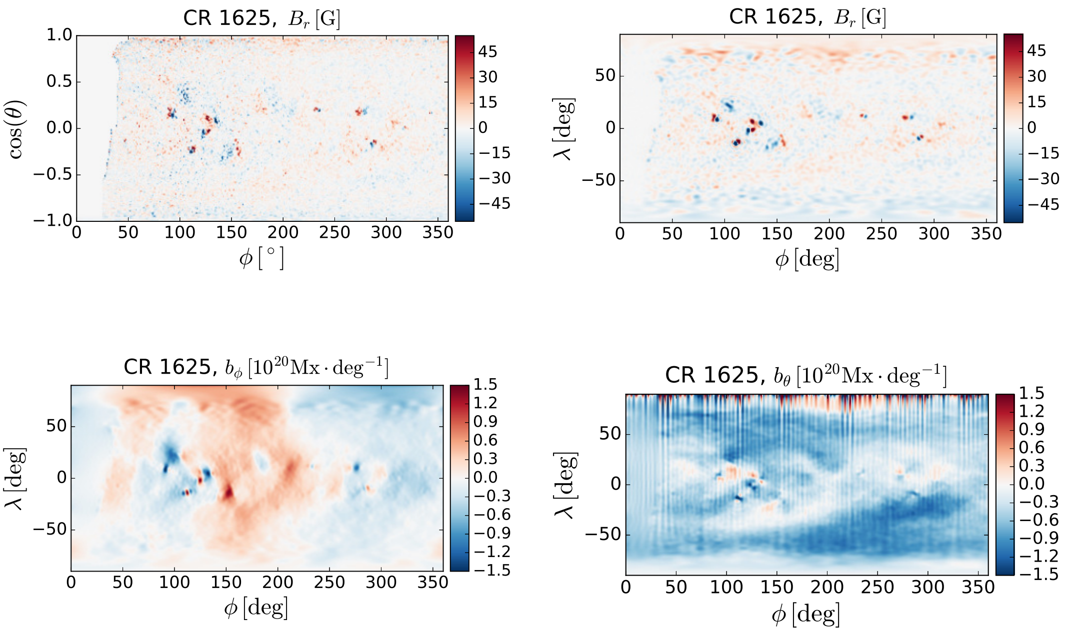

Figure 4.1: Initial condition of the simulations. *Top left:* Synoptic magnetogram corresponding to CR 1625. *Top right:* Synoptic magnetogram corresponding to CR 1625, remapped to an equiangular grid and resampled to the highest angular degree order, l, used to compute the potential field extrapolation. *Bottom left:* Radial integral of the azimuthal field across the convection zone, b_ϕ, extrapolated from the surface field. *Bottom right:* Radial integral of the θ component of the magnetic field across the convection zone, b_θ, extrapolated from the surface field. Red and blue indicate opposite polarities in all the maps.

4.2 Methods

4.2.1 Model

We consider a mean field approach based on horizontal averages,

$$B_j = \langle B_j \rangle + B_j', \tag{4.1}$$

where $j = \{r, \theta, \phi\}$,

$$\langle B_j \rangle(\theta, \phi) = \frac{\int_{\theta-\delta}^{\theta+\delta} \int_{\phi-\delta}^{\phi+\delta} B_j \sin\theta' \, \mathrm{d}\phi' \mathrm{d}\theta'}{\int_{\theta-\delta}^{\theta+\delta} \int_{\phi-\delta}^{\phi+\delta} \sin\theta' \, \mathrm{d}\phi' \mathrm{d}\theta'}, \tag{4.2}$$

and δ is the scale over which the average is performed. Using $\delta \sim 2 - 3^\circ$ is enough to ensure some scale separation with respect to the larger turbulence correlation lengths at the surface (those of supergranulation). In the remainder of the paper we drop the angle brackets for clarity, and refer to the j-th component of the averaged magnetic field by B_j.

Our model consists of two two-dimensional domains in the (ϕ, θ) plane, representing the surface of the Sun and the convection zone, respectively. The evolution of the surface magnetic field, assumed to be radial, is governed by the surface flux transport equation (DeVore et al. 1984):

$$\begin{aligned}\frac{\partial B_r}{\partial t} =& -\Omega_{R_\odot}(\theta)\frac{\partial B_r}{\partial \phi} - \frac{1}{R_\odot \sin\theta}\frac{\partial}{\partial\theta}\left[u_M(\theta)B_r\sin\theta\right] \\ &+ \frac{\eta_H}{R_\odot^2}\left[\frac{1}{\sin\theta}\frac{\partial}{\partial\theta}\left(\sin\theta\frac{\partial B_r}{\partial\theta}\right) + \frac{1}{\sin^2\theta}\frac{\partial^2 B_r}{\partial\phi^2}\right] \\ &+ S(\theta,\phi,t), \end{aligned} \tag{4.3}$$

where $\Omega_{R_\odot}$ is the differential rotation, u_M is the meridional flow and η_H is the surface diffusivity associated to the convective flows. The emergence of new flux is described by the source term $S(\theta, \phi, t)$.

The first term in Eq. (4.3) describes the transport of the surface field by the solar differential rotation. We use the differential rotation profile inferred by correlation tracking of magnetic features by Hathaway and Rightmire (2011):

$$\Omega_{R_\odot}(\theta) = 14.437 - 1.48\cos^2\theta - 2.99\cos^4\theta \quad [^\circ/\text{day}]. \tag{4.4}$$

The second term in Eq. (4.3) corresponds to the surface meridional flow. Following van Ballegooijen et al. (1998), we model the meridional flow as:

$$u_M = -11\cos(2\theta) \quad [\text{ms}^{-1}]. \tag{4.5}$$

This expression captures the main characteristics of the observed meridional flow (see Hathaway and Rightmire 2011).

The third term in Eq. (4.3) describes the dispersal of magnetic flux on the surface by means of random convective flows modeled as a diffusion process (see Leighton 1964, Martin-Belda and Cameron 2016). We use a surface diffusivity of $\eta_H = 250\,\text{km}^2\text{s}^{-1}$, as indicated by observations (Schrijver and Martin 1990, Jafarzadeh et al. 2014).

The source term $S(\theta, \phi, t)$ represents new emergences, and is built from synoptic magnetograms (see Sec. 4.2.2).

The azimuthal field in the convection zone is represented in our model by the azimuthal flux per unit colatitude, i.e.:

$$b_\phi = \int_{R_\text{b}}^{R_\odot} B_\phi r \mathrm{d}r. \tag{4.6}$$

In the above expression, R_b refers to the bottom of the convection zone and $R_\odot$ is the solar radius.

Following Cameron and Schüssler (2017), we make the following assumptions regarding the plasma flows and the structure of the internal magnetic field of the Sun:

1. The magnetic field is purely radial in the near-surface shear layer (NSSL), owing to strong downwards turbulent pumping.
2. The magnetic field does not penetrate the radiative interior.
3. The poloidal field does not penetrate the tachocline. This assumption of the model is partly justified by Spruit (2011), who noted that the tachocline cannot support large shear stresses, which would be present if the poloidal field did penetrate the tachocline.

4. The radial shear is negligible in the region between the tachocline and the NSSL. This is based on helioseismic inference of the rotation rate in the deep interior and the NSSL (Christensen-Dalsgaard and Schou 1988).

To derive an evolution equation for b_ϕ, we integrate the azimuthal component of the induction equation in radius. The resulting equation reads (see Appendix 4.A):

$$\begin{aligned}\frac{\partial b_\phi}{\partial t} &= R_\odot^2\,\Omega_{R_\odot}\sin\theta\, B_r \\ &+ b_\theta \sin\theta \left.\frac{\mathrm{d}\Omega}{\mathrm{d}\theta}\right|_{R_{\mathrm{NSSL}}} + \frac{\partial(b_\theta\sin\theta)}{\partial\theta}\Omega_{R_{\mathrm{NSSL}}} \\ &+ \frac{\eta_0}{R_\odot^2}\left[\frac{1}{\sin\theta}\frac{\partial}{\partial\theta}\left(\sin\theta\frac{\partial b_\phi}{\partial\theta}\right) + 2\frac{\cos\theta}{\sin^2\theta}\frac{\partial b_\theta}{\partial\phi} - \frac{b_\phi}{\sin^2\theta}\right. \\ &+ \left.\frac{1}{\sin^2\theta}\frac{\partial^2 b_\phi}{\partial\phi^2}\right] - \frac{1}{R_\odot}\frac{\partial(\bar{u}b_\phi)}{\partial\theta} + S_\phi(\theta,\phi,t),\end{aligned} \tag{4.7}$$

where $\Omega_{R_{\mathrm{NSSL}}}$ is the differential rotation at the bottom of the NSSL, $\bar{u}$ is an effective return meridional flow, η_0 is the effective diffusivity of the azimuthal field, $S_\phi(\theta,\phi,t)$ is a source term associated to flux emergence, and

$$b_\theta = \int_{R_{\mathrm{T}}}^{R_{\mathrm{NSSL}}} B_\theta r\,\mathrm{d}r. \tag{4.8}$$

In the above expression, R_{T} refers to the top of the tachocline and R_{NSSL} refers to the bottom of the NSSL. The quantity b_θ is calculated in terms of b_ϕ and B_r in Appendix 4.B.

The first three terms in Eq. (4.7) describe the generation of azimuthal flux by differential rotation and the azimuthal flux transport. Here, B_r is the radial field at the surface, which is constrained by observation and evolves according to Eq. (4.3). The radially integrated θ-component of the magnetic field, b_θ, can be obtained in terms of b_ϕ and B_r from the solenoidality condition $\nabla\cdot\mathbf{B} = \mathbf{0}$ (see Appendix 4.B). The differential rotation profile is evaluated at the bottom of the NSSL. The analysis of helioseismic data by Barekat et al. (2014) suggests that the radial shear in this layer is independent of latitude. Following these authors, we adopt

$$\Omega_{R_{\mathrm{NSSL}}}(\theta) = \Omega_{R_\odot}(\theta) + 0.53 \quad [^\circ/\mathrm{day}]. \tag{4.9}$$

The fourth term of Eq. (4.7) describes the turbulent diffusion of azimuthal flux. Following Cameron and Schüssler (2016), we assumed the following form for the diffusivity in the derivation of Eq. (4.7):

$$\eta(r) = \eta_0\frac{r^2}{R_\odot^2}, \tag{4.10}$$

where η_0 is a free parameter of our model. Cameron and Schüssler (2016) used the properties of the decay phase of the sunspot cycles to estimate $\eta_0 \sim 150 - 450\,\mathrm{km^2s^{-1}}$.

The fifth term corresponds to the advection of the azimuthal flux by an effective equatorward flow, which we model as

$$\bar{u} = u_0\cos(2\theta) \quad [\mathrm{ms^{-1}}], \tag{4.11}$$

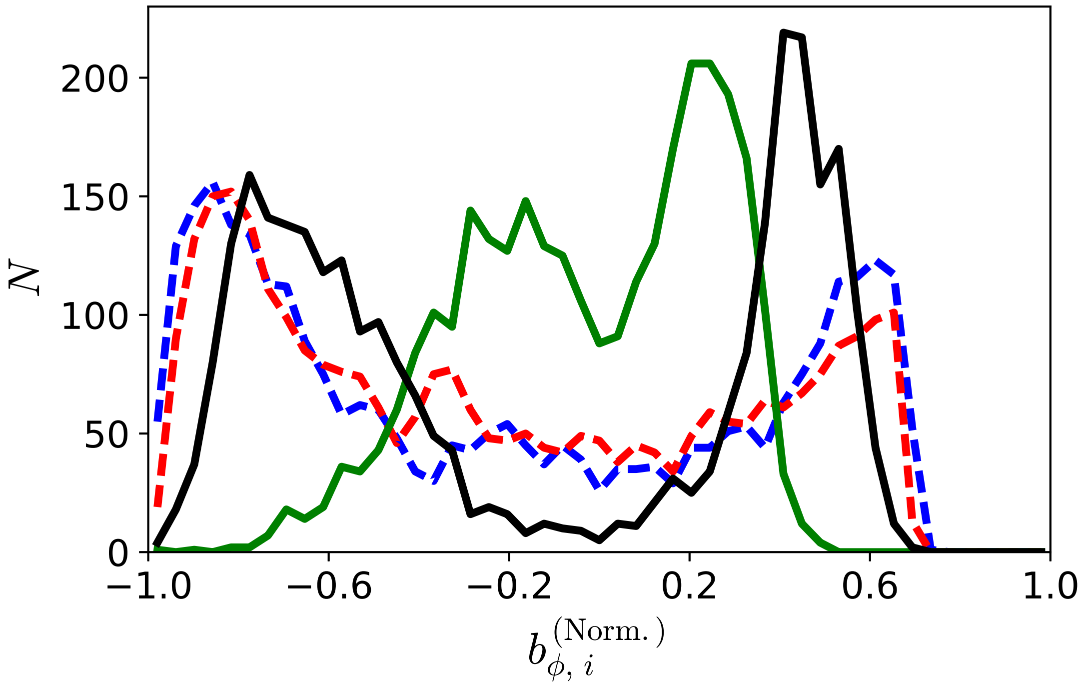

Figure 4.2: Number of emergences (N) as a function of the normalized underlying azimuthal flux density ($b_{\phi,i}^{(\mathrm{Norm.})}$). The different curves correspond to different choices of the free parameters. *Continuous black line:* $u_0 = 3\,\mathrm{m\,s^{-1}}$ and $\eta_0 = 100\,\mathrm{km^2s^{-1}}$. *Dashed blue line:* $u_0 = 5\,\mathrm{m\,s^{-1}}$ and $\eta_0 = 400\,\mathrm{km^2s^{-1}}$. *Dashed red line:* $u_0 = 1\,\mathrm{m\,s^{-1}}$ and $\eta_0 = 25\,\mathrm{km^2s^{-1}}$. *Continuous green line:* $u_0 = 6\,\mathrm{m\,s^{-1}}$ and $\eta_0 = 600\,\mathrm{km^2s^{-1}}$.

where u_0 is a free parameter of the model. This flow can correspond to a return meridional flow (Wang et al. 1991, Durney 1995) or equatorward pumping (Guerrero and de Gouveia Dal Pino 2008).

The solenoidality condition requires that the surface magnetic field connects to the sub-surface field. Hence, a source term in Eq. (4.7) is needed to ensure the connectivity of the surface field sources to the field in the convection zone. In order to calculate $S_\phi(\theta, \phi, t)$, we extrapolate the surface sources downward via a potential field solution (see Sec. 4.2.2).

Our model, therefore, consists of: (a) a two-dimensional domain representing the surface of the Sun, in which the (radial) surface field evolves according to Eq. (4.3); (b) a two-dimensional domain representing the convection zone, in which the radial integral of the azimuthal magnetic field evolves according to Eq. (4.7); and (c) the coupling of both domains through the emergences, represented by the source terms, and the solenoidality condition.

4.2.2 Treatment of the source terms

The source term in Eq. (4.3), which represents the emergence of flux on the solar surface, was calculated using SOLIS synoptic magnetograms. Let B_r^n be the radial magnetic

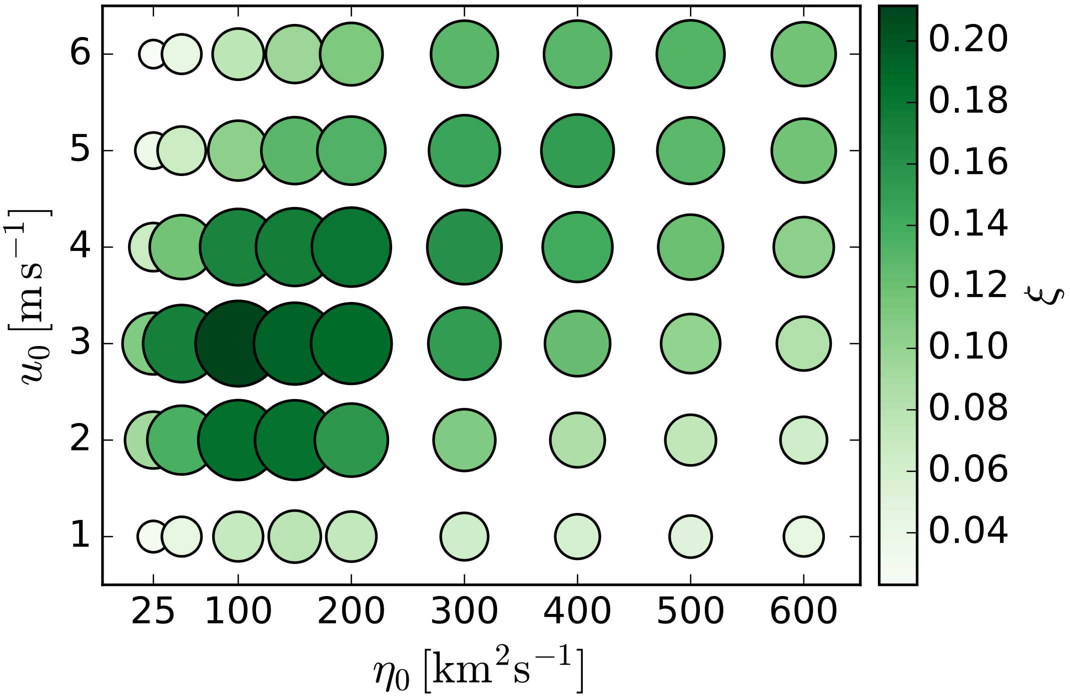

Figure 4.3: Distribution of the quantity $\xi = \sum_c N_c|b_{\phi,c}| \Big/ \sum_c N_c/|b_{\phi,c}|$ as a function of the parameters u_0 and η_0. Each circle represents a run. The size of each circle is proportional to the quantity ξ, which measures the adjustment of the run to our requirement that the simulated azimuthal flux lies underneath the observed active regions. For better visualization, we also encode the value of ξ in the colour of the circles.

field corresponding to carrington rotation (CR) n, as given by the corresponding synoptic magnetogram. The field associated with emergences during CR n is computed as

$$\Delta B_r(\theta, \phi, t^n) = B_r^n - \tilde{B}_r^n, \tag{4.12}$$

where $\tilde{B}_r^n$ is the magnetic field from the previous magnetogram evolved for one rotation using Eq. (4.3). This expression is related to the surface source term $S(\theta, \phi, t)$ through

$$\Delta B_r(\theta, \phi, t^n) = \int_{t^{n-1}}^{t^n} S(\theta, \phi, t)\,\mathrm{d}t. \tag{4.13}$$

In practice, we add ΔB_r to the simulated surface field every carrington rotation. The synoptic magnetograms are corrected by multiplying the positive values by a factor such that the resulting net magnetic flux on the surface is zero. Apart from describing flux emergences, the surface source term also corrects for the errors of the SFT model and errors in individual synoptic magnetograms.

The surface field B_r must connect with the field in the convection zone so that $\nabla \cdot \mathbf{B} = 0$ is maintained. The connectivity of the surface sources with the subsurface field is achieved through the source term in Eq. (4.7), which we calculate by performing a downwards potential field extrapolation of $\Delta B_r(\theta, \phi, t^n)$. Let $\Delta B_\phi(\theta, \phi, t^n)$ be the azimuthal component

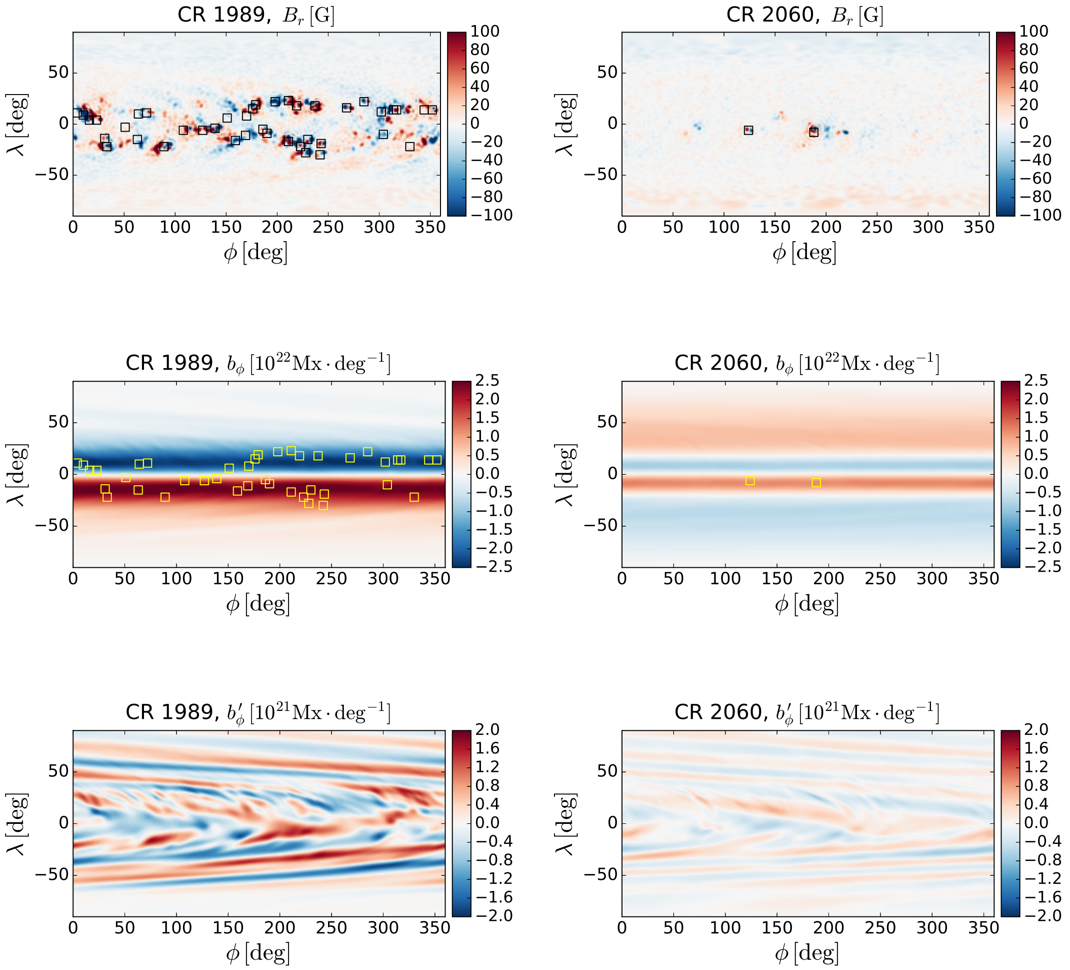

Figure 4.4: Surface field (B_r), azimuthal flux density (b_ϕ) and its non-axisymmetric component (b'_ϕ), for CR 1987 (close to the middle of cycle 23) and CR 2060 (near the end of that cycle). Red and blue represent opposite polarities. The squares on the top and middle rows represent observed emergence sites, extracted from the USAF/NOAA sunspot group database.

of the extrapolated field, and $\Delta b_\phi = \int_{R_b}^{R_\odot} \Delta B_\phi r \, \mathrm{d}r$. The source term in Eq. (4.7), $S_\phi(\theta, \phi, t^n)$, is related to $\Delta b_\phi(\theta, \phi, t^n)$ through

$$\Delta b_\phi(\theta, \phi, t^n) = \int_{t^{n-1}}^{t^n} S_\phi(\theta, \phi, t) \, \mathrm{d}t. \tag{4.14}$$

The extrapolated Δb_ϕ is added to the simulated b_ϕ every rotation, at the same time ΔB_r is added to the surface field.

The potential field extrapolation of $\Delta B_r(\theta, \phi, t^n)$ is more easily done using spherical harmonics, for which it is convenient to remap the synoptic magnetograms onto a grid equally spaced in θ, rather than in $\cos\theta$. The remapping prevents large errors near the poles, which arise from the poorer spatial resolution of the synoptic magnetograms at high latitudes. A discussion of this problem can be found in Tóth et al. (2011).

The value of the magnetic field at each point of the new equiangular grid is interpolated linearly from the magnetogram (old grid). The magnetic field at the poles is not known, which makes it appropriate to perform the interpolation in Fourier space by expanding

$$B_r(\theta, \phi, t^n) = \sum_m a_m(\theta, t^n) e^{im\phi}. \tag{4.15}$$

At the poles, regularity of B_r translates into the following boundary conditions for a_m:

$$\left.\frac{\partial a_0(\theta, t^n)}{\partial \theta}\right|_{\theta=0,\pi} = 0; \tag{4.16}$$

$$a_{m\neq 0}(\theta = 0, \pi; t^n) = 0. \tag{4.17}$$

The value of the Fourier coefficient at point of colatitude θ^* of the new grid is given by:

$$a_m(\theta^*, t^n) = a_m(\theta^-, t^n) + \frac{a_m(\theta^+, t^n) - a_m(\theta^-, t^n)}{\theta^+ - \theta^-}(\theta^* - \theta^-), \tag{4.18}$$

where θ^- and θ^+ are the points of the old grid adjacent to θ^* in the θ direction. For the points of the new grid that are located between the north pole and the northernmost grid point of the old grid, θ_0^+, Eqs. (4.16) and (4.17) lead to:

$$a_0(\theta^*, t^n) = a_0(\theta_0^+, t^n); \tag{4.19}$$

$$a_{m\neq 0}(\theta^*, t^n) = \frac{a_{m\neq 0}(\theta_0^+, t^n)}{\theta_0^+}\theta^*. \tag{4.20}$$

For grid points between the southernmost point of the old grid, θ_0^-, and the south pole, we have:

$$a_0(\theta^*, t^n) = a_0(\theta_0^-, t^n); \tag{4.21}$$

$$a_{m\neq 0}(\theta^*, t^n) = a_{m\neq 0}(\theta_0^-, t^n) - \frac{a_{m\neq 0}(\theta_0^-, t^n)}{\pi - \theta_0^-}(\theta^* - \theta_0^-). \tag{4.22}$$

Since the maximum angular order of the spherical harmonic analysis is limited by an anti-aliasing condition, the decomposition of B_r in spherical harmonics has the effect of slightly smoothing the magnetograms (see the top row of Fig. 4.1).

4.2.3 Setup and calibration

The initial condition of the simulations was computed as a potential field extrapolation of the first magnetogram of the series. This was taken at CR 1625, which corresponds to the end of cycle 20 in March, 1975. Figure 4.1 shows the raw magnetogram, the remapped version used to build the surface field source, and the extrapolated b_ϕ and b_θ. The sign of b_ϕ indicates the direction of the integrated azimuthal field. In our chosen coordinate system, a positive value of b_ϕ corresponds to azimuthal field pointing in the sense of rotation of the Sun. The sign of b_θ is predominantly negative, which reflects the sign of the axial dipole at this cycle minimum. The irregularities of b_θ near the north pole are probably related to the noise of the magnetogram, and diffuse very quickly once the simulation starts.

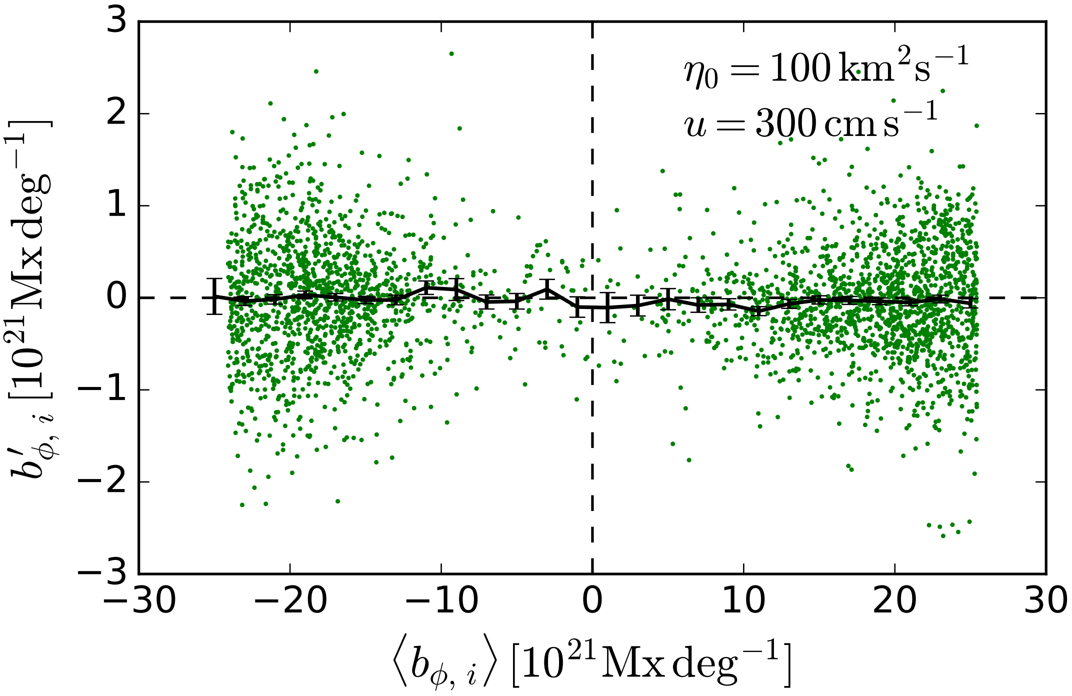

Figure 4.5: Non-axisymmetric component of the azimuthal flux underlying each emergence in cycle 23 ($b'_{\phi,i}$) versus its axisymmetric component ($\langle b_{\phi,i}\rangle$). The emergences are represented by green points. The black line represents the average of $b'_{\phi,i}$ over all emergences inside bins of $2 \cdot 10^{21}$ Mx deg^{-1} width. The error bars denote the standard error of the mean.

To calibrate the model, we required that the simulated azimuthal flux lie radially below the active regions observed on the Sun during cycle 22. We ran simulations with different values of the free parameters for cycles 21, 22 and 23. The strength of the return flow, u, was varied between 1 and 6 m s^{-1}, and the diffusivity η_0 was varied between 25 and 600 km^{2}s^{-1}. The simulations were let run for cycle 21 for initialization. The active region data (latitude, longitude and area) was extracted from the USAF/NOAA sunspot group database. We evaluate the azimuthal flux density underlying every emergence location, $b_{\phi,i} = b_\phi(\lambda_i, \phi_i)$, as close in time as possible, but always prior, to the time of observed maximum area of the active region (here the index i runs over the emergences). In the case of backside emergences, there can be a significant delay between these two times (as large as half a rotation). Note, however, that the change in azimuthal flux density on time scales shorter than one rotation is, in most cases, small as the non-axisymmetric component represents less than 3% of the total azimuthal flux density on average.

Figure 4.2 shows a few examples of the distribution of emergences according to their underlying azimuthal flux density for various combinations of parameters. Different values of η_0 give rise to different global magnitudes of the azimuthal flux density so, for easier comparison, we normalized $b_{\phi,i}$ to its maximum value in each simulation. The emergences were grouped in bins of width $4 \cdot 10^{-2}$ to reduce noise. The two peaks in the distribution of the active regions reflect the equatorial antisymmetry of the azimuthal flux.

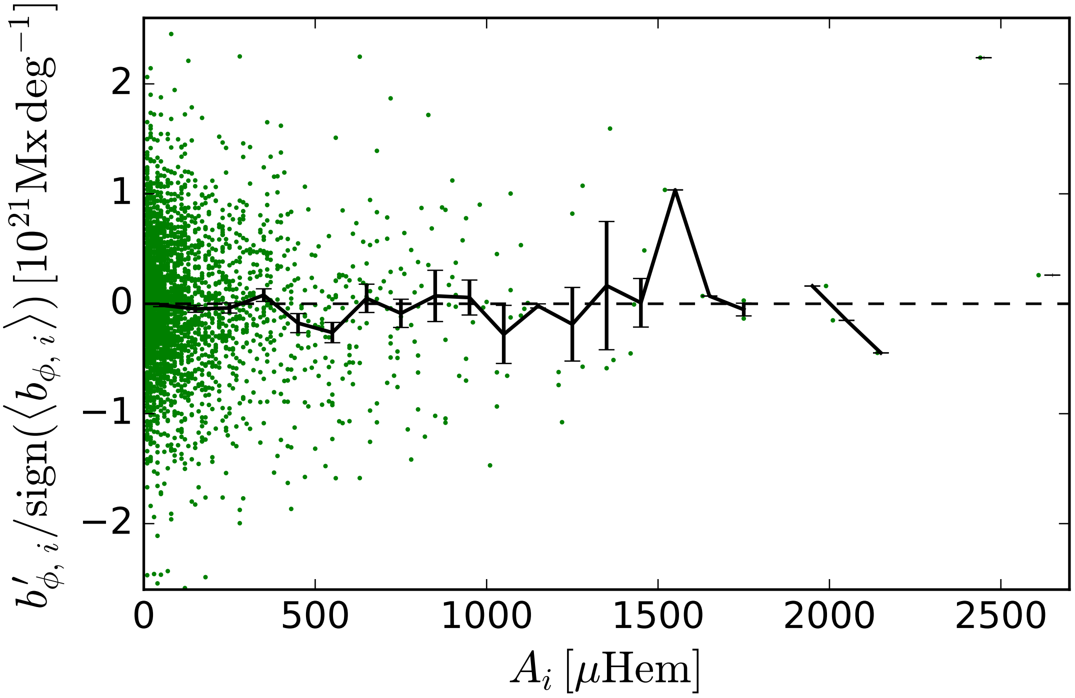

Figure 4.6: Excess azimuthal flux density above the azimuthal mean underlying each emergence in cycle 23 ($b'_{\phi,i}/\mathrm{sign}(\langle b_{\phi,i}\rangle)$) versus the area of the emergence (A_i). The emergences are represented by green points. The black line represents the average of $b'_{\phi,i}/\mathrm{sign}(\langle b_{\phi,i}\rangle)$ over all emergences inside area bins of width 100 μHem. The error bars denote the standard error of the mean.

In cycle 22, the underlying azimuthal flux is mainly positive in the northern hemisphere and negative in the southern hemisphere. The case with $u_0 = 3\,\mathrm{m\,s^{-1}}$ and $\eta_0 = 100\,\mathrm{km\,s^{-2}}$ (black line) corresponds best to the requirement that the simulated azimuthal flux be preferentially located underneath the emergences. In the other three cases, the two-peak structure is not so conspicuous, and there are more emergences where there is little or no simulated azimuthal flux.

To find the parameter combinations that yield two well-separated peaks, we considered the quantity

$$\xi = \frac{\sum_c N_c |b_{\phi,c}|}{\sum_c N_c / |b_{\phi,c}|}, \tag{4.23}$$

where c runs through the $b_{\phi,i}$ bins and $b_{\phi,c}$ is the mid-point of each bin. The value of ξ will be bigger for the simulations where the emergences occur farther away from the places where $b_\phi \sim 0$. Figure 4.3 shows the value of ξ for all test runs carried out. We find that the combination $u = 3\,\mathrm{m\,s^{-1}}$ and $\eta_0 = 100\,\mathrm{km^2 s^{-1}}$ maximizes ξ. These parameters are close to the range found by Cameron and Schüssler (2017) for the operation of the solar dynamo in an updated Leighton model. We proceed to the analysis of the data from cycle 23 using the azimuthal flux density maps generated in the simulation using the above parameter values.

4.3 Results for cycle 23

4.3.1 Angular distribution and evolution of azimuthal flux

Our analysis, which integrates the azimuthal field in the radial direction, allows us to infer the latitudinal and longitudinal structure of the sub-surface field from the observed surface field and large scale flows.

The top row of Fig. 4.4 shows the observed surface field near the activity maximum of Cycle 23 (CR 1987) and towards the end of that cycle (CR 2060). Squares indicate the emergence sites from the USAF/NOAA sunspot record. Some of the emergences do not seem to correspond to strong concentrations of magnetic field in the magnetograms, and some features in the magnetograms do not have a counterpart in the active region record. A possible cause for the mismatch in the first case could be the loss of information in the low-resolution magnetograms. In the second case, one possibility is that small sunspot groups that emerged on the far side of the Sun lacked spots when the region rotated onto the visible side. In this case, the flux content of the active regions is still present in the synoptic magnetogram, and therefore included in the source term.

The middle row of 4.4 shows the inferred maps of azimuthal flux density. The magnetic activity sits mainly on top of the azimuthal flux system. The azimuthal flux corresponding to CR 1987 presents a structure that is strongly axisymmetric and antisymmetric about the equator. The strongest concentration of azimuthal flux occurs at $\sim 15^\circ$ of latitude in both hemispheres. At CR 2060, most of the azimuthal flux has diffused and cancelled across the equator, and a new azimuthal flux system of opposite polarity, corresponding to the new cycle, has begun to develop at higher latitudes from the winding-up of the reversed poloidal field.

The bottom row of Fig. 4.4 shows the non-axisymmetric part of the integrated azimuthal field, calculated as $b'_\phi = b_\phi - \langle b_\phi \rangle$, where $\langle b_\phi \rangle$ is the azimuthal mean of b_ϕ. The magnitude of b'_ϕ represents, on average, $\sim 3\%$ of the total azimuthal flux density. This non-axisymmetric structure arises from the emergence process (which is the only non-axisymmetric ingredient of our model), and tends to diffuse away towards the end of the cycle, when the number of emergences is smaller.

4.3.2 Impact of the non-axisymmetric structure on the emergence process

In order to investigate whether the non-axisymmetric structure of the azimuthal flux influences the emergence process, we consider the deviation of the azimuthal flux density underlying each active region from the azimuthally averaged azimuthal flux density at the latitude of emergence, $\langle b_{\phi,i} \rangle$. The result is shown in Fig. 4.5. As seen in Sec. 4.2.3, the bipolar distribution of events reflects the strong antisymmetry of the azimuthal field about the equator. The active regions for which $\langle b_{\phi,i} \rangle < 0$ are mainly located in the north hemisphere, while those with $\langle b_{\phi,i} \rangle > 0$ correspond to the south hemisphere.

An influence of the non-axisymmetric structure of the azimuthal flux on the triggering of the emergence process would lead to a non-zero average value of $b'_{\phi,i}$ in each hemisphere. For example, if emergences at a given latitude tended to occur at longitudes where the azimuthal flux density is above the azimuthal mean, averaging $b'_{\phi,i}$ over all the

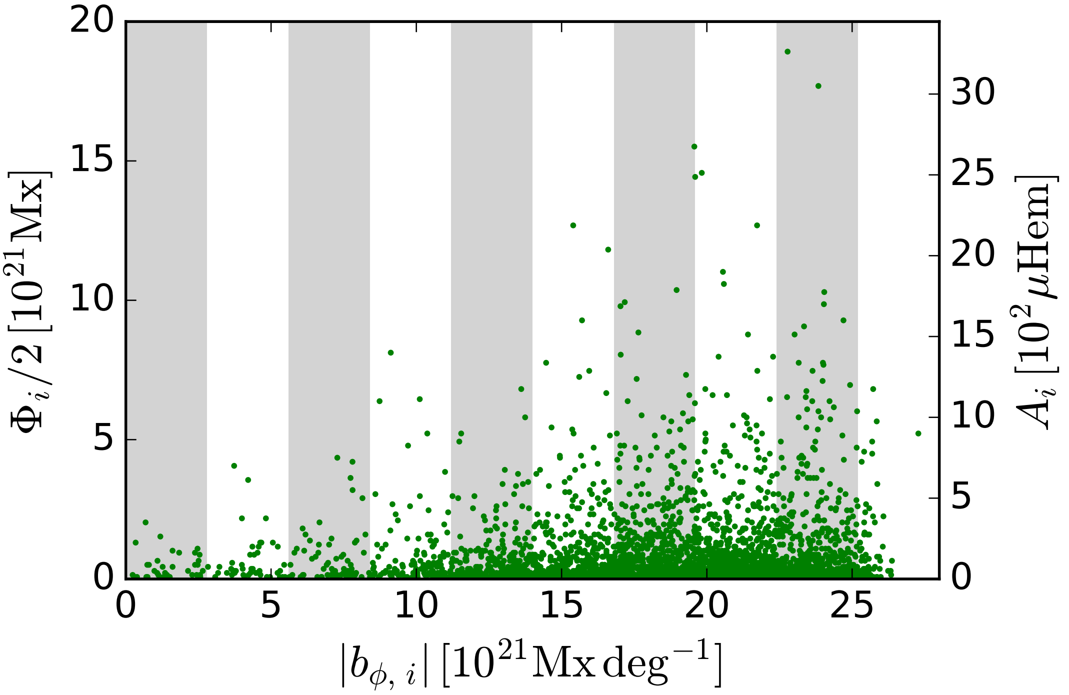

Figure 4.7: Emerged magnetic flux (Φ_i) versus underlying azimuthal flux density for the active regions recorded over cycle 23. Each green point represents an emergence. The stripes in the background indicate azimuthal flux density ranges. The area of the emergences is represented on the right-hand-side vertical axis.

emergences for which $\langle b_{\phi,i}\rangle > 0$ would yield a positive value. In the other hemisphere, the average $b'_{\phi,i}$ would be smaller than zero. Computing these averages yields

$$\bar{b}'_{\phi,i}(\langle b_{\phi,i}\rangle < 0) = (0.1 \pm 1.7)\cdot 10^{19}\mathrm{Mx\,deg}^{-1};$$
$$\bar{b}'_{\phi,i}(\langle b_{\phi,i}\rangle > 0) = (-4.5 \pm 1.4)\cdot 10^{19}\mathrm{Mx\,deg}^{-1}.$$

The average value of $b'_{\phi,i}$ in each hemisphere results very close to zero, in relative terms. Therefore, we do not find a significant correlation between the location of the emergence events and the departures from axisymmetry of the sub-surface azimuthal flux.

Next, we consider the possible influence of the non-axisymmetric structure on the active region areas. Figure 4.6 shows the excess of azimuthal flux density above the azimuthal average beneath each active region, $b'_{\phi,i}/\mathrm{sign}(\langle b_{\phi,i}\rangle)$, versus the active region area, A_i. Again, there is no significant deviation from zero, which suggests that the inferred non-axisymmetric structure of the sub-surface azimuthal flux is unrelated to the area of the emerged active region.

4.3.3 Relationship between azimuthal and emerged flux

Here we study the relationship between the flux contained in an active region and the azimuthal flux density underneath the emergence site. Figure 4.7 shows the flux of each

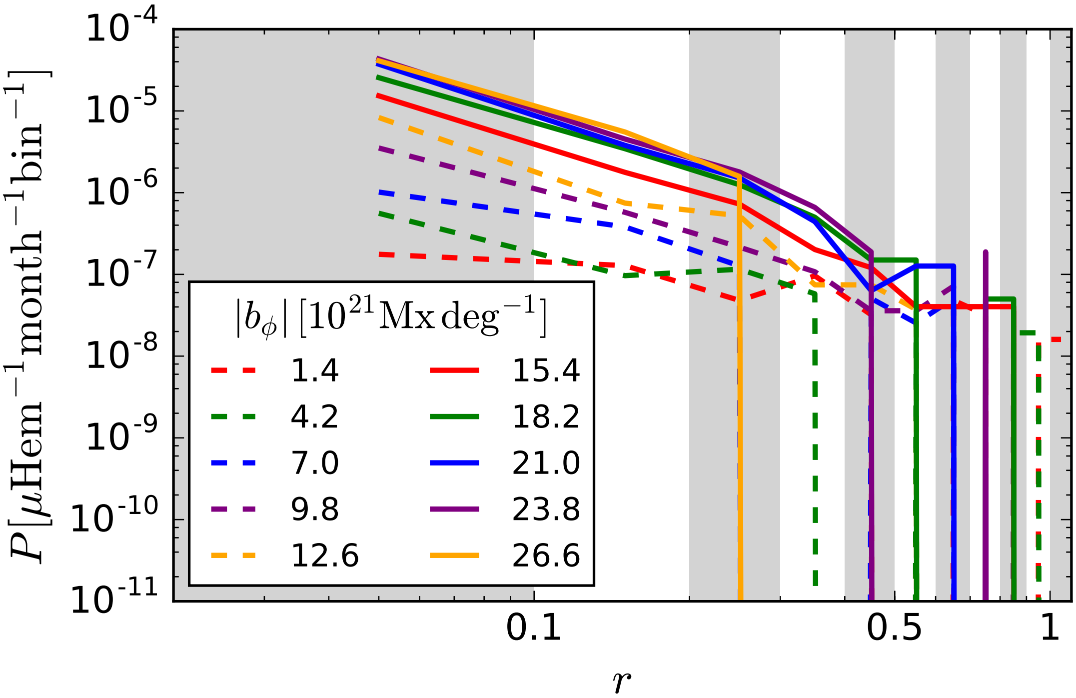

Figure 4.8: Probability of emergence per unit time, per unit area and per flux ratio bin (P) as a function of the ratio between the emerged flux and the azimuthal flux underlying the emergence site (r). The different colours correspond to the ranges of azimuthal flux density represented in Fig. 4.7. The numbers in the legend refer to the mid points of the azimuthal flux ranges. The stripes in the background indicate flux ratio bins of width 0.1.

active region in the sunspot group record at the time of maximum development, Φ_i, versus the unsigned underlying azimuthal flux density, $|b_{\phi,i}|$. Since we used SOLIS synoptic magnetograms to feed our simulations, we want to compare with fluxes comparable to those from SOLIS. The flux contained in each active region was calculated from its sunspot group area (obtained from the USAF/NOAA sunspot database) by using the cross-calibration factors in Table 2 of Muñoz-Jaramillo et al. (2015). The resulting relationship is $\Phi_i\,[\mathrm{Mx}] = 1.44 \cdot 10^{19} A_i\,[\mu\mathrm{Hem}]$. A factor 1/2 is introduced to account for the fact that the two polarities of the active region are part of a single Ω-shaped magnetic structure that crosses the solar surface twice.

Using the emergences shown in Fig. 4.7 we estimate the probability of emergence as a function of the ratio between the flux content of the emerged active region and the azimuthal flux available within one degree colatitude directly beneath it,

$$r_i = \frac{\Phi_i}{2\int_{1\,\mathrm{deg}} b_{\phi,i}\,\mathrm{d}\theta}. \tag{4.24}$$

To do so, we bin the data according to the ratio r_i (with bins of size 0.1) and the underlying azimuthal flux density, $b_{\phi,i}$ (with bins of size $2.8 \cdot 10^{21}\,\mathrm{Mx\,deg}^{-1}$). We thus obtain the number of emergences in each $(r_i, b_{\phi,i})$ bin. These are converted to a probability of emergence per unit area and unit time as a function of r by dividing the number of emer-

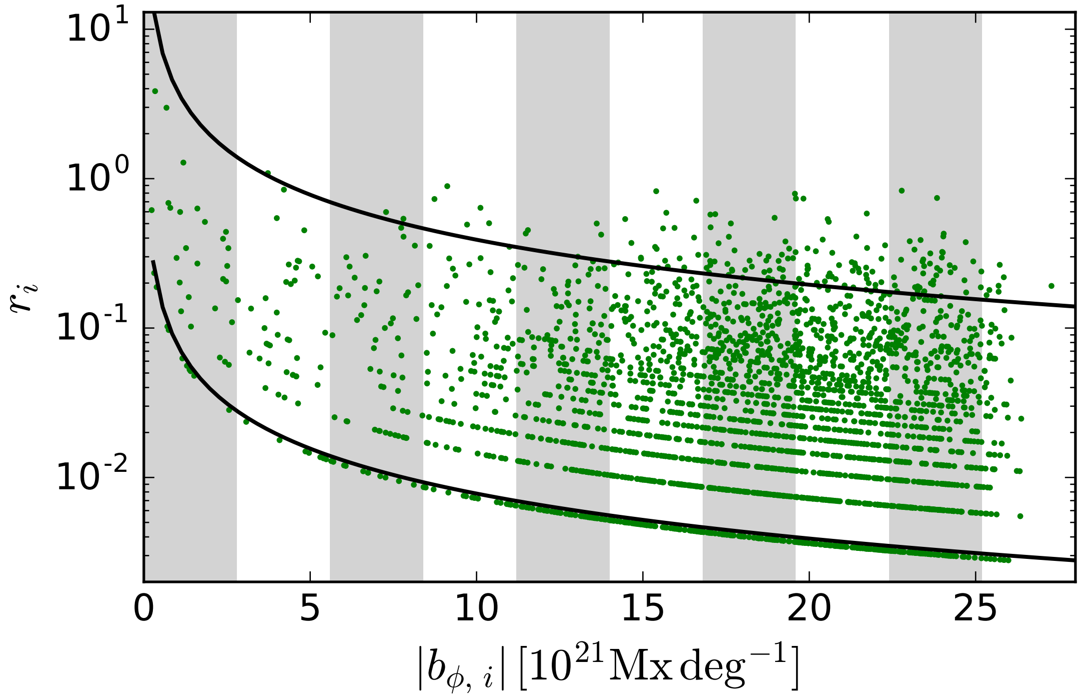

Figure 4.9: Ratio of the emerged flux to the underlying azimuthal flux (r_i) versus the azimuthal flux density beneath the emergence location for the active regions recorded during cycle 23. Each green point represents an emergence. The stripes in the background indicate azimuthal flux ranges. The two continuous curves separate ephemeral regions (below the lower curve), medium-sized regions (between the two curves) and large active regions (above the upper curve) by their flux content, according to Table 5.1 of Schrijver and Zwaan (2008). These fluxes have been converted from fluxes as given by Kitt Peak magnetograms to fluxes as given by SOLIS magnetograms by using the cross-calibration constants in Muñoz-Jaramillo et al. (2015).

gences in each $b_{\phi,i}$ bin by the cycle-averaged area of the subsurface domain covered by the corresponding azimuthal flux density range, and the duration of cycle 23. The resulting probability distributions are plotted in Fig. 4.8. Each coloured line corresponds to a different azimuthal flux density range. The distributions decrease rapidly for flux ratios greater than 0.4, suggesting that emergences whose flux comprises more than 40% of the azimuthal flux available underneath the emergence site are rare events.

The probability distributions shown in Fig. 4.8 seem to converge as we consider stronger azimuthal flux ranges. For the upper end of azimuthal flux ranges the probability of emergence is very similar. The lower probabilities obtained for emergences with smaller underlying azimuthal fluxes are due to a detection bias. To illustrate this, we plot the flux ratio of the emergences as a function of the underlying azimuthal flux density (Fig. 4.9). The two curves separate ephemeral, medium and large active regions. Active regions lying closer to the lower curve have a lifetime of days, while the lifetime of those closer to the upper curve approaches weeks. Many smaller active regions will not appear in the USAF/NOAA sunspot catalog, either because they emerge and decay on the backside of the Sun or because they do not have enough flux to form spots or pores. Thus, the probability distributions corresponding to lower azimuthal density fluxes (indicated by dashed lines in Fig. 4.8) are substantially affected by this detection bias. The fact that the less affected distributions (corresponding to larger amounts of underlying azimuthal flux) seem to converge suggests that the probability of emergence is a function of the ratio of the emerged flux and the azimuthal flux underlying the emergence site.

4.4 Summary and conclusion

We have provided a non-axisymmetric model of the magnetic flux transport in the Sun, based on the Babcock-Leighton dynamo framework. Using synoptic magnetograms as an input, we inferred the latitudinal and longitudinal distribution of azimuthal flux (per unit colatitude) and its evolution over three cycles.

We calibrated our model by requiring that the azimuthal flux in Cycle 22 in our simulations lied mainly radially underneath the activity belts. This led to a return meridional flow (and/or latitudinal pumping) having an amplitude of $u_0 = 3\,\mathrm{ms}^{-1}$ and an effective diffusivity for the azimuthal field of $\eta_0 = 100\,\mathrm{km}^2\mathrm{s}^{-1}$. These values are in the range found by Cameron and Schüssler (2017) for the operation of the solar dynamo.

The azimuthal flux system is highly axisymmetric and antisymmetric about the equator. The departures from axisymmetry represent, on average, approximately 3% of the azimuthal flux at a given location. We found that the non-axisymmetric structure does not have a significant impact on the location of the emergences or their observed properties. We also found that the probability of emergence is a function of the ratio of the flux content of the emerged active region and the underlying azimuthal flux.

Aknowledgements

D.M.B. acknowledges postgraduate fellowship of the International Max Planck Research School on Physical Processes in the Solar System and Beyond.

This work utilizes SOLIS data obtained by the NSO Integrated Synoptic Program (NISP), managed by the National Solar Observatory, which is operated by the Association of Universities for Research in Astronomy (AURA), Inc. under a cooperative agreement with the National Science Foundation.

This work was carried out in the context of Deutsche Forschungsgemeinschaft SFB 963 "Astrophysical Flow Instabilities and Turbulence" (Project A16).

We thank Manfred Schüssler for his valuable suggestions and his thorough revision of this manuscript.

Appendix

4.A The radial integral of the ϕ component of the induction equation

We derive the evolution equation for the azimuthal flux per unit colatitude,

$$b_\phi = \int_{R_\mathrm{b}}^{R_\odot} B_\phi r \,\mathrm{d}r, \tag{4.25}$$

under the assumptions specified in Sec. 4.2.1.

The ϕ component of the induction equation in spherical coordinates, (r, θ, ϕ), can be written as follows:

$$\begin{aligned} r\frac{\partial B_\phi}{\partial t} &= \frac{\partial}{\partial r}(ru_\phi B_r - ru_r B_\phi) - \frac{\partial}{\partial \theta}(u_\theta B_\phi - u_\phi B_\theta) \\ &\quad - \frac{1}{\sin\theta}\frac{\partial \eta}{\partial r}\frac{\partial B_r}{\partial \phi} + \frac{\partial}{\partial r}\left[\eta \frac{\partial}{\partial r}(rB_\phi)\right] \\ &\quad + \frac{\eta}{r}\left[\frac{1}{\sin\theta}\frac{\partial}{\partial\theta}\left(\sin\theta\frac{\partial B_\phi}{\partial\theta}\right) + \frac{1}{\sin^2\theta}\frac{\partial^2 B_\phi}{\partial\phi^2}\right. \\ &\quad \left. + \frac{2}{\sin\theta}\frac{\partial B_r}{\partial\phi} + \frac{2\cos\theta}{\sin^2\theta}\frac{\partial B_\theta}{\partial\phi} - \frac{B_\phi}{\sin^2\theta}\right], \end{aligned} \tag{4.26}$$

where we have assumed $\eta = \eta(r)$.

The first row of Eq. (4.26) includes the advection and shear terms. Integrating the shear terms radially, we obtain

$$\begin{aligned} \left.\frac{\partial b_\phi}{\partial t}\right|_\mathrm{shear} &= \int_{R_\mathrm{b}}^{R_\odot} \frac{\partial}{\partial r}(ru_\phi B_r)\,\mathrm{d}r + \int_{R_\mathrm{b}}^{R_\odot} \frac{\partial}{\partial\theta}(u_\phi B_\theta)\,\mathrm{d}r \\ &= \left[ru_\phi B_r\right]_{R_\mathrm{b}}^{R_\odot} + \frac{\partial}{\partial\theta}\int_{R_\mathrm{b}}^{R_\odot} u_\phi B_\theta\,\mathrm{d}r \\ &= R_\odot^2 \Omega_{R_\odot}\sin\theta B_r|_{R_\odot} + \frac{\partial}{\partial\theta}\int_{R_\mathrm{b}}^{R_\odot} r\Omega\sin\theta B_\theta\,\mathrm{d}r. \end{aligned} \tag{4.27}$$

In the above equation, $B_r|_{R_\mathrm{b}}$ vanishes since we assume that the magnetic field does not penetrate the radiative interior. With $B_\theta = 0$ in the NSSL, we can change the upper limit of integration of the integral in Eq. (4.27) to R_NSSL. The lower limit can be changed to the top of the tachocline, R_T, since there is no poloidal field in the convection zone part of the tachocline. In the new integration domain, Ω depends only on θ, so we can move it outside of the integral. This yields

$$
\begin{aligned}
\left.\frac{\partial b_\phi}{\partial t}\right|_{\text{shear}} &= R_\odot^2 \Omega_{R_\odot} \sin\theta B_r|_{R_\odot} \\
&+ \frac{\partial}{\partial\theta}\left(\Omega_{R_{\text{NSSL}}} \sin\theta \int_{R_{\text{T}}}^{R_{\text{NSSL}}} r B_\theta \,\mathrm{d}r\right) \\
&= R_\odot^2 \Omega_{R_\odot} \sin\theta B_r|_{R_\odot} \\
&+ b_\theta \sin\theta \left.\frac{\mathrm{d}\Omega}{\mathrm{d}\theta}\right|_{R_{\text{NSSL}}} + \frac{\partial(b_\theta \sin\theta)}{\partial\theta}\Omega_{R_{\text{NSSL}}},
\end{aligned}
\tag{4.28}
$$

where we have defined

$$
b_\theta = \int_{R_{\text{T}}}^{R_{\text{NSSL}}} B_\theta r \,\mathrm{d}r. \tag{4.29}
$$

The radial integral of the radial advection term in Eq. (4.26), $\int_{R_{\text{b}}}^{R_\odot} \partial(u_r B_\phi)/\partial r \,\mathrm{d}r$, vanishes since both u_r and B_ϕ vanish at R_{b} and $R_\odot$. Integrating the latitudinal advection term yields

$$
\begin{aligned}
\left.\frac{\partial b_\phi}{\partial t}\right|_{\text{adv.}} &= -\int_{R_{\text{b}}}^{R_\odot} \frac{\partial}{\partial\theta}(u_\theta B_\phi)\,\mathrm{d}r \\
&= -\frac{\partial}{\partial\theta}\int_{R_{\text{b}}}^{R_\odot} u_\theta B_\phi \,\mathrm{d}r \\
&= -\frac{\partial}{\partial\theta}\left[\frac{\bar{u}_R}{R_\odot}\int_{R_{\text{b}}}^{R_\odot} r B_\phi \,\mathrm{d}r\right] \\
&= -\frac{1}{R_\odot}\frac{\partial(\bar{u} b_\phi)}{\partial\theta},
\end{aligned}
\tag{4.30}
$$

where $\bar{u}$ is a weighted average of the meridional flow over the convection zone,

$$
\bar{u}(\theta) = R_\odot \overline{\left(\frac{u_\theta(r,\theta)}{r}\right)}. \tag{4.31}
$$

The diffusion term in Eq. (4.26) reads:

$$
\begin{aligned}
r\left.\frac{\partial B_\phi}{\partial t}\right|_{\text{diff.}} &= -\frac{1}{\sin\theta}\frac{\partial\eta}{\partial r}\frac{\partial B_r}{\partial\phi} + \frac{\partial}{\partial r}\left[\eta\frac{\partial}{\partial r}(rB_\phi)\right] \\
&+ \frac{\eta}{r}\left[\frac{1}{\sin\theta}\frac{\partial}{\partial\theta}\left(\sin\theta\frac{\partial B_\phi}{\partial\theta}\right) + \frac{1}{\sin^2\theta}\frac{\partial^2 B_\phi}{\partial\phi^2}\right. \\
&+ \left.\frac{2}{\sin\theta}\frac{\partial B_r}{\partial\phi} + \frac{2\cos\theta}{\sin^2\theta}\frac{\partial B_\theta}{\partial\phi} - \frac{B_\phi}{\sin^2\theta}\right].
\end{aligned}
\tag{4.32}
$$

The integral of the radial part, $\int_{R_{\text{b}}}^{R_\odot} \frac{\partial}{\partial r}\left[\eta\frac{\partial}{\partial r}(rB_\phi)\right] \mathrm{d}r$, vanishes since there is no diffusive flux transport across the boundaries. Following results of Cameron and Schüssler (2016), we assume an effective diffusivity of azimuthal flux

$$
\eta(r) = \eta_0 \frac{r^2}{R_\odot^2}. \tag{4.33}
$$

Substituting the above expression in Eq. (4.32) and integrating the rest of the diffusion terms leads to:

$$\begin{aligned}\left.\frac{\partial b_\phi}{\partial t}\right|_{\text{diff.}} = \frac{\eta_0}{R_\odot^2}\Bigg[&\frac{1}{\sin\theta}\frac{\partial}{\partial\theta}\left(\sin\theta\frac{\partial b_\phi}{\partial\theta}\right)\\ &+2\frac{\cos\theta}{\sin^2\theta}\frac{\partial b_\theta}{\partial\phi}-\frac{b_\phi}{\sin^2\theta}+\frac{1}{\sin^2\theta}\frac{\partial^2 b_\phi}{\partial\phi^2}\Bigg].\end{aligned} \tag{4.34}$$

Combining Eqs. (4.28), (4.30), and (4.34), and introducing the source term that is necessary to ensure connectivity with the surface sources, we obtain the final form of the equation:

$$\begin{aligned}\frac{\partial b_\phi}{\partial t} =& R_\odot^2\,\Omega_{R_\odot}\sin\theta\,B_r\\ &+b_\theta\sin\theta\left.\frac{\mathrm{d}\Omega}{\mathrm{d}\theta}\right|_{R_{\text{NSSL}}}+\frac{\partial(b_\theta\sin\theta)}{\partial\theta}\Omega_{R_{\text{NSSL}}}\\ &+\frac{\eta_0}{R_\odot^2}\Bigg[\frac{1}{\sin\theta}\frac{\partial}{\partial\theta}\left(\sin\theta\frac{\partial b_\phi}{\partial\theta}\right)+2\frac{\cos\theta}{\sin^2\theta}\frac{\partial b_\theta}{\partial\phi}-\frac{b_\phi}{\sin^2\theta}\\ &+\frac{1}{\sin^2\theta}\frac{\partial^2 b_\phi}{\partial\phi^2}\Bigg]-\frac{1}{R_\odot}\frac{\partial(\bar{u}b_\phi)}{\partial\theta}+S_\phi(\theta,\phi,t).\end{aligned} \tag{4.35}$$

To simplify the notation and keep consistency with Eq. (4.3), we write B_r instead of $B_r|_{R_\odot}$ to refer to the radial field at the surface.

4.B Calculation of b_θ

The quantity b_θ can be calculated in terms of b_ϕ and $B_r|_{R_\odot}$ from the solenoidality condition, $\nabla\cdot\mathbf{B}=0$. Writing the divergence operator in spherical coordinates leads to

$$r\frac{\partial(B_\theta\sin\theta)}{\partial\theta} = -\sin\theta\frac{\partial(r^2B_r)}{\partial r}-r\frac{\partial B_\phi}{\partial\phi}. \tag{4.36}$$

Integrating over the convection zone and using the definitions (4.25) and (4.29) we obtain

$$\begin{aligned}\frac{\partial(b_\theta\sin\theta)}{\partial\theta} &= -\sin\theta[r^2B_r]_{R_{\text{b}}}^{R_\odot}-\frac{\partial b_\phi}{\partial\phi}\\ &= -\sin\theta R_\odot^2B_r|_{R_\odot}-\frac{\partial b_\phi}{\partial\phi},\end{aligned} \tag{4.37}$$

where we have used $B_r|_{R_{\text{b}}}=0$ and $B_\theta|_{R_{\text{b}}<r<R_{\text{T}}}=B_\theta|_{R_{\text{NSSL}}<r<R_\odot}=0$. Integrating now in θ yields

$$b_\theta = -\frac{1}{\sin\theta}\left(\int_0^\theta\sin\theta' R_\odot^2B_r\,\mathrm{d}\theta'+\int_0^\theta\frac{\partial b_\phi}{\partial\phi}\,\mathrm{d}\theta'\right), \tag{4.38}$$

where, again, B_r denotes now the surface field.

5 Conclusions and future work

In this thesis, we considered the non-axisymmetric transport of magnetic flux in the Sun, with a focus on its role on the global dynamo. In the fisrt two papers (Chs. 2 and 3), we studied the way the near-surface, converging flows around active regions, which are non-axisymmetric, affect the build-up of the global axial dipole moment, defined as

$$D_M = \sqrt{\frac{3}{4\pi}} \int_0^{2\pi} \int_0^{\pi} B_r(\phi, \theta) \cos\theta \sin\theta \, \mathrm{d}\theta \mathrm{d}\phi, \tag{5.1}$$

where B_r is the surface magnetic field, assumed to be purely radial. The axial dipole moment at the end of a given cycle is a good precursor of the strength of the next cycle (Upton and Hathaway 2014).

The contribution of a single BMR to the global axial dipole in the presence of surface diffusion and a meridional flow was studied by Wang and Sheeley (1991). This contribution evolves on a time scale of years, and depends strongly on the speed of the meridional flow and latitude of emergence. An axially symmetric azimuthal flow has no impact on D_M, so these authors do not consider differential rotation. In the presence of inflows, however, it is necessary to include the differential rotation in the analysis of the surface transport of flux. We found that the axial dipole moment of a BMR normally decreases with respect to its initial value over the first month of evolution. When the orientation of the BMR is sufficiently close to the E-W direction, the interplay between the inflows, the differential rotation and the diffusion leads to an increased contribution to the global axial dipole (Martin-Belda and Cameron 2016).

We also studied the way inflows affect the axial dipole moment over a full cycle. The aggregate action of the inflows decreases the axial dipole moment at the end of a cycle, compared to a no-inflows scenario. The magnitude of this decrease depends on the activity level: the stronger the cycle, the larger the reduction. This dependence can provide a saturation mechanism for the global dynamo (Martin-Belda and Cameron 2017a).

In the third paper, we used a flux-transport model based on the updated BL model of Cameron and Schüssler (2017) to infer maps of the sub-surface toroidal flux density from synoptic magnetrograms. The non-axisymmetric structure arising from the emergence process is, on average, weak compared to the axisymmetric part. Owing to its weakness, it plays a negligible role on the flux emergence process. We found that the probability of emergence per unit surface area and per unit time is a function of the ratio between the BMR's flux contents and the amount of toroidal flux underlying the emergence site (Martin-Belda and Cameron 2017b).

In future work, the model of Spruit (2003) for the inflows can be tested. The inflows could be reproduced by using radiative MHD simulations of near-surface magnetoconvection. A parameter study could help in understanding the way the inflows respond to strong magnetic fields. A parametrization of the inflows based on this study could possibly solve the clumping problem discussed in Ch. 3.

Another possible line of work is to construct an FTD model of the solar dynamo combining the results presented in this thesis. Including the inflows towards active regions requires that the treatment of the surface transport of magnetic flux be non-axisymmetric. The departures from axial symmetry in the toroidal flux system are, however, small. An axisymmetric treatment of the evolution of the toroidal field would thus be a good first approximation. Both domains would be coupled by a poloidal source term based on the probabilities of emergence per unit time and unit surface area inferred from observations in Ch. 4. By running simulations spanning many cycles, we could ascertain the relative importance of the inflows and the BMR tilt scattering in the modulation of the solar cycle.

A third possibility is to construct a fully non-axisymmetric dynamo model to study the effects of varying the transport parameters and the emergence rate. This may help to determine if the departures from axial symmetry play a more important role on the global dynamos in other solar-like stars.

Bibliography

H. Alfvén. Existence of Electromagnetic-Hydrodynamic Waves. *Nature*, 150:405–406, October 1942. doi:10.1038/150405d0.

K. Augustson, A. S. Brun, M. Miesch, and J. Toomre. Grand Minima and Equatorward Propagation in a Cycling Stellar Convective Dynamo. *ApJ*, 809:149, August 2015. doi:10.1088/0004-637X/809/2/149.

H. D. Babcock. The Sun's Polar Magnetic Field. *ApJ*, 130:364, September 1959. doi:10.1086/146726.

H. D. Babcock and W. C. Livingston. Changes in the Sun's Polar Magnetic Field. *Science*, 127:1058, May 1958.

H. W. Babcock. The Topology of the Sun's Magnetic Field and the 22-YEAR Cycle. *ApJ*, 133:572, March 1961. doi:10.1086/147060.

H. W. Babcock and H. D. Babcock. Mapping the Magnetic Fields of the Sun. *PASP*, 64: 282, December 1952. doi:10.1086/126495.

H. W. Babcock and H. D. Babcock. The Sun's Magnetic Field, 1952-1954. *ApJ*, 121:349, March 1955. doi:10.1086/145994.

A. Barekat, J. Schou, and L. Gizon. The radial gradient of the near-surface shear layer of the Sun. *A&A*, 570:L12, October 2014. doi:10.1051/0004-6361/201424839.

I. Baumann, D. Schmitt, M. Schüssler, and S. K. Solanki. Evolution of the large-scale magnetic field on the solar surface: A parameter study. *A&A*, 426:1075–1091, November 2004. doi:10.1051/0004-6361:20048024.

L. Biermann. Der gegenwärtige Stand der Theorie konvektiver Sonnenmodelle. *Vierteljahresschrift der Astronomischen Gesellschaft*, 76:194–200, 1941.

F. H. Bigelow. The solar corona. *Smithsonian Institute, Washington*, 1889.

A. Bonanno, D. Elstner, G. Rüdiger, and G. Belvedere. Parity properties of an advection-dominated solar alpha ^{2} Omega-dynamo. *A&A*, 390:673–680, August 2002. doi:10.1051/0004-6361:20020590.

S. I. Braginskii. Self-excitation of a magnetic field during the motion of a highly conducting fluid. *Zh. Eksperim. i. Teor. Fiz.*, Vol: 47, September 1964.

B. P. Brown, M. K. Browning, A. S. Brun, M. S. Miesch, and J. Toomre. Persistent Magnetic Wreaths in a Rapidly Rotating Sun. *ApJ*, 711:424–438, March 2010. doi:10.1088/0004-637X/711/1/424.

D. Brunt. The General Magnetic Field of the Sun. *Astronomische Nachrichten*, 196:169, October 1913. doi:10.1002/asna.19131961302.

E. Bullard and H. Gellman. Homogeneous Dynamos and Terrestrial Magnetism. *Philosophical Transactions of the Royal Society of London Series A*, 247:213–278, November 1954. doi:10.1098/rsta.1954.0018.

P. Caligari, F. Moreno-Insertis, and M. Schussler. Emerging flux tubes in the solar convection zone. 1: Asymmetry, tilt, and emergence latitude. *ApJ*, 441:886–902, March 1995. doi:10.1086/175410.

P. Caligari, M. Schüssler, and F. Moreno-Insertis. Emerging Flux Tubes in the Solar Convection Zone. II. The Influence of Initial Conditions. *ApJ*, 502:481–492, July 1998. doi:10.1086/305875.

R. H. Cameron and M. Schüssler. Are the strengths of solar cycles determined by converging flows towards the activity belts? *A&A*, 548:A57, December 2012. doi:10.1051/0004-6361/201219914.

R. H. Cameron and M. Schüssler. The crucial role of surface magnetic fields for the solar dynamo. *Science*, 347:1333–1335, March 2015. doi:10.1126/science.1261470.

R. H. Cameron and M. Schüssler. The turbulent diffusion of toroidal magnetic flux as inferred from properties of the sunspot butterfly diagram. *A&A*, 591:A46, June 2016. doi:10.1051/0004-6361/201527284.

R. H. Cameron and M. Schüssler. An update of Leighton's solar dynamo model. *A&A*, 599:A52, March 2017. doi:10.1051/0004-6361/201629746.

R. H. Cameron, J. Jiang, D. Schmitt, and M. Schüssler. Surface Flux Transport Modeling for Solar Cycles 15-21: Effects of Cycle-Dependent Tilt Angles of Sunspot Groups. *ApJ*, 719:264–270, August 2010. doi:10.1088/0004-637X/719/1/264.

R. H. Cameron, A. Vögler, and M. Schüssler. Decay of a simulated mixed-polarity magnetic field in the solar surface layers. *A&A*, 533:A86, September 2011. doi:10.1051/0004-6361/201116974.

R. H. Cameron, D. Schmitt, J. Jiang, and E. Işık. Surface flux evolution constraints for flux transport dynamos. *A&A*, 542:A127, June 2012. doi:10.1051/0004-6361/201218906.

R. C. Carrington. On the Distribution of the Solar Spots in Latitudes since the Beginning of the Year 1854, with a Map. *MNRAS*, 19:1–3, November 1858. doi:10.1093/mnras/19.1.1.

R. C. Carrington. *Observations of the spots on the sun: from November 9, 1853, to March 24, 1861, made at Redhill.* Williams and Norgate, 1863.

P. Charbonneau. Dynamo models of the solar cycle. *Living Reviews in Solar Physics*, 7 (3), 2010. doi:10.12942/lrsp-2010-3.

P. Charbonneau. *Solar and Stellar Dynamos: Saas-Fee Advanced Course 39*. Springer-Verlag Berlin Heidelberg, 2013. doi:10.1007/978-3-642-32093-4.

P. Chatterjee and A. R. Choudhuri. On Magnetic Coupling Between the Two Hemispheres in Solar Dynamo Models. *Sol. Phys.*, 239:29–39, December 2006. doi:10.1007/s11207-006-0201-6.

P. Chatterjee, D. Nandy, and A. R. Choudhuri. Full-sphere simulations of a circulation-dominated solar dynamo: Exploring the parity issue. *A&A*, 427:1019–1030, December 2004. doi:10.1051/0004-6361:20041199.

A. R. Choudhuri. Prospects for predicting cycle 24. *Journal of Astrophysics and Astronomy*, 29:41–47, March 2008. doi:10.1007/s12036-008-0005-2.

A. R. Choudhuri, M. Schussler, and M. Dikpati. The solar dynamo with meridional circulation. *A&A*, 303:L29, November 1995.

J. Christensen-Dalsgaard and J. Schou. Differential rotation in the solar interior. In E. J. Rolfe, editor, *Seismology of the Sun and Sun-Like Stars*, volume 286 of *ESA Special Publication*, December 1988.

D. H. Clark and F. R. Stephenson. An Interpretation of the Pre-Telescopic Sunspot Records from the Orient. *QJRAS*, 19:387, December 1978.

T. G. Cowling. The magnetic field of sunspots. *MNRAS*, 94:39–48, November 1933. doi:10.1093/mnras/94.1.39.

T. G. Cowling. On the Sun's general magnetic field. *MNRAS*, 105:166, 1945. doi:10.1093/mnras/105.3.166.

T. G. Cowling. The growth and decay of the sunspot magnetic field. *MNRAS*, 106:218, 1946. doi:10.1093/mnras/106.3.218.

M. Dasi-Espuig, S. K. Solanki, N. A. Krivova, R. Cameron, and T. Peñuela. Sunspot group tilt angles and the strength of the solar cycle. *A&A*, 518:A7, July 2010. doi:10.1051/0004-6361/201014301.

M. L. De Rosa and C. S. Schrijver. Consequences of large-scale flows around active regions on the dispersal of magnetic field across the solar surface. In *Proceedings of SOHO 18/GONG 2006/HELAS I, Beyond the spherical Sun*, volume 624, page 12, 2006.

C. R. DeVore, J. P. Boris, and N. R. Sheeley, Jr. The concentration of the large-scale solar magnetic field by a meridional surface flow. *Sol. Phys.*, 92:1–14, May 1984. doi:10.1007/BF00157230.

M. Dikpati and P. Charbonneau. A Babcock-Leighton Flux Transport Dynamo with Solar-like Differential Rotation. *ApJ*, 518:508–520, June 1999. doi:10.1086/307269.

S. D'Silva and A. R. Choudhuri. A theoretical model for tilts of bipolar magnetic regions. *A&A*, 272:621, May 1993.

L. D. V. Duarte, J. Wicht, M. K. Browning, and T. Gastine. Helicity inversion in spherical convection as a means for equatorward dynamo wave propagation. *MNRAS*, 456:1708–1722, February 2016. doi:10.1093/mnras/stv2726.

B. R. Durney. On a Babcock-Leighton dynamo model with a deep-seated generating layer for the toroidal magnetic field. *Sol. Phys.*, 160:213–235, September 1995. doi:10.1007/BF00732805.

W. M. Elsasser. On the origin of the earth's magnetic field. *Phys. Rev.*, 55:489–498, Mar 1939. doi:10.1103/PhysRev.55.489.

W. M. Elsasser. The earth's interior and geomagnetism. *Rev. Mod. Phys.*, 22:1–35, Jan 1950. doi:10.1103/RevModPhys.22.1.

Y. Fan. Magnetic Fields in the Solar Convection Zone. *Living Reviews in Solar Physics*, 6:4, December 2009. doi:10.12942/lrsp-2009-4.

Y. Fan. Magnetic fields in the solar convection zone. *Living Reviews in Solar Physics*, 6 (4), 2009. doi:10.12942/lrsp-2009-4.

Y. Fan, G. H. Fisher, and A. N. McClymont. Dynamics of emerging active region flux loops. *ApJ*, 436:907–928, December 1994. doi:10.1086/174967.

M. Ghizaru, P. Charbonneau, and P. K. Smolarkiewicz. Magnetic Cycles in Global Large-eddy Simulations of Solar Convection. *ApJ*, 715:L133–L137, June 2010. doi:10.1088/2041-8205/715/2/L133.

L. Gizon. Helioseismology of Time-Varying Flows Through The Solar Cycle. *Sol. Phys.*, 224:217–228, October 2004. doi:10.1007/s11207-005-4983-9.

L. Gizon and M. Rempel. Observation and modeling of the solar-cycle variation of the meridional flow. *Sol. Phys.*, 251(1-2):241–250, 2008. ISSN 0038-0938. doi:10.1007/s11207-008-9162-3.

L. Gizon, T. L. Duvall, Jr., and R. M. Larsen. Probing Surface Flows and Magnetic Activity with Time-Distance Helioseismology. In P. Brekke, B. Fleck, and J. B. Gurman, editors, *Recent Insights into the Physics of the Sun and Heliosphere: Highlights from SOHO and Other Space Missions*, volume 203 of *IAU Symposium*, page 189, 2001.

L. Gizon, A. C. Birch, and H. C. Spruit. Local Helioseismology: Three-Dimensional Imaging of the Solar Interior. *Annual Review of Astronomy and Astrophysics*, 48:289–338, September 2010. doi:10.1146/annurev-astro-082708-101722.

A. Goel and A. R. Choudhuri. The hemispheric asymmetry of solar activity during the last century and the solar dynamo. *Research in Astronomy and Astrophysics*, 9:115–126, January 2009. doi:10.1088/1674-4527/9/1/010.

I. González Hernández, R. Howe, R. Komm, and F. Hill. Meridional Circulation During the Extended Solar Minimum: Another Component of the Torsional Oscillation? *ApJ*, 713:L16–L20, April 2010. doi:10.1088/2041-8205/713/1/L16.

G. Guerrero and E. M. de Gouveia Dal Pino. Turbulent magnetic pumping in a Babcock-Leighton solar dynamo model. *A&A*, 485:267–273, July 2008. doi:10.1051/0004-6361:200809351.

D. A. Haber, B. W. Hindman, J. Toomre, R. S. Bogart, R. M. Larsen, and F. Hill. Evolving Submerged Meridional Circulation Cells within the Upper Convection Zone Revealed by Ring-Diagram Analysis. *ApJ*, 570:855–864, May 2002. doi:10.1086/339631.

G. E. Hale. On the Probable Existence of a Magnetic Field in Sun-Spots. *ApJ*, 28:315, November 1908a. doi:10.1086/141602.

G. E. Hale. Solar Vortices. *PASP*, 20:203, August 1908b. doi:10.1086/121821.

G. E. Hale. Preliminary Results of an Attempt to Detect the General Magnetic Field of the Sun. *ApJ*, 38:27, July 1913. doi:10.1086/142013.

G. E. Hale. Solar Magnetism. *Nature*, 136:703–705, November 1935. doi:10.1038/136703a0.

G. E. Hale and S. B. Nicholson. The Law of Sun-Spot Polarity. *ApJ*, 62:270, November 1925. doi:10.1086/142933.

G. E. Hale, F. Ellerman, S. B. Nicholson, and A. H. Joy. The Magnetic Polarity of Sun-Spots. *ApJ*, 49:153, April 1919. doi:10.1086/142452.

D. H. Hathaway. The Solar Cycle. *Living Reviews in Solar Physics*, 12:4, September 2015. doi:10.1007/lrsp-2015-4.

D. H. Hathaway and L. Rightmire. Variations in the Axisymmetric Transport of Magnetic Elements on the Sun: 1996-2010. *ApJ*, 729:80, March 2011. doi:10.1088/0004-637X/729/2/80.

H. Hotta and T. Yokoyama. Solar Parity Issue with Flux-transport Dynamo. *ApJ*, 714: L308–L312, May 2010. doi:10.1088/2041-8205/714/2/L308.

H. Hotta, M. Rempel, and T. Yokoyama. Large-scale magnetic fields at high Reynolds numbers in magnetohydrodynamic simulations. *Science*, 351:1427–1430, March 2016. doi:10.1126/science.aad1893.

R. Howard. Evidence for large-scale velocity features on the sun. *ApJ*, 228:L45–L50, February 1979. doi:10.1086/182900.

R. Howard and B. J. Labonte. The sun is observed to be a torsional oscillator with a period of 11 years. *ApJ*, 239:L33–L36, July 1980. doi:10.1086/183286.

E. Işık. A Mechanism for the Dependence of Sunspot Group Tilt Angles on Cycle Strength. *ApJ*, 813:L13, November 2015. doi:10.1088/2041-8205/813/1/L13.

S. Jafarzadeh, R. H. Cameron, S. K. Solanki, A. Pietarila, A. Feller, A. Lagg, and A. Gandorfer. Migration of Ca II H bright points in the internetwork. *A&A*, 563:A101, March 2014. doi:10.1051/0004-6361/201323011.

J. Jiang, P. Chatterjee, and A. R. Choudhuri. Solar activity forecast with a dynamo model. *MNRAS*, 381:1527–1542, November 2007. doi:10.1111/j.1365-2966.2007.12267.x.

J. Jiang, E. Işik, R. H. Cameron, D. Schmitt, and M. Schüssler. The Effect of Activity-related Meridional Flow Modulation on the Strength of the Solar Polar Magnetic Field. *ApJ*, 717:597–602, July 2010. doi:10.1088/0004-637X/717/1/597.

M. J. Käpylä, P. J. Käpylä, N. Olspert, A. Brandenburg, J. Warnecke, B. B. Karak, and J. Pelt. Multiple dynamo modes as a mechanism for long-term solar activity variations. *A&A*, 589:A56, May 2016. doi:10.1051/0004-6361/201527002.

P. J. Käpylä, M. J. Mantere, and A. Brandenburg. Cyclic Magnetic Activity due to Turbulent Convection in Spherical Wedge Geometry. *ApJ*, 755:L22, August 2012. doi:10.1088/2041-8205/755/1/L22.

B. B. Karak. Importance of Meridional Circulation in Flux Transport Dynamo: The Possibility of a Maunder-like Grand Minimum. *ApJ*, 724:1021–1029, December 2010. doi:10.1088/0004-637X/724/2/1021.

B. B. Karak and R. Cameron. Babcock-Leighton Solar Dynamo: The Role of Downward Pumping and the Equatorward Propagation of Activity. *ApJ*, 832:94, November 2016. doi:10.3847/0004-637X/832/1/94.

L. L. Kitchatinov and S. V. Olemskoy. Does the Babcock-Leighton mechanism operate on the Sun? *Astronomy Letters*, 37:656–658, September 2011. doi:10.1134/S0320010811080031.

J. Larmor. How could a rotating body such as the sun become a magnet. *Report B.A.A.S.*, 159:412, 1919.

J. Larmor, Sir. The magnetic field of sunspots. *MNRAS*, 94:469, March 1934. doi:10.1093/mnras/94.5.469.

R. B. Leighton. Transport of Magnetic Fields on the Sun. *ApJ*, 140:1547, November 1964. doi:10.1086/148058.

R. B. Leighton. A Magneto-Kinematic Model of the Solar Cycle. *ApJ*, 156:1, April 1969. doi:10.1086/149943.

D. H. Mackay, E. R. Priest, and M. Lockwood. The Evolution of the Sun's Open Magnetic Flux - II. Full Solar Cycle Simulations. *Sol. Phys.*, 209:287–309, October 2002a. doi:10.1023/A:1021230604497.

D. H. Mackay, E. R. Priest, and M. Lockwood. The Evolution of the Sun's Open Magnetic Flux - I. A Single Bipole. *Sol. Phys.*, 207:291–308, June 2002b. doi:10.1023/A:1016249917230.

V. I. Makarov and A. G. Tlatov. The large-scale solar magnetic field and 11-year activity cycles. *Astronomy Reports*, 44(11):759–764, 2000. ISSN 1562-6881. doi:10.1134/1.1320502.

D. Martin-Belda and R. H. Cameron. Surface flux transport simulations: Effect of inflows toward active regions and random velocities on the evolution of the Sun's large-scale magnetic field. *A&A*, 586:A73, February 2016. doi:10.1051/0004-6361/201527213.

D. Martin-Belda and R. H. Cameron. Inflows towards active regions and the modulation of the solar cycle: A parameter study. *A&A*, 597:A21, 2017a. doi:10.1051/0004-6361/201629061.

D. Martin-Belda and R. H. Cameron. Evolution of the Sun's non-axisymmetric toroidal field. *A&A*, 603:A53, July 2017b. doi:10.1051/0004-6361/201730509.

V. Martínez Pillet, B. W. Lites, and A. Skumanich. Active Region Magnetic Fields. I. Plage Fields. *ApJ*, 474:810–842, January 1997. doi:10.1086/303478.

E. W. Maunder. The sun and sun-spots, 1820-1920. *MNRAS*, 82:534–543, June 1922. doi:10.1093/mnras/82.9.534.

A. Muñoz-Jaramillo, M. Dasi-Espuig, L. A. Balmaceda, and E. E. DeLuca. Solar Cycle Propagation, Memory, and Prediction: Insights from a Century of Magnetic Proxies. *ApJ*, 767:L25, April 2013. doi:10.1088/2041-8205/767/2/L25.

A. Muñoz-Jaramillo, R. R. Senkpeil, J. C. Windmueller, E. C. Amouzou, D. W. Longcope, A. G. Tlatov, Y. A. Nagovitsyn, A. A. Pevtsov, G. A. Chapman, A. M. Cookson, A. R. Yeates, F. T. Watson, L. A. Balmaceda, E. E. DeLuca, and P. C. H. Martens. Small-scale and Global Dynamos and the Area and Flux Distributions of Active Regions, Sunspot Groups, and Sunspots: A Multi-database Study. *ApJ*, 800:48, February 2015. doi:10.1088/0004-637X/800/1/48.

N. J. Nelson, B. P. Brown, A. S. Brun, M. S. Miesch, and J. Toomre. Magnetic Wreaths and Cycles in Convective Dynamos. *ApJ*, 762:73, January 2013. doi:10.1088/0004-637X/762/2/73.

N. J. Nelson, B. P. Brown, A. S. Brun, M. S. Miesch, and J. Toomre. Buoyant Magnetic Loops Generated by Global Convective Dynamo Action. *Sol. Phys.*, 289:441–458, February 2014. doi:10.1007/s11207-012-0221-4.

A. A. Norton, P. Charbonneau, and D. Passos. Hemispheric Coupling: Comparing Dynamo Simulations and Observations. *Space Sci. Rev.*, 186:251–283, December 2014. doi:10.1007/s11214-014-0100-4.

E. N. Parker. Hydromagnetic Dynamo Models. *ApJ*, 122:293, September 1955. doi:10.1086/146087.

G. Ruediger and L. L. Kichatinov. Alpha-effect and alpha-quenching. *A&A*, 269:581–588, March 1993.

K. H. Schatten, P. H. Scherrer, L. Svalgaard, and J. M. Wilcox. Using dynamo theory to predict the sunspot number during solar cycle 21. *Geophys. Res. Lett.*, 5:411–414, May 1978. doi:10.1029/GL005i005p00411.

C. J. Schrijver. Simulations of the photospheric magnetic activity and outer atmospheric radiative losses of cool stars based on characteristics of the solar magnetic field. *ApJ*, 547(1):475, 2001.

C. J. Schrijver and K. L. Harvey. The photospheric magnetic flux budget. *Sol. Phys.*, 150: 1–18, March 1994. doi:10.1007/BF00712873.

C. J. Schrijver and Y. Liu. The global solar magnetic field through a full sunspot cycle: Observations and model results. *Sol. Phys.*, 252(1):19–31, 2008. ISSN 1573-093X. doi:10.1007/s11207-008-9240-6.

C. J. Schrijver and S. F. Martin. Properties of the large- and small-scale flow patterns in and around AR 19824. *Sol. Phys.*, 129:95–112, September 1990. doi:10.1007/BF00154367.

C. J. Schrijver and C. Zwaan. *Solar and Stellar Magnetic Activity*. October 2008.

A. Schuster. Transaction of Section A, p634. *Report B.A.A.S.*, 1892.

H. Schwabe. Sonnenbeobachtungen im Jahre 1843. Von Herrn Hofrath Schwabe in Dessau. *Astronomische Nachrichten*, 21:233, February 1844.

H. B. Snodgrass. Magnetic rotation of the solar photosphere. *ApJ*, 270:288–299, July 1983. doi:10.1086/161121.

S. K. Solanki. Smallscale Solar Magnetic Fields - an Overview. *Space Sci. Rev.*, 63: 1–188, March 1993. doi:10.1007/BF00749277.

G. Spörer. Über die Periodizität der Sonnenflecken seit dem Jahre 1618, vornehmlich in Bezug auf die heliographische Breite derselben, und Hinweis auf eine erhebliche Störung dieser Periodizität während eines langen Zeitraumes. *Vierteljahrsschrift der Astronomischen Gesellschaft*, 22:223–229, 1887.

H. C. Spruit. Heat flow near obstacles in the solar convection zone. *Sol. Phys.*, 55:3–34, November 1977. doi:10.1007/BF00150871.

H. C. Spruit. Origin of the torsional oscillation pattern of solar rotation. *Sol. Phys.*, 213: 1–21, March 2003. doi:10.1023/A:1023202605379.

H. C. Spruit. *Theories of the Solar Cycle: A Critical View*, page 39. 2011.

M. Steenbeck and F. Krause. On the Dynamo Theory of Stellar and Planetary Magnetic Fields. I. AC Dynamos of Solar Type. *Astronomische Nachrichten*, 291:49–84, January 1969. doi:10.1002/asna.19692910201.

M. Steenbeck, F. Krause, and K. H. Rädler. Berechnung der mittleren lorentz-feldstärke für ein elektrisch leitendes medium in turbulenter, durch coriolis-kräfte beeinflußter bewegung. *Zeitschrift für Naturforschung A*, 21(4):369–376, 1966.

M. J. Thompson, J. Toomre, E. R. Anderson, H. M. Antia, G. Berthomieu, D. Burtonclay, S. M. Chitre, J. Christensen-Dalsgaard, T. Corbard, M. De Rosa, C. R. Genovese, D. O. Gough, D. A. Haber, J. W. Harvey, F. Hill, R. Howe, S. G. Korzennik, A. G. Kosovichev, J. W. Leibacher, F. P. Pijpers, J. Provost, E. J. Rhodes, Jr., J. Schou, T. Sekii, P. B. Stark, and P. R. Wilson. Differential Rotation and Dynamics of the Solar Interior. *Science*, 272:1300–1305, May 1996. doi:10.1126/science.272.5266.1300.

G. Tóth, B. van der Holst, and Z. Huang. Obtaining Potential Field Solutions with Spherical Harmonics and Finite Differences. *ApJ*, 732:102, May 2011. doi:10.1088/0004-637X/732/2/102.

L. Upton and D. H. Hathaway. Predicting the Sun's Polar Magnetic Fields with a Surface Flux Transport Model. *ApJ*, 780:5, January 2014. doi:10.1088/0004-637X/780/1/5.

M. Švanda, A. G. Kosovichev, and J. Zhao. Effects of Solar Active Regions on Meridional Flows. *ApJ*, 680:L161, June 2008. doi:10.1086/589997.

A. A. van Ballegooijen, N. P. Cartledge, and E. R. Priest. Magnetic Flux Transport and the Formation of Filament Channels on the Sun. *ApJ*, 501:866–881, July 1998. doi:10.1086/305823.

A. Vögler. On the effect of photospheric magnetic fields on solar surface brightness . Results of radiative MHD simulations. *Mem. Soc. Astron. Italiana*, 76:842, 2005.

Y.-M. Wang and N. R. Sheeley. Understanding the Geomagnetic Precursor of the Solar Cycle. *ApJ*, 694:L11–L15, March 2009. doi:10.1088/0004-637X/694/1/L11.

Y.-M. Wang and N. R. Sheeley, Jr. Magnetic flux transport and the sun's dipole moment - New twists to the Babcock-Leighton model. *ApJ*, 375:761–770, July 1991. doi:10.1086/170240.

Y.-M. Wang, A. G. Nash, and N. R. Sheeley, Jr. Evolution of the sun's polar fields during sunspot cycle 21 - Poleward surges and long-term behavior. *ApJ*, 347:529–539, December 1989a. doi:10.1086/168143.

Y.-M. Wang, A. G. Nash, and N. R. Sheeley, Jr. Magnetic flux transport on the sun. *Science*, 245:712–718, August 1989b. doi:10.1126/science.245.4919.712.

Y.-M. Wang, N. R. Sheeley, Jr., and A. G. Nash. A new solar cycle model including meridional circulation. *ApJ*, 383:431–442, December 1991. doi:10.1086/170800.

Y.-M. Wang, E. Robbrecht, and N. R. Sheeley, Jr. On the Weakening of the Polar Magnetic Fields during Solar Cycle 23. *ApJ*, 707:1372-1386, December 2009. doi:10.1088/0004-637X/707/2/1372.

A. D. Wittmann and Z. Xu. A catalogue of sunspot observations from 165 BC to AD 1684. *Vistas in Astronomy*, 31:127, 1988. doi:10.1016/0083-6656(88)90189-4.

R. Wolf. Abstract of his latest Results. *MNRAS*, 21:77, January 1861. doi:10.1093/mnras/21.3.77.

A. R. Yeates. Coronal Magnetic Field Evolution from 1996 to 2012: Continuous Non-potential Simulations. *Sol. Phys.*, 289:631–648, February 2014. doi:10.1007/s11207-013-0301-0.

A. R. Yeates, D. Nandy, and D. H. Mackay. Exploring the Physical Basis of Solar Cycle Predictions: Flux Transport Dynamics and Persistence of Memory in Advection- versus Diffusion-dominated Solar Convection Zones. *ApJ*, 673:544-556, January 2008. doi:10.1086/524352.

H. Yoshimura. Solar-cycle dynamo wave propagation. *ApJ*, 201:740–748, November 1975. doi:10.1086/153940.

J. Zhao and A. G. Kosovichev. Torsional Oscillation, Meridional Flows, and Vorticity Inferred in the Upper Convection Zone of the Sun by Time-Distance Helioseismology. *ApJ*, 603:776–784, March 2004. doi:10.1086/381489.

Publications

Refereed publications

- *Surface flux transport simulations: Effect of inflows toward active regions and random velocities on the evolution of the Sun's large-scale magnetic field* D. Martin-Belda and R. H. Cameron, Astronomy & Astrophysics 586, A73 (2016), DOI 10.1051/0004-6361/201527213.
- *Inflows towards active regions and the modulation of the solar cycle: A parameter study* D. Martin-Belda and R. H. Cameron, Astronomy & Astrophysics 597, A21 (2017), DOI 10.1051/0004-6361/201629061.
- *Evolution of the Sun's non-axisymmetric toroidal field* D. Martin-Belda and R. H. Cameron, Astronomy & Astrophysics 603, A53 (2017), DOI 10.1051/0004-6361/201730509.

Conference contributions

- *May 2015* Stellar and Planetary Dynamos (Göttingen, Germany). Poster: Effect of inflows towards active regions on the Sun's large scale field
- *April 2016* Space Climate 6 (Levi, Finland). Poster: Inflows towards active regions and the modulation of the solar cycle
- *August 2016* Solar and Stellar Magnetic Fields (M16) (Goslar, Germany) Talk: Non-axisymmetric structure of the Sun's toroidal field
- *November 2016* 17th MHD days (Göttingen, Germany). Talk: Non-axisymmetric evolution of the Sun's toroidal flux

Acknowledgements

The first thank you goes to my supervisor Robert Cameron for his excellent mentoring over the last three years and a half. I also thank Manfred Schüssler for his patience and priceless advice in what I found to be a most challenging task: paper writing. I also want to thank my supervisor at the university, Laurent Gizon, for his guidance.

I am also extremely grateful to the school coordinator, Sonja Schuh, for her support, her hard work on improving the school and for making many problems easier for the students (and especially for those with an allergy to paperwork, such as myself).

I want to thank the International Max Planck Research School for Solar System Science at the University of Göttingen for the support and the top-level education I have received over these years.

It is impossible to individually thank all the people who have supported me, in one way or another, over these three and a half years. I cannot skip mentioning some, though. Thanks to my parents, Juan Luis and Catalina, and to my siblings, Rut, Ester, Isaac, Teresa, Juan and Loreto. Thanks to my partners in crime Francisco, Michél, Ivan, Ricardo, Jack and Alessandro. To my wonderful officemates Franziska, Iulia and Theo. To Holly, Fatima and Sabrina. To Belén and Nan. To Emanuele and Nathalie. To Elisabeth.

I want to especially thank Emanuele, Theo, Jörn and Atefeh for their invaluable help and feedback.

This thesis is dedicated to my parents.

Curriculum vitae

Personal Details

Name: David Martín Belda
Date of birth: 30. March 1984
Place of birth: Salamanca
Present Citizenship: Spanish

Education

10.2013 – 04.2017: **PhD studies**
International Max Plank Research School for Solar System Science at the University of Göttingen, Göttingen, Germany.
Title of thesis: *Non-axisymmetric magnetic flux transport in the Sun*
Advisors: Robert Cameron, Manfred Schüssler, Laurent Gizon

10.2011 – 9.2013: **Master of Science (Astrophysics)**
Universidad de La Laguna, Tenerife, Spain
Title of thesis: *Numerical simulations of the transverse oscillations of multi-threaded coronal loops*
Advisors: Manuel Luna Bennasar, Ángel de Vicente

09.2002 – 02.2011: **Graduate in Physics**
Universidad de Salamanca, Salamanca, Spain